POOL BOILING OF R-134a AND R-123 ON SMOOTH AND ENHANCED TUBES

by

EVRAAM I. GORGY

B.S., Cairo University, Egypt, 2001

A THESIS

submitted in partial fulfillment of the requirements for the degree

MASTER OF SCIENCE

Department of Mechanical And Nuclear Engineering
College of Engineering

KANSAS STATE UNIVERSITY
Manhattan, Kansas

2008

Approved by:

Co-Major Professor
Steven J. Eckels

Co-Major Professor
Bruce R. Babin

Copyright

EVRAAM I. GORGY

2008

Abstract

This project studied the pool boiling of R-134a and R-123 on smooth and enhanced tubes. This is the 1st phase of ASHRAE project RP-1316 "Experimental Evaluation of The Heat Transfer Impacts of Tube Pitch in a Highly Enhanced Surface Tube Bundle". A Turbo BII-HP and a Turbo BII-LP enhanced tubes were used in this study. These tubes were manufactured and donated by Wolverine Tube, Inc. Four different boiling cases were tested, R-134a on smooth tube, R-123 on smooth tube, R-134a on Turbo BII-HP tube, and R-123 on Turbo BII-LP tube. The first step in this study was performing a modified Wilson plot analysis, once completed, the average and local refrigerant heat transfer coefficients were determined. This thesis also presents the enthalpy-based heat transfer analysis (EBHT), a new method for determining the heat exchanger's overall heat transfer coefficient as a function of the enthalpy change of incompressible fluids.

The test tubes' outer diameter is 19.05 mm and length is 1 m. Tests were conducted in a single tube test section, in which the test tube was water heated. All tests were conducted at a saturation temperature of 4.44 °C. The heat flux range is 9.2-126.6 kW/m² for testing with R-134a on smooth tube, 9.2-58 kW/m² for R-123 on smooth tube, 4.1-135.1 kW/m² for R-134a on Turbo BII-HP tube and 4.7-59.8 kW/m² for R-123 on Turbo BII-LP tube. Results show that the heat transfer coefficient increases with heat flux for all cases except the case of R-134a on Turbo BII-HP tube, where it experiences a trend change.

Part of this study was comparing the smooth and enhanced tubes performances. R-134a Turbo BII-HP tube to smooth tube heat transfer coefficient ratio changes from 4 at low heat flux to 1.7 at high heat flux. R-123 Turbo BII-LP tube to smooth tube heat transfer coefficient ratio changes from 24 at low heat flux to 7 at high heat flux. The performance of Turbo BII-HP and Turbo BII-LP was found to be very similar over the tested heat flux range of the Turbo BII-LP tube. Comparison plots with available literature are presented.

Table of Contents

List of Figures viii
List of Tables x
Acknowledgements xi
Dedication xii
Nomenclature xiii
CHAPTER 1 - Introduction 1
1.1 Introduction. 1
1.2 Pool Boiling Mechanism. 1
1.3 Scope of The Research. 2
1.4 Organization of The Document. 3
CHAPTER 2 - Literature Review 5
2.1 Introduction. 5
2.2 Review of Previous Work. 6
2.3 Experimental Techniques. 14
2.4 Tube Types. 15
2.5 Modeling. 16
2.6 Conclusion. 17
CHAPTER 3 - Facility Description 18
3.1 Introduction. 18
3.2 Test Section. 21
3.2.1 The instrumented tube. 26
3.2.2 The function of the wire wraps (swirls). 28
3.2.3 The hydraulic diameter and characteristic length definitions. 29
3.2.4 The thin film RTD's. 29
3.2.5 RTD's calibration. 30
3.2.6 The refrigerant saturated pressure and temperature measurements. 31
3.3 The Water Circuit. 32
3.4 Refrigerant Circuit. 33

3.5 Facility Operation. 34
3.6 Data Acquisition. 34
3.7 Conclusion. 35
CHAPTER 4 - Data Reduction 36
4.1 Introduction. 36
4.2 Finite Heat Transfer Analysis. 37
4.3 Total Heat Transfer Analysis. 39
4.4 The Average Heat transfer Coefficient Analysis. 40
4.4.1 The enthalpy-based heat transfer analysis (EBHT). 41
4.4.1.1 The governing equations of the enthalpy-based heat transfer analysis. 42
4.4.2 The water side heat transfer coefficient. 44
4.4.3 The modified Wilson plot technique. 45
4.5 The Local Refrigerant Heat Transfer Coefficient Analysis. 47
4.5.1 Comments on the use of the water side heat transfer coefficient in the local analysis. 48
4.5.2 The local heat flux. 49
4.5.4 The water temperature gradient. 50
4.5.5 The Monte Carlo Simulation of the local temperature curve fit. 50
4.6 Uncertainty Analysis. 51
4.6.1 Inputs. 51
4.6.1.1 Temperature uncertainty. 51
4.6.1.2 Saturation temperature uncertainty for R-134a. 52
4.6.1.3 Saturation temperature uncertainty for R-123. 53
4.6.1.4 Water pressure uncertainty. 54
4.6.1.5 Water specific heat uncertainty. 54
4.6.1.6 Water density Uncertainty. 54
4.6.1.7 Water heat transfer coefficient uncertainty. 55
4.6.1.8 Length uncertainty. 55
4.6.2 Average refrigerant heat transfer coefficient uncertainty. 56
4.6.3 Local Refrigerant Heat Transfer Coefficient Uncertainty. 57
4.6.3.1 Uncertainty of the local temperature slope. 57
4.6.3.2 Uncertainty of the local temperature. 59

4.7 Conclusion. 59
CHAPTER 5 - Results 60
5.1 Average Heat Transfer Coefficient Results. 60
5.1.1 Modified Wilson Plot Results. 60
5.1.2 R-134a and R-123 smooth tube results. 64
5.1.3 R-134a and R-123 enhanced tubes results. 66
5.1.4 Smooth to enhanced comparison plots. 68
5.1.5 Turbo BII HP and Turbo BII LP comparison. 69
5.2 Local Heat Transfer Coefficient Results. 70
5.2.1 Test tube water temperature profile. 70
5.2.2 R-134a and R-123 smooth tube results. 73
5.2.3 R-134a and R-123 enhanced tube results. 74
5.3 Average and Local Results Comparison. 76
5.4 Conclusion. 79
CHAPTER 6 - Overall Conclusion 80
6.1 Research Conclusion 80
6.2 Recommendations 82
Bibliography 83
Appendix A - Data Tables 86
Appendix B - Mathcad Example Calculation Sheet 110

List of Figures

Figure 3-1 General shematic of the entire system 19
Figure 3-2 Picture of the test facility. 20
Figure 3-3 Side view of the test facility.....21
Figure 3-4 Cross sectional view of the test section. 23
Figure 3-5 Close up on the test section water entrance. 24
Figure 3-6 Clope up on the test section 24
Figure 3-7 Test section side view. 25
Figure 3-8 Instrumented tube.....27
Figure 3-9 Close up on the instrumented tube.....27
Figure 3-10 Instrumended tube cross section and flow pattern. 29
Figure 3-11 RTD element inside an encapsulant.....30
Figure 3-12 Picture of the RTD's size. 30
Figure 4-1 1-D finite control volume.....37
Figure 5-1 R-134a on smooth tube modified Wilson plot. 62
Figure 5-2 R-123 on smooth tube modified Wilson plot. 62
Figure 5-3 R-134a on Turbo BII HP tube modified Wilson plot. 62
Figure 5-4 R-123 on Turbo BII LP tube modified Wilson plot. 63
Figure 5-5 R-134a on smooth tube average heat transfer coefficient plot. 65
Figure 5-6 R-123 on smooth tube average heat transfer coefficient plot. 65
Figure 5-7 R-134a on Turbo BII HP tube average heat transfer coefficient plot. 67
Figure 5-8 R-123 on Turbo BII LP tube average heat transfer coefficient plot. 67
Figure 5-9 R-134a Turbo BII HP tube and smooth tube comparison. 68
Figure 5-10 R-123 Turbo BII LP tube and smooth tube comparison plot. 69
Figure 5-11 Turbo BII HP and Turbo BII LP comparison plot. 70
Figure 5-12 R-134a smooth tube temperature profile plot. 71
Figure 5-13 R-123 smooth tube temperature profile plot. 71
Figure 5-14 R-134a Turbo BII HP tube temperature profile plot. 72

Figure 5-15 R-123 Turbo BII LP tube temperature profile plot. 72
Figure 5-16 R-134a on smooth tube local heat transfer coefficient plot. 73
Figure 5-17 R-123 on smooth tube local heat transfer coefficient plot. 74
Figure 5-18 R-134a on Turbo BII HP tube local heat transfer coefficient plot. 75
Figure 5-19 R-123 on Turbo BII LP tube local heat transfer coefficient plot. 75
Figure 5-20 R-134a smooth tube average and local comparison plot. 77
Figure 5-21 R-123 smooth tube average and local comparison plot. 75
Figure 5-22 R-134a Turbo BII HP tube average and local comparison plot. 75
Figure 5-23 R-123 Turbo BII LP average and local comparison plot. 78

List of Tables

Table 1-1 Test range. 3
Table 3-1 Test tubes details 26
Table 5-1 Modified Wilson plot summary table. 63
Table 6-1 R-134a on smooth tube average data 86
Table 6-2 R-134a on smooth tube local data 87
Table 6-3 R-123 on smooth tube average data 91
Table 6-4 R-123 on smooth tube local data 91
Table 6-5 R-123 on Turbo BII LP tube average data 95
Table 6-6 R-123 on Turbo BII LP tube local data 96
Table 6-7 R-134a on Turbo BII HP Tube average data 100
Table 6-8 R-134a on Turbo BII HP tube local data 101

Acknowledgements

"Because the LORD was with Joseph and gave him success in whatever he did" Genesis 39:23. I would like to express my gratefulness to the Lord for granting me the success in this work. Prof. Steven Eckels has done a great job pushing this research forward with his precious experience and knowledge, dedicating a lot of his time and efforts even with his responsibilities as a director of the Institute of Environmental Research and as a professor. Working with him "enhanced" my experience and knowledge in the two phase flow field. I would like to thank Prof. Bruce Babin for all his support and trust in the work of this research, Prof. Babin is a talented instructor. The comments and reviews of Prof. Daniel Swenson were very beneficial and I am thankful for him. I would like to thank Prof. Terry Beck for his hard work in teaching the advanced heat transfer courses at K-State. I am appreciative to the ASHREA RP-1316 project's committee for supervising this project and giving their useful comments on the work. Also, to the Trane research team and their valuable comments.

Eric Waters helped in designing and building the facility as well as the data acquisition system, for all of that I am thankful. Also, to Larry Waters (Eric's father) who we called many times during building the facility to take his advice. I am grateful for all IER Engineers including, Luke Schooler (who has done a wonderful job in building the facility and making the system's pictures and drawings), Jim Mason, Jared Selland, Brandon Hagman, and Aaron Lindh. I am thankful for David Huddleston and Tim Sobering from The Electronics Design Laboratory at K-State for their help in designing and manufacturing the RTD's.

I am grateful to the support and prayers of my family (every member of the family). I am appreciative for all of my friends, IER staff and students, Erin Carlson (the academic program director in the MNE department), and my fellow graduate students.

Dedication

To the faithful of St. Mary Orthodox Church in El-Fayoum City, Egypt

Nomenclature

A	Surface area
$A(x)$	Surface area applied on a distance x
A_i	Tube's inner surface area
A_o	Tube's outer surface area
C	Integration constant
C_1	Integration constant
C_2	Integration constant
C_3	Integration constant
C_p	Water specific heat at constant pressure
$C_{p,h}$	Hot side specific heat at constant pressure
$C_{p,c}$	Cold side specific heat at constant pressure
C_i	Water heat transfer coefficient correction factor
C_o	Refrigerant heat transfer coefficient correlation's constant
D_h	Hydraulic diameter
D_o	Test tube outer diameter
D_i	Test tube inner diameter
D_w	Wire diameter
$EBHT$	Enthalpy based heat transfer analysis
$\dot{E}_{in}$	Rate of inlet energy
$\dot{E}_{out}$	Rate of outlet energy
$\dot{E}_{gen}$	Rate of generated energy
E_{st}	Stored energy

f	Friction coefficient
h_r	Refrigerant heat transfer coefficient
$h_{r,a}$	Average refrigerant heat transfer coefficient
$h_{r,l}$	Local refrigerant heat transfer coefficient
h_i	Water heat transfer coefficient
h_w	Corrected water heat transfer coefficient
i_f	Refrigerant liquid enthalpy
i_g	Refrigerant vapor enthalpy
i_{in}	Water inlet enthalpy
i_{out}	Water outlet enthalpy
k_c	Copper thermal conductivity
k_w	Water thermal conductivity
L	Length
L_c	Characteristic length
$\dot{m}$	Water mass flow rate
$\dot{m}_h$	Hot side mass flow rate
$\dot{m}_c$	Cold side mass flow rate
n	Heat flux exponent
Nu_D	Nusselt number
P_{in}	Water inlet pressure
P_{out}	Water outlet pressure
P_h	Hot side pressure
P_c	Cold side pressure
ΔP	Water pressure drop
q''_{local}	Local heat flux
Q	Total rate of heat transfer

R_{wall}	Tube wall thermal resistance
Re_D	Reynolds number
R	Electric resistance
ρ	Water density
T_{in}	Water inlet temperature
T_{out}	Water outlet temperature
$T_{wall,in}$	Tube inner wall temperature
$T_{wall,out}$	Tube outer wall temperature
T_h	Water temperature
T_{hot}	Hot side temperature
T_{cold}	Cold side temperature
T_{local}	Local RTD's temperature measurement
ΔT_1	The temperature difference between the inlet hot side and the outlet cold side
ΔT_2	The temperature difference between the outlet hot side and the inlet cold side
T_∞	Refrigerant saturation temperature
U	Overall heat transfer coefficient
U_o	Heat exchanger's overall heat transfer coefficient
U_{local}	Local overall heat transfer coefficient
u_T	Uncertainty in the temperature measurement
$u_{T_{sat,134a}}$	Uncertainty in the refrigerant saturation temperature of R-134a
$u_{T_{sat,123}}$	Uncertainty in the refrigerant saturation temperature of R-123
$u_{T_{local}}$	Uncertainty in the local temperature measurement
u_{dTdx}	Uncertainty in the temperature slope
u_{C_p}	Uncertainty in the water specific heat
u_ρ	Uncertainty in the water density

$u_{h_{r,a}}$	Uncertainty in the average refrigerant heat transfer coefficient
$u_{h_{r,l}}$	Uncertainty in the local refrigerant heat transfer coefficient
v_h	Hot side specific volume
v_c	Cold side specific volume
V	Water velocity
W	Wire warp pitch
x	Distance

CHAPTER 1 - Introduction

1.1 Introduction.

Shell and tube heat exchangers are widely used in the refrigeration industry. Many of the evaporators used in large capacity units are of the shell and tube type heat exchangers. These evaporators are either in-tube boiling or shell-side boiling. In the case of the in-tube boiling, the refrigerant flows and boils inside the tubes. Flooded evaporators, like the ones used in centrifugal chillers, are of the shell-side boiling kind, in which the water flows inside of the tube bundle while refrigerant flows in the shell and on the outer surface of the horizontal tube bundle.

In flooded evaporators, refrigerant enters the evaporator from the bottom in a sub-cooled state and boils as it moves up on the tube bundle and exists from the top of the evaporator in the saturated vapor state or the super heated state depending on the amount of heat flux imposed by the water. The increase in quality causes an increased velocity as the refrigerant moves through the bundle. Two types of boiling heat transfer occur inside the flooded evaporator. The top portion of the tube bundle is exposed to convective boiling heat transfer and the bottom row tubes are exposed to pool boiling heat transfer.

This research presents a shell side pool boiling study. Pool boiling is an important consideration for tubes at the bottom of large flooded evaporators. To simulate the lower portion of theses bundles, a single tube test section was constructed. The test section incorporates a single 1 m long test tube. Unlike most of the studies done on pool boiling of refrigerants where the test tube was electrically heated, this research presents the pool boiling study with a water heated tube. The objective is to determine the refrigerant side pool boiling, and the water side heat transfer coefficients.

1.2 Pool Boiling Mechanism.

Pool boiling occurs when a still liquid around a heated tube reaches its boiling point and bubbles begin to form. Surface enhancement on the tube often helps bubble generation by

providing nucleation sites. Pool boiling in general has four different regimes, free convection boiling, nucleate boiling, transition boiling and film boiling. Many textbooks and researchers have described the boiling curve, like Nukiyama's saturated water boiling curve (Incropera and Dewitt (2002)), and the different regimes of pool boiling.

This project focuses only on the nucleate boiling regime, which is the common operating regime for industrial applications like refrigeration systems and nuclear reactors. The nucleate boiling regime is divided into two regions, the isolated bubbles region and the jets-and-columns region. Initially isolated bubbles begin to form on the tube surface in the nucleation sites. As the heat flux increases, bubble coalescence starts. This causes jets and columns of vapor to leave the tube surface. As the heat flux continues to increase, the fluid reaches its point of maximum heat flux, which is known as the CHF (critical heat flux). At this point, the vapor generation begins to inhibit the liquid flow back to the tube surface, thus beginning to decrease performance. Beyond the CHF point the boiling curve moves to the transition regime then the film boiling regime.

1.3 Scope of The Research.

This project is the 1st phase of ASHRAE project RP-1316 "Experimental Evaluation of The Heat Transfer Impacts of Tube Pitch in a Highly Enhanced Surface Tube Bundle". RP-1316 is focused on shell side boiling research, where the tube bundle is water heated. The test tubes (Turbo BII HP and Turbo BII LP) were manufactured and donated by Wolverine Tube, Inc.

This thesis presents a complete pool boiling study including the following. The first step in this study was performing a modified Wilson plot analysis, once completed, the average and local refrigerant heat transfer coefficients were determined. Tests were conducted for R-134a and R-123 on smooth tube, R-134a on Turbo B-II HP tube and R-123 on Turbo BII LP tube. Both Turbo BII's are externally and internally enhanced.

This phase of the study provides two important pieces of information for the 2nd phase of the project. First, the water side heat transfer coefficient correlations will be used to model the

tube side of the tube bundle. Second, the refrigerant pool boiling coefficient will be useful in modeling the tube bundle which includes both nucleate boiling and convective components.

Correlations can not simply be used for the water side heat transfer coefficient because of the presence of the internal enhancement. Specially, the micro-fins affect the accuracy of measuring both the characteristic length and the hydraulic diameter. For this reason, the Gnielinski correlation needs a correction factor multiplier. This correction factor is determined using the modified Wilson plot technique. All the Wilson plot data and the complete pool boiling data are taken at a saturation temperature of 4.4 °C. Table 1-1 shows the range of the test conditions.

Table 1-1 Test range.

	R-134a Smooth Tube	**R-123 Smooth Tube**	**R-134a Turbo BII HP Tube**	**R-123 Turbo BII LP Tube**
Heat Flux Range (kW/m^2)	9.2-126.6	9.2-58	4.1-135.1	4.7-59.8
Reynolds Number (× 1000)	8-62	9-52	7 -38.5	5-31

1.4 Organization of The Document.

Chapter two of this thesis gives a pool boiling literature review from 1991 onward. The literature review reports on single tube pool boiling of refrigerants with an emphasis on papers including R-134a or R-123 on the tubes used in this study. Chapter three gives a description of the facility built for this project. The facility description includes detailed drawings and explanation of the test section. It also presents a description of the water and the refrigerant circuits and detailed explanation of the equipments and instrumentations in each circuit.

Chapter four presents the data reduction techniques. The data reduction includes the methods and equations used for determining the average and local refrigerant heat transfer

coefficients. Also, it includes a new method, called the enthalpy-based heat transfer analysis (EBHT), for determining the heat exchanger's overall heat transfer coefficient as a function of the water enthalpy. And it ends with the uncertainty analysis of the components used in the average and local refrigerant heat transfer coefficients equations.

Chapter five presents the results of the four tested cases, R-134a and R-123 on smooth tube, R-134a on Turbo BII HP tube, and R-123 on Turbo BII LP tube. It starts with presenting the modified Wilson plot analysis. Results for the average and local heat transfer coefficients are presented next. The final section compares the various tubes and refrigerants. The overall conclusion and future recommendations of this document are presented in chapter six.

CHAPTER 2 - Literature Review

2.1 Introduction.

Pool boiling has been a significant research area for many years, even up to today. Some researchers provides information on the pool boiling regimes for different fluids, such as Nukiyama's (1934) boiling curve for saturated water at atmospheric pressure. In addition, others are trying to understand and define the parameters that affect pool boiling, such as the influence of surface roughness. Berensen (1962) showed that increased surface roughness can cause a large increase in heat flux. This led to the development of the enhanced surfaces. The enhanced surface provides the nucleation sites for trapping the vapor and hence the better bubbles generation.

Moreover, it has been found that the surface-fluid combination influences boiling heat transfer. Therefore, for each surface-fluid combination, the quality of the pool boiling is evaluated by measuring the heat flux and determining the boiled fluid's heat transfer coefficient. The curves of the heat flux versus the heat transfer coefficient at a certain saturation temperature are one of the significant conclusions in the published papers on pool boiling. For example, some researchers have shown that saturation temperature for certain fluids does not have a large effect on the heat transfer coefficient as it is shown later in this chapter.

This literature review focuses on the boiling of refrigerants, mostly for R-134a and R-123. This is useful for comparing the results of this research project with previous studies, comparison charts are provided in the results chapter of this thesis. This literature review is presented by first offering a useful summary of the papers of interest. This summary is followed by sections that focus on some components which help understanding the work done on refrigerant pool boiling. The review covers the period from 1991 onward. For work prior to this time, the reader is referred to Pais and Webb (1991). A number of things are assumed in the following discussion. For example, the refrigerant heat transfer coefficient discussed below is

based on an equivalent area unless otherwise noted. Also, the statement “heat transfer coefficient” always refers to the refrigerant heat transfer coefficient or will be stated otherwise.

2.2 Review of Previous Work.

Hahne et al. (1991) studied the pool boiling of R-11 on finned tubes experimentally and theoretically. The tubes used were finned with 19 and 26 fins per inch (fpi). The 19 fpi had 18.74 mm OD and the 26 fpi had 18.89 mm OD. Tests were made at a saturation temperature of 23.31 °C. The heat flux range was 1-50 kW/m². The single finned tubes had a smaller heat transfer coefficient than that of the plain tube when the heat flux is less than 1 kW/m². However, when the heat flux exceeds 1 kW/m², the finned tubes heat transfer coefficient exceeds that of the plain tube. Based on Mikic and Rohsenow correlation for plain tubes, the authors developed a new theory for the finned tubes. This theoretical study was made by calculating the effect of the fins, the bubble dynamics, and the interaction between the heat transfer mechanisms of boiling and natural convection. The calculated results agreed well with the experimental results.

Webb and Pais (1991) experimentally studied the pool boiling of R-11, 12, 22, 113, 123 and 134a on three tube geometries. The test tubes used were 26 (fpi), Turbo-B and GEWA-SE. Tests were made at a saturation temperature of 27 °C. The tubes were 165 mm long and 19.05 mm OD. The heat flux range was 3-70 kW/m². For R-134a, the Turbo-B tube provided the highest performance. Its heat transfer coefficient is approximately 20% below that of the R-11 on the same tube. Also, GEWA-SE provided the highest performance with R-134a. Its heat transfer coefficient is 10% below that of R-12 on the same tube. No single tube geometry provided the highest performance with all refrigerants. The optimum geometry for each tube may vary for different refrigerants. Comparison charts of the test results with, Chen et al., and Starner for R-11 and Jung, and Bergles (1989) for R-113 were included in the paper.

Webb and Pais (1992) presented an extended review of (1991) study. This study had the same refrigerants, test tube dimensions, and heat flux range, but at a different boiling saturation temperature. Also, two more test tubes were added to the study. The data was taken at a saturation temperature of 4.44 °C, and the tubes added to the study were a plain tube and a GEWA-TX19. The Cooper correlation and Stephan-Abdelsalam correlation were used to predict

the data of the plain tube. The Cooper correlation agreed better with the experimental data than Stephan-Abdelsalam's. The heat transfer coefficient for a given heat flux increases with an increase of saturation temperature for all tube geometries. The curve fit of the experimental data was developed in the form $h = C\left(q''\right)^n$. The values of C and n were provided in a table. It should be noted that n had always a positive sign for all the refrigerants.

Memory et al. (1995) presented their single tube nucleate pool boiling of R-114 and R-114-oil mixtures on smooth and enhanced surfaces. The test tubes used were; smooth tube, GEWA-K, GEWA-T, GEWA-YX, TURBO-B, THERMOEXCEL-HE, and HIGH FLUX. Tests were made at a saturation temperature of 2.2 °C. The tubes were 450 mm long and 15.9 mm OD. Oil concentrations of 0%, 5% and 10% were used. The heat flux range was 0.6-100 kW/m². For pure R-114, the finned tubes typically provided enhancements between 3 and 4, and the re-entrant cavity tubes provided enhancements of more than 10 at low heat fluxes, decreasing to around 4 at high heat fluxes. For R-114-oil mixtures, at 3% concentration, the finned tubes performance increased with heat flux at first before dropping. For the re-entrant cavity tubes, as the oil concentration increased, the performance was dropping off steadily. The smooth tube data of the pure R-114 was compared with those of Wanniarachchi et al. and the data agreed closely. Also, the data agreed when it was compared with the predicted values obtained using Cooper correlation for the smooth tube.

Webb et al. (1995) studied the pool boiling of R-123 with oil mixtures of enhanced tubes. The test tubes used were; plain tube, GEWA-SE, TURBO-B and porous surface tube. Tests were made at a saturation temperature of 4.4 °C. The heat transfer calculations were based on the heater's active length, which is 117.8 mm. Oil concentrations from 0-10% were used. The heat flux range was 1-60 kW/m². For oil concentrations less than 2%, the experimental results indicated that there was no significant decrease in the heat transfer coefficient over the range of tubes tested. The heat transfer coefficient tends to decrease as the oil concentration increases. The heat transfer coefficient of the porous tube decreased less than of the enhanced tubes. The experimental results of the 0% oil concentration were compared with Webb and Pais (1992), and the data agreed closely.

Chien and Webb (1996) presented the first part of a parametric study of the effect of tunnel dimensions on nucleate boiling on structured surfaces. The study was made on R-11 and R-123. The test tubes had two different fin base shapes, rectangular and circular and three fpi, 35, 40, and 50. The tubes were then wrapped with a 50 µm thick copper sheet. The copper sheet was pored with a pore making tool with pore diameters (0.12-0.28 mm) and pore pitches of (0.75-3.0 mm). This configuration provided a surface similar to that of the Thermoexcel-E tube. The tubes were 19.1 mm OD and 140 mm long. Tests were made at a saturation temperature of 26.7 °C. The heat flux range was 2-70 kW/m². Increasing the fin height from 0.5 to 0.9 mm significantly increased the heat transfer coefficient on the 35 and 40 fpi tubes. For high fins, increasing the fin height from 0.8 to 1.5 mm didn't significantly increase the boiling performance. 0.7-1.0 mm was a recommended fin height. Tubes with a small fin base radius resulted in higher boiling heat transfer performance. The heat transfer performance of R-11 and R-123 was similar at the saturation temperature tested for the enhanced and Turbo-B tubes.

Chien and Webb (1996) presented the second part of a parametric study of nucleate boiling on structured surfaces. This paper studied the effect of the pore diameter and pore pitch. They explained the relationship between pore pitch and pore diameter. The dry-out heat flux increases with increased total open area, and with larger the pore size. An important conclusion is, at a certain reduced heat flux, part of the tunnel will become flooded and this results in decreasing the performance. Smaller pore size will prevent flooding at the reduced heat flux. The boiling coefficient is strongly controlled by the pore size at a certain heat flux.

Chiou et al. (1997) studied the pool boiling of R-22, R-124 and R-134a on a plain tube. Tests were conducted at saturation temperatures of 4.4 °C and 27 °C, and reduced pressures of 0.1 and 0.2. The tube dimensions were 100 mm long and 17.8 mm OD. The heat flux range was 0.1-110 kW/m². The heat transfer coefficient for R-124 was the smallest due to its low reduced pressure. The data agreed closely with the Webb and Pais' (1991) and (1992) and Cooper correlation, however the data didn't agree either with the Mostinski correlation or the Stephan-Abdelsalam correlation. A modified Blöchl (1991) method was proposed as a semi-analytical model. It satisfactorily predicted the experimental data as well as Webb and Pais' data.

Hsieh and Weng (1997) studied the nucleate pool boiling from coated surfaces in R-134a and R-407c. The ten test tubes used were; a smooth/plain tube (the material is not mentioned, but it is most likely to be copper), copper plasma spray, molybdenum plasma spraying, aluminum (L and H) flame spraying, Zink flame spraying, , and four different pitted coating on a copper surface. Tests were made at a saturation temperature of 4.4 °C. The tube dimensions were 330 mm long and 19 mm OD. The heat flux range was 0.6-62 kW/m². Boiling heat transfer was enhanced by a thin layer of porous matrix coated on the heating surface, with an enhancement of up to 1.5 ~ 2.5 times. Pitted coating surfaces gave the best performance over heat flux range for R-134a, while the plasma spraying surface performed well for R-407c. The refrigerant properties seem to have a significant effect on the three different enhanced tubes. The smooth tube data agreed closely with the Stephan-Abdelsalam's correlation. The Al. tube data agreed closely with the Cornwell and Houston correlation. For the Bier et al. correlation, all tubes data didn't seem to agree. A correlation was developed for plasma and flame spraying surfaces of the boiling data with mean pore diameter and porosity of the substrate surface in terms of Reynolds number, Jacob number, constant heat flux number and geometric scale factor.

Chang and You (1997) presented their study of boiling heat transfer from micro-porous cylindrical surfaces in FC-87 and R-123. The six test tubes used were; a plain 15.6 mm OD, ABM-coated plain 15.6 mm OD, low-fin 13.7 mm OD, ABM-coated low-fin 13.7 mm OD, High-flux 12.7 mm OD, and Turbo-B 17.2 mm OD. The tubes length was 72 mm. The tests were conducted in saturated FC-87 and R-123 at 1 atm. The heat flux range was 2-256 kW/m². The CHF values were determined for all the tubes for the boiling of FC-87 and R-123. The data of the plain tube in R-123 agreed with Webb and Pais' data. The data of the plain tube in FC-87 agreed with the Churchill and Chu correlation. ABM-coated plain tube showed enhancements of 200 to 380% for FC-87 and 140 to 280% for R-123. For the low-fin ABM coated tube 15 to 60% enhancement for the heat transfer coefficient over the non-coated low fin tube. The High-flux tube showed better performance than the Turbo-B, however the Turbo-B had the best performance at the CHF. The Turbo-B provided enhancements 91% for FC-87 and 46% for R-123 over the plain tube.

Saidi, et al. (1999) studied the pool boiling of R-123 on 1923 fins/m and 752 fins/m tubes. The test tubes were 50 mm long and 17.1 mm OD. The data was taken at a saturation temperature of 26.7 °C. The heat flux range was 1.5-70 kW/m². Data was compared with that of the plain, GEWA-K26, GEWA-SE, GEWA-TX19 and Turbo-B tubes studied by Webb and Pais. The two tubes had 130-240% enhancement ratios relative to the plain tube.

Tatara and Payver (2000) studied the pool boiling of pure R-134a from a single Turbo-BII-HP tube. The heat flux range was 8-40 kW/m². The tube was 211.51 mm long and 19.05 mm OD. Data were taken at a saturation temperature of 4.4 °C. The wall temperature was measured by locating thermocouples inside the wall thickness. The heat transfer coefficients were 60-90% greater than that of the Turbo-B tube.

Kim and Choi (2000) presented nucleate pool boiling of R-11, R-123 and R-134a on structured enhanced tubes having pores with connecting gaps. Three tubes of pore sizes 0.2 mm, 0.23 mm, 0.27 mm were used. The tubes geometry was similar to that of Turbo-B. The test tubes were 170 mm long and 18.8 mm OD. The data were taken at a saturation temperature of 26.7 °C and 4.4 °C. The heat flux range was 1-50 kW/m². Results were compared with those of Chein and Webb (1998). Although, the tubes of Chein and Webb are different than those used in Kim and Choi (2000), data seems to agree. At a heat flux of 40 kW/m², the heat transfer coefficient was greater than that of the smooth tube by, 6.5 times for R-11, 6 times for R-123 and 5.0 times for R-134a. Two models were developed, one for both R-11 and R-123 and one for R-134a. The correlations have parameters proposed by Cooper for plain tube and additional parameters for the pore sizes. The correlations predicted the experimental data within ± 20%.

Hsieh and Yang (2001) studied the nucleate pool boiling from coated and spirally wrapped tubes in R-134a and R-600a at low and moderate heat flux. Eight test tubes were used; copper smooth, copper smooth with helical wires wrapped 2º, copper smooth with helical wires wrapped 1.5º, copper smooth with helical wires wrapped 1º, porous molybdenum, porous molybdenum with helical wires wrapped 1º, porous copper and porous copper with helical wires wrapped 1º. The test tubes were 210 mm long and 20 mm OD. The heat flux range was 0.1-30 kW/m². The tests were conducted at a saturation temperature of 18 °C. The data of the copper

smooth tube with helical wires wrapped 1.5º tube agreed with Stephan-Abdelsalam correlation. Data was compared with that of Hsieh and Weng, and there seems to be agreement. Correlations of the thermal performance of each individual tube were developed. Bubble diameter and frequency were studied for both refrigerants under the heat flux range 0.6-1 kW/m².

Chein and Webb (2001) studied the effect of geometry and fluid properties on the performance of tunnel and pore enhanced boiling surfaces. Study included both R-134a and R-22 on twelve test tubes. The test tubes were 140 mm long and 18-19.5 mm OD. The heat flux range was 2-80 kW/m². The tests were conducted at a saturation temperature of 26.7 °C. The wall thermocouples were attached on the tube inner wall. The authors have previously published experimental work which identifies the effect of geometric dimensions on the boiling performance of "tunneled" enhanced boiling surfaces for R-11 and R-123. The effect of pore diameter and pore pitch for R-134a and R-22 are similar to that for R-123. Specifically, larger pore diameter provided performance benefits as long as tunnel flooding is avoided. Tunnel flooding causes less boiling performance degradation and occurs at a lower heat flux for R-134a and R-22 than that for R-123. The boiling performance for R-134a and R-22 is less sensitive to the pore diameter/pitch, but more sensitive to fin base radius than R-123. Higher fin height, greater fin density, and smaller fin base radius are preferred for R-123, R-134a and R-22. The authors compared this study's results with their previous works in the same field.

Jung et al. (2004) presented a nucleate boiling heat transfer study of R-22, R-134a, R-125 and R-32 on various enhanced tubes. Four tubes were used; plain, low fin 26 fpi, Turbo-B, and Thermoexcel-E. The data was taken at a saturation temperature of 7 °C. The tubes were 152 mm long and 18.6-18.8 mm OD. The heat flux range was 10-80 kW/m². For a plain and low fin tubes, refrigerants with higher vapor pressure showed higher heat transfer coefficients. For Turbo-B and Thermoexcel-E tubes, R-125 showed a peculiar behavior exhibiting much reduced heat transfer coefficients. The heat transfer enhancement ratios of the low fin, Turbo-B and Thermoexcel-E tubes were 1.09-1.68, 1.77-5.41, 1.64-8.77 respectively.

Robinson and Thome (2004) studied the local bundle boiling heat transfer coefficient of R-410A, R-134a, and R-507A on a Turbo BII tube bundle**.** The pool boiling study made in this research was a part of a full bundle investigation. The R-134a and R-410A data was taken at saturation temperature of 4.4 °C, and the data of R-507A was taken at saturation temperature of 4.6 °C. The heat flux range was 16.3-40.1 kW/m². This study is the first study of this literature review to use water as the heating source. The range of the water's Reynolds number was 8,800-20,000.The tube was 1000 mm long and 19.05 mm OD. A modified Wilson plot method was used to determine both of the water heat transfer coefficient and a correlation for the refrigerant heat transfer coefficient as a function of the heat flux in the form $h = C\left(q''\right)^n$. The following are the resulted models.

$$h_{o,pool,R-134a} = 30,944q^{-0.042}$$

$$h_{o,pool,R-507a} = 37,334q^{-0.055}$$

$$h_{o,pool,R-410a} = 43,520q^{-0.063}$$

A Ln-Ln chart was developed for the comparison with previous works. The heat transfer coefficients associated with the boiling curves for each refrigerant are increasing with the saturation pressure of the corresponding refrigerant. The pool boiling coefficients for this tube are nearly independent of heat flux and, in fact, decrease slightly with increasing the heat flux. The leading coefficient of the Gnielinski correlation was 2.8.

Robinson and Thome (2004) studied the local bundle boiling heat transfer coefficient of R-134a on a plain tube bundle. The pool boiling study made in this research was a part of a full bundle investigation. The data was taken at saturation temperature of 4.5 °C. This study is the second study of this literature review to use water as the heating source. The range of the water's Reynolds number was 9,840-18,800. The heat flux range was 14.36-26.3 kW/m². Wilson plot method was conducted to determine both of the water heat transfer coefficient and a correlation

of the refrigerant heat transfer coefficient as a function of the heat flux in the form $h = C\left(q''\right)^n$. The resulted model was $h_{o,pool,R-134a} = 10.56q^{0.66}$. It is notable that the fitted value for the heat flux exponent (0.66) is practically the same as that in the Cooper pool boiling correlation (0.67). The data agreed closely with Cooper correlation, a roughness factor of 5.7 microns was used for the Cooper correlation. The leading coefficient of the Gnielinski correlation was 1.0.

Robinson and Thome (2004) studied the local bundle boiling heat transfer coefficient of R-134a and R-507A on an integral finned tube. The pool boiling study that was done in this research was a part of a full bundle investigation. The data was taken at saturation temperatures of 4.7 °C for R-507a and 4.5 °C for R-134a. This study is the third study of this literature review to use water as the heating source. The range of the water's Reynolds number was 8,800-20,000. The heat flux range was 16.3-34.5 kW/m². Modified Wilson plot method was conducted to determine both of the water heat transfer coefficient and a correlation of the refrigerant heat transfer coefficient as a function of the heat flux in the form $h = C\left(q''\right)^n$. The leading coefficient of the Gnielinski correlation was 2.2. The resulted models were,

$$h_{o,pool,R-134a} = 90.11q^{0.436}$$

$$h_{o,pool,R-507a} = 93.35q^{0.448}$$

Ribatski and Thome (2006) presented a nucleate pool boiling study of R-134a on enhanced tubes. The tubes used were; High-Flux, GEWA-B, Turbo-CSL, and Turbo-BII HP. The data was taken at saturation temperatures of 5 °C, 10 °C and 20 °C. The heat flux range was 20-70 kW/m². This study is the fourth study of this literature review to use water as the heating source. The range of the water's Reynolds number was 6,000-16,000.The tubes were 554 mm long and 19.05 mm OD. Six Thermocouples, each pair of two was located at three different positions along the axis of an insert tube in the middle of the test tube. They were protruded from the insert tube to measure the water temperature in the annulus between the test tube and the insert tube.

Ribatski and Thome used the modified Wilson plot method to determine both of the water heat transfer coefficient and a correlation of the refrigerant heat transfer coefficient as a function of the heat flux in the form $h = C\left(q''\right)^n$. The value of n was 0.7. The six thermocouples help the determination of the local heat transfer coefficients as a function of the tube length. The effect of the saturation temperature on the heat transfer coefficient was almost negligible. Except for the Turbo-CSL, the heat transfer coefficient presented either a slight decrease in its value or an almost constant value with increasing heat flux. The High-Flux surface provided by far the highest heat transfer performance. Heat transfer enhancement ratios of the High-Flux, GEWA-B, Turbo-CSL and Turbo-BII tubes were 4.9-21.3, 2.4-5.2, 2.4-2.9, and 1.8-7.0, respectively, compared to a plain tube.

Yang and Fan (2006) presented a pool boiling study of R-134a and R-404A on porous and structured tubes. The tubes used were; smooth, GEWA-TX, Turbo-B, and a porous tube. The tubes OD's are as follows; 18.0 mm, 18.8 mm, 18.8 mm, 19.56 mm, respectively and all the tubes had a length of 100 mm. The data was taken at saturation temperatures of 4.4 °C and 26.7 °C. The heat flux range was 0.8-120 kW/m². Thermocouples were installed on the tubes' inner wall. The smooth tube's results agreed with the Cooper correlation for R-134a better than the data of the R-404A for both saturation temperatures. The results showed that the heat transfer coefficients increase with increasing the heat flux for the smooth and structured tubes. For the porous tube, the dependence of the heat transfer coefficients on the heat flux was not significant. At low heat flux the porous tube provided the highest performance.

2.3 Experimental Techniques.

The majority of the papers summarized above used an electric heater for heating the test tube. The electric heater provides a constant heat flux for the test section. This is a different boundary condition than that obtained when using water for heating the test tube. In the case of water, a temperature drop across the test section can be observed and, in fact, it simulates the actual evaporators. Since both Turbo BII HP and Turbo BII LP are internally enhanced tubes, their boiling performance is best tested with water heating so the effect of the internal micro-fins

on the water side heat transfer coefficient can be evaluated. Most of the papers above used thermocouples for measuring the tube wall temperature. Thus, the refrigerant heat transfer coefficient can easily be calculated using the electric resistances analogy. Most the researchers of this literature review drilled holes in the tube wall for attaching the wall thermocouples.

The papers summarized above are electrically heated except the work of Robinson and Thome (2004) and Ribatski and Thome (2006), which is water heated. Also, the refrigerant heat transfer coefficient reported in the published papers was measured as an average and no local measurements or investigations were reported. Although, the experimental work made by Robinson and Thome (2004) involves the measurement of the water temperature drop along the test tube, the local heat transfer coefficient was not reported in their papers.

2.4 Tube Types.

The most used tubes are from four major families, the Turbo B family (manufactured by Wolverine), the GEWA family (manufactured by Wieland-Werke), the Thermoexcel family (manufactured by Hitachi) and the integral finned tubes (manufactured by Hitachi). Those major family can be expanded to, plain, integral finned tubes, 19 and 26 fins per inch (fpi), 1923 fins/m, 752 fins/m tubes, GEWA-SE, GEWA-TX, GEWA-TX19, GEWA-K, GEWA-T, GEWA-YX, THERMOEXCEL-E, THERMOEXCEL-HE, High-Flux, GEWA-B, Turbo-B, Turbo-CSL, and Turbo-BII HP.

Chien and Webb (1996) made their own test tubes. The test tubes had two different fin base shapes, rectangular and circular and three fpi, 35, 40, and 50. Also, Hsieh and Weng (1997) studied ten test tubes; a plain tube, copper plasma spray, molybdenum plasma spraying, aluminum (L and H) flame spraying, Zink flame spraying, , and four different pitted coating on a copper surface. Kim and Choi (2000) presented their study on structured enhanced tubes having pores with connecting gaps. Three tubes were used; 0.2 mm, 0.23 mm, 0.27 mm pore sizes. The tubes geometry was similar to that of Turbo-B.

Chang and You (1997) presented their study on six test tubes; a plain, ABM-coated plain, low-fin, ABM-coated low-fin, High-flux and Turbo-B. Shou-Shing Hsieh and Tsung-Ying Yang (2001) presented their study on eight test tubes; copper smooth, copper smooth with helical wires wrapped 2º, copper smooth with helical wires wrapped 1.5º, copper smooth with helical wires wrapped 1º, porous molybdenum, porous molybdenum with helical wires wrapped 1º, porous copper and porous copper with helical wires wrapped 1º. Liang-Han Chein and Relph L. Webb (2001) studied twelve test tubes made specifically for their study.

2.5 Modeling.

For smooth tubes, the Cooper correlation is the most widely used for comparing the results of experimental work. Stephan-Abdelsalam correlation is sometimes used for smooth tube as well. Although these two correlations are well known in the pool boiling field, the constants associated with each correlation, like surface roughness, need to be determined accurately according to the application in which they are used.

The most used model in both and enhanced tubes is $h = C\left(q''\right)^n$ where the heat transfer coefficient is just a function of the heat flux. The constants of the equations are different for each tube-fluid combination. It was recommended one should be conservative in applying this model, since it is does not work on a wide range of heat flux.

Some such as E. Hahne et al. (1991) who have developed a theoretical approach for modeling finned tubes. This theoretical study was made by calculating the effect of the fins, the bubble dynamics, and the interaction between the heat transfer mechanisms of boiling and natural convection. The model was verified with the experimental results. Chiou et al. (1997) proposed a modified Blöchl method as a semi-analytical model, the model was verified with the experimental results. Based on the obtained experimental results, Hsieh and Weng (1997) developed a correlation for plasma and flame spraying surfaces of the boiling data with mean pore diameter and porosity of the substrate surface in terms of Reynolds number, Jacob number, constant heat flux number and geometric scale factor. Kim and Choi (2000) developed two models, one for R-11 and R-123 and the other for R-134a, the correlations predicted the

experimental data within ± 20%. Hsieh and Yang (2001) developed correlations of the thermal performance of each individual tested tube. External verification of these models has not yet appeared in the literature.

2.6 Conclusion.

Surface enhancement is the most studied area in the pool boiling field. Electric heating was found to be a widely used method for providing the heat to the test tube. The Turbo B family (Turbo B and Turbo BII), the Thermoexcel family, and the GEWA family (GEWA-SE, GEWA-TX, etc.) show their good performance's reputation among the boiling tubes. Cooper and Stephan-Abdelsalam correlations are commonly used for comparing the experimental results of smooth tubes. The most used model for the heat transfer coefficient is $h = C\left(q''\right)^n$ or the heat transfer coefficient is just a function of the heat flux, although later on in this thesis some restriction will be found on the usage of this model. Chien and Webb (1996) Part II presented an important conclusion which is at a certain reduced heat flux, part of the tunnel will become flooded and this results in decreasing the performance.

CHAPTER 3 - Facility Description

3.1 Introduction.

The test facility is designed for evaluating the single tube pool boiling heat transfer performance of smooth and enhanced tubes in a pool of R-134a and R-123. The enhanced tubes are Turbo BII HP and Turbo BII LP. Both Turbo BII HP and Turbo BII LP are designed and manufactured by Wolverine Tube, Inc. Turbo BII HP is used for high pressure refrigerant, like R-134a, and Turbo BII LP is used for low pressure refrigerants, like R-123. The test tubes are water heated. The facility is equipped with the necessary instrumentation for determining both the average and the local refrigerant heat transfer coefficients.

The test facility comprises of four main components, single tube test section (shell and tube heat exchanger), condenser (brazed plate heat exchanger), two electric water heaters, and two water pumps. Figure 3-1 shows a general schematic of the entire system. The water is driven by the two pumps through the test section and the entire water circuit. The refrigerant is driven by gravity, or natural circulation. In which, the liquid refrigerant exits the condenser at a higher elevation than the test section's entrance pipes while the vapor exits from the top of the test section directly to the condenser. This chapter discusses the detailed configuration of each component in the system. Actual pictures of the test facility are shown in Figure 3-2 and Figure 3-3.

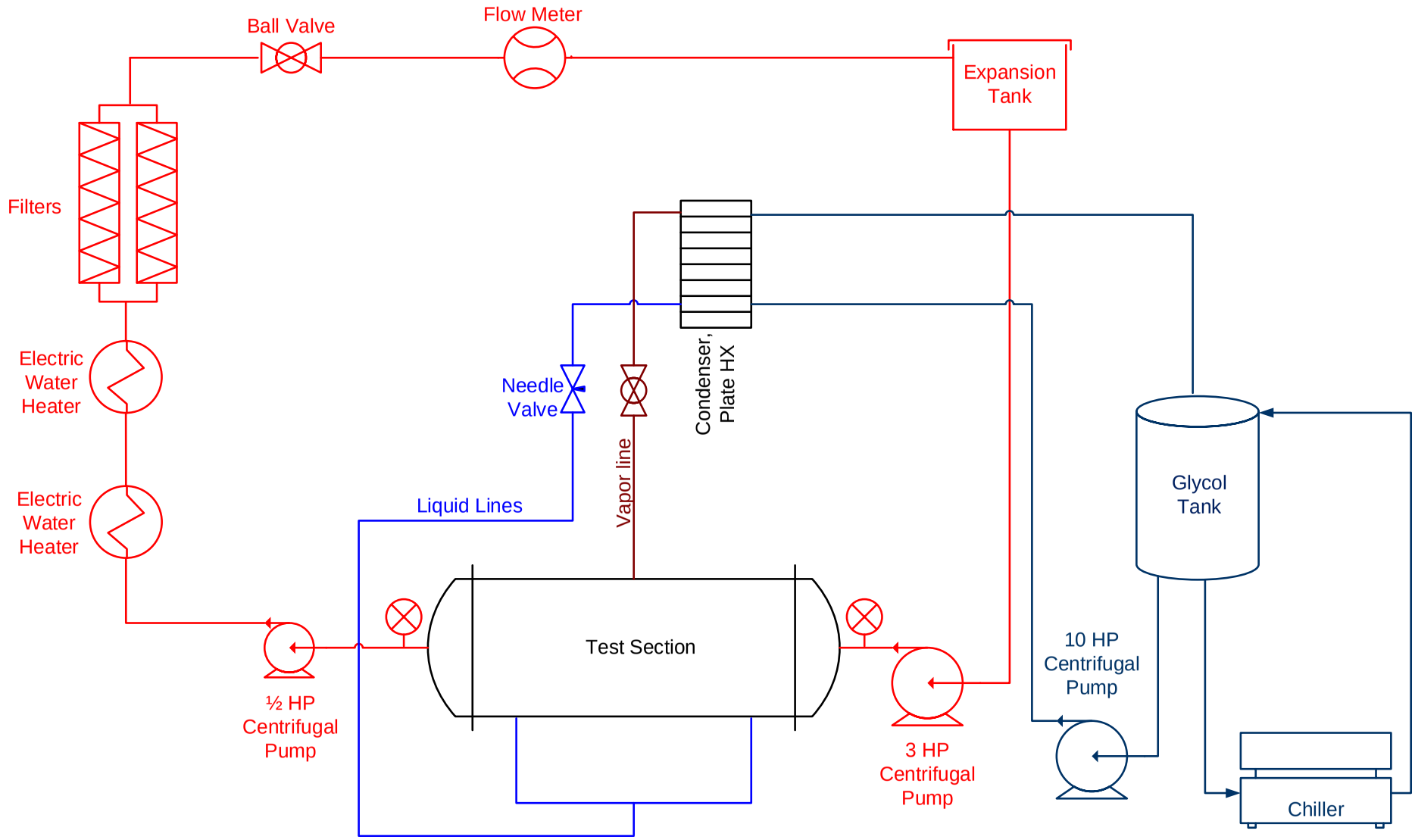

Figure 3-1 General schematic of the entire system.

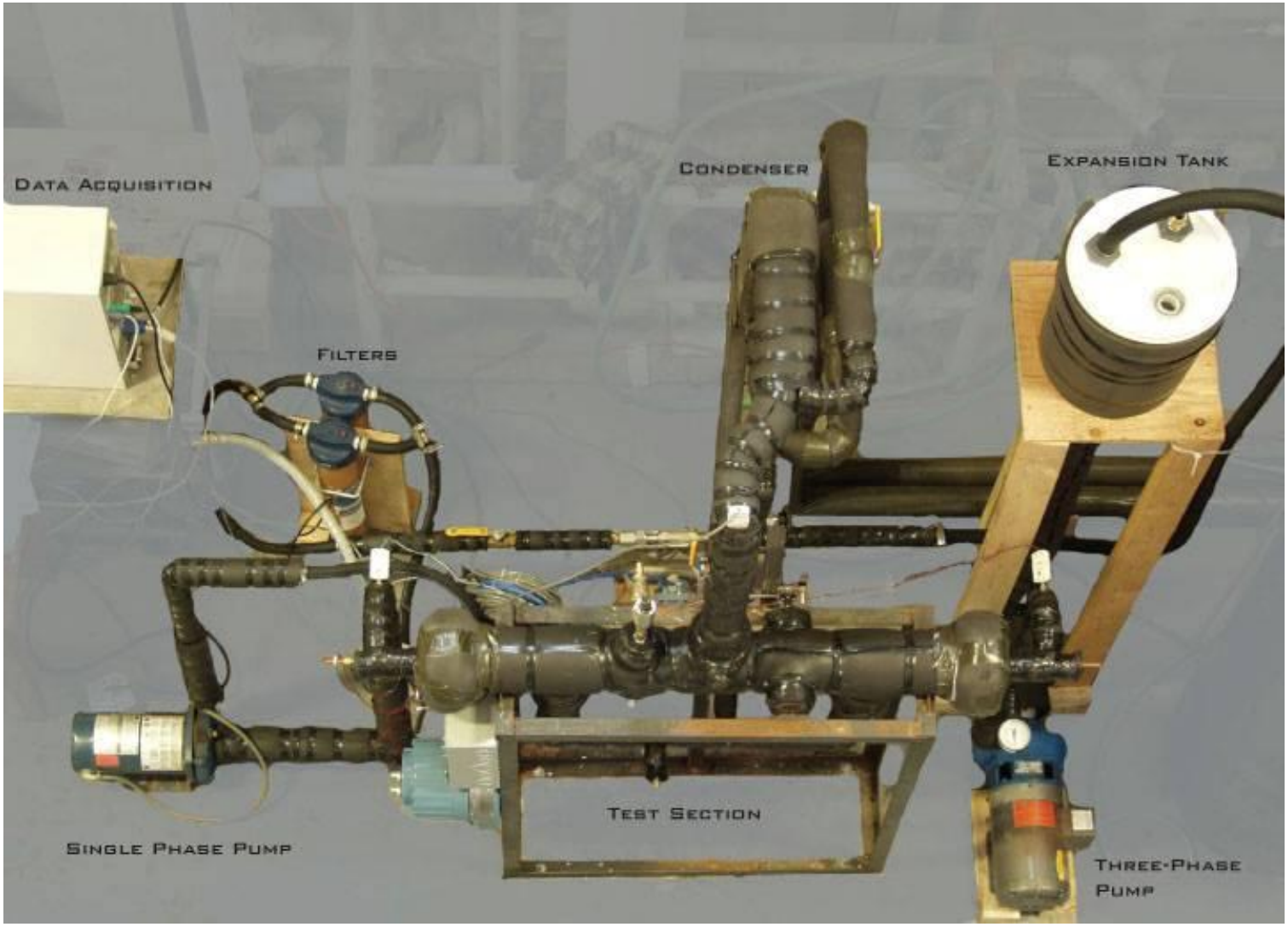

Figure 3-2 Picture of the test facility

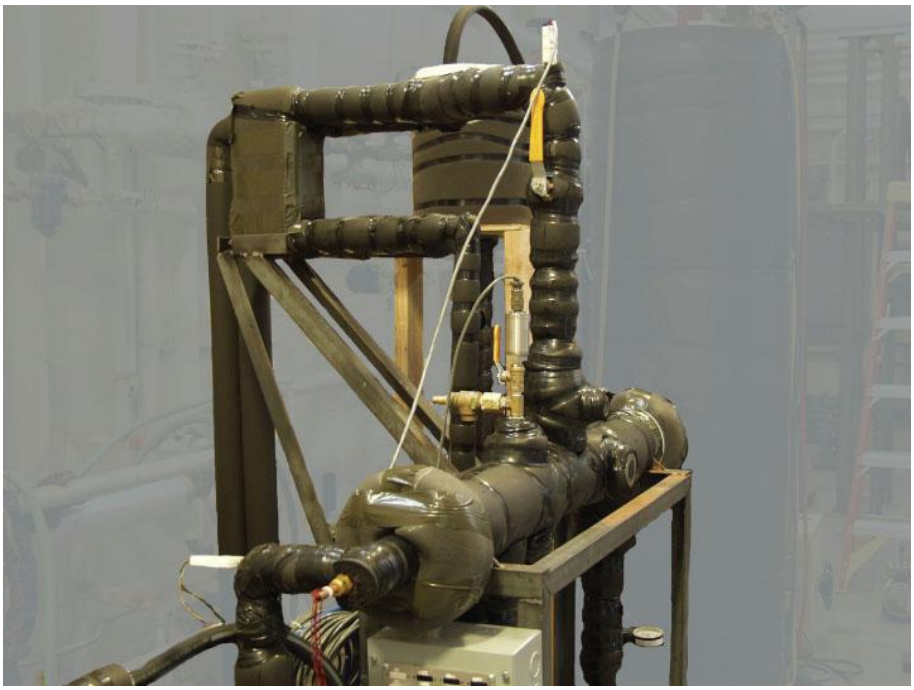

Figure 3-3 Side view the test facility

3.2 Test Section.

The test section is similar to an industrial shell and tube heat exchanger, but employs only one tube (the test tube). The design criteria of the test section are the test tube outer diameter and length and the shell inside diameter. The shell inside diameter was selected to keep the test tube fully immersed in liquid at all test conditions and allow enough vapor space for the vapor to leave the test section unrestricted.

The refrigerant flows in the shell of the test section and boils on the outer surface of the test tube. The liquid refrigerant enters the test section through two inlet pipes, while the vapor exists from the outlet pipe in the center of the test section. The vapor leaving the test section flows to the condenser in a 38.1 mm (1.5 in.) diameter tube, where it changes phase, leaving the condenser as a liquid and then return back to the test section. A perforated plate is fixed underneath the test tube to evenly distribute the liquid refrigerant around the test tube.

On the water side, two pressure transducers are installed on both sides of the test section. Each one is installed on the tee that connects the test tube to the water port (entering on one side or leaving on the other side of the test section) and the instrumented tube. The water pressure transducers are manufactured by Setra model 280E. Its measuring range is 0-689.47 kPa abs. (0-100 PSAI). Figures 3-4, 3-5, 3-6 and 3-7 show different cross sections and views of the test section. The following subsections provide more details on specific components in the test section.

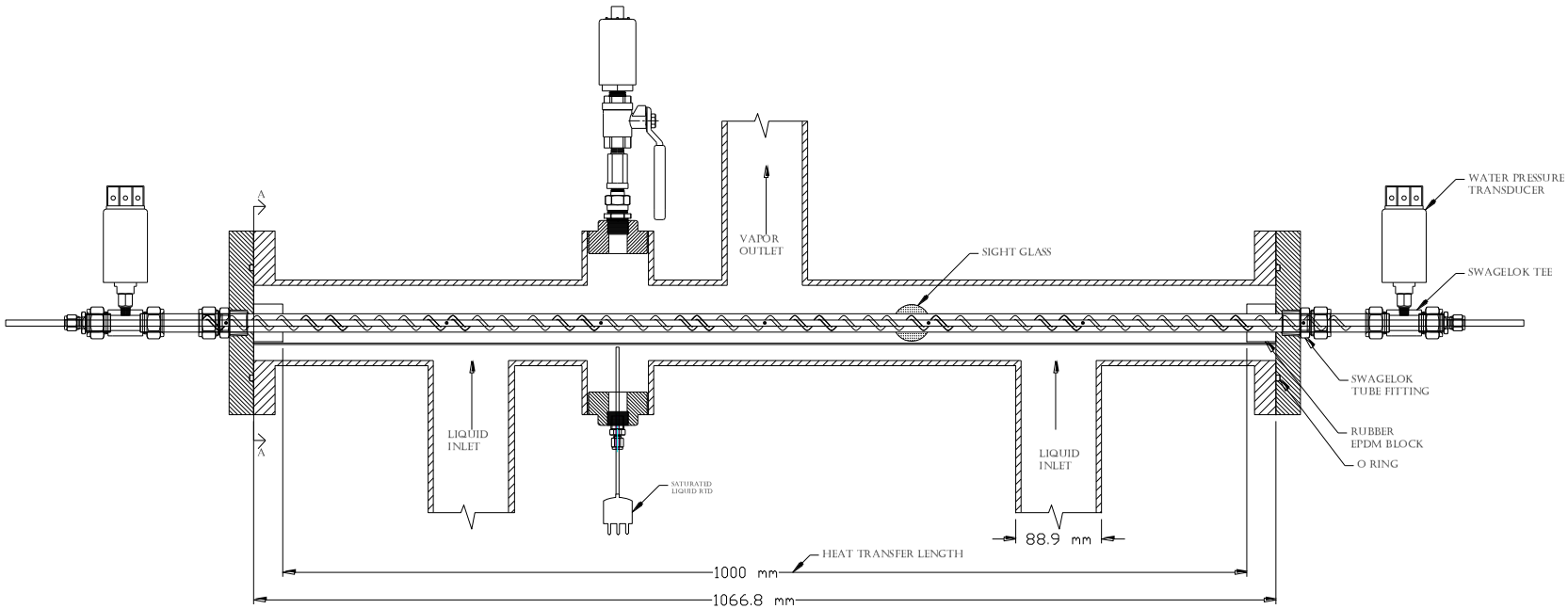

Figure 3-4 Cross sectional view of the test section

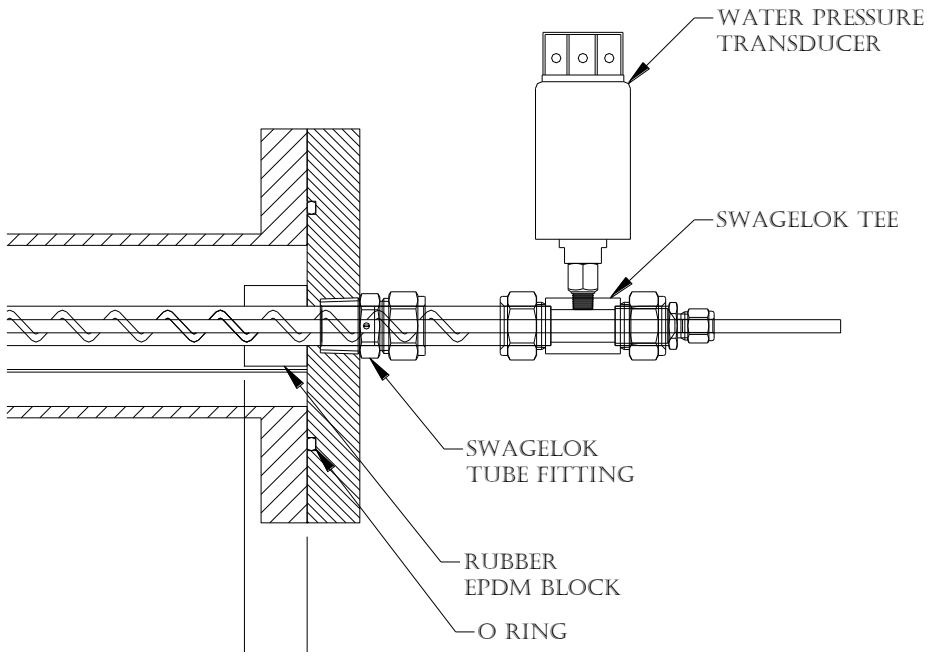

Figure 3-5 Close up on the test section water entrance

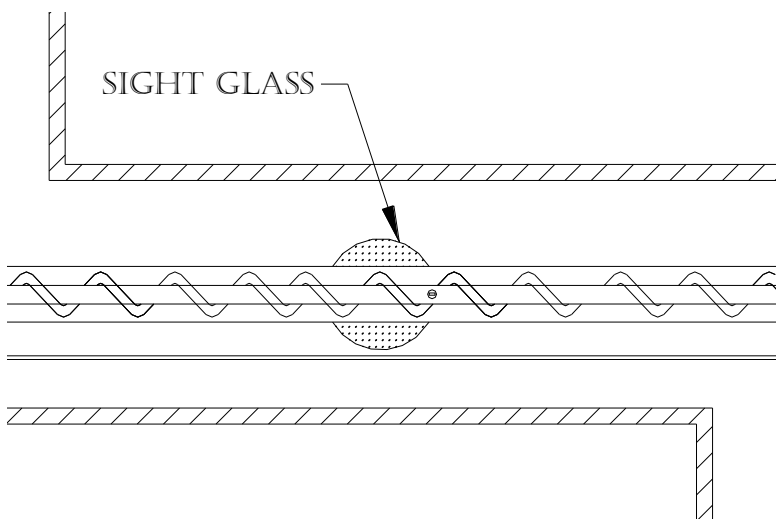

Figure 3-6 Close up on the test section

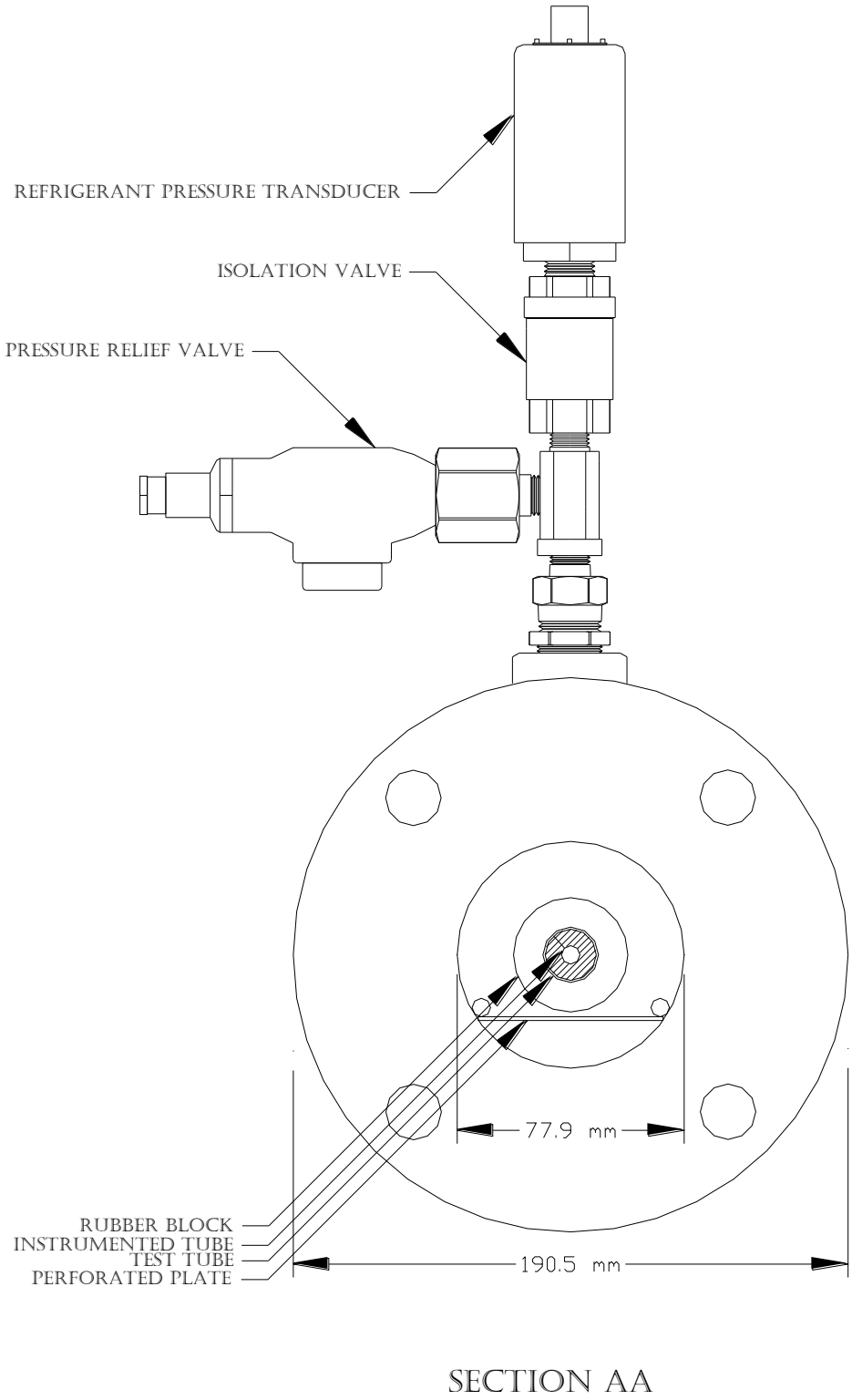

Figure 3-7 Test section side view

3.2.1 The instrumented tube.

The water entering the test section flows within the test tube and the instrumented tube. The instrumented tube (shown in Figure 3-8 and Figure 3-9) has two purposes, one is to increase the water velocity and thus the water heat transfer coefficient, and the other is to mount seven RTD's on its outer surface. The higher the water heat transfer coefficient, the better the resolution on the determination of the refrigerant heat transfer coefficient.

Two of the seven RTD's, the outer most two RTD's, are used for measuring the inlet and outlet temperatures as indicated in Figure 3-8. The inlet and outlet RTD's are located at the endplates of the test section. The advantage of their locations is to decrease the ambient loss effect on the temperature measurements. The other five RTD's are evenly distributed along the instrumented tube.

The instrumented tube is made of stainless steel and is 1.57 m (62 in.) long, its outer diameter is 6.35 mm (1/4 in.) and has a wall thickness of 0.254 mm (0.01 in.). The instrumented tube is centered inside the 1.3 m (51.5 in) long and 19.05 mm (3/4 in.) nominal diameter test tube. Thicknesses and more specifications on the test tubes are provided in Table 3-1 below.

Table 3-1 Test tubes details

	Outside Diameter mm (inch)	**Nominal Wall mm (inch)**	**Fin Per Inch**	**Finished Fin OD mm (inch)**	**Min. Wall Under Fins mm (inch)**	**Root Diameter mm (inch)**
Smooth Tube	19.05 (3/4)	0.635(0.025)	----	----	----	----
Turbo BII HP	19.05 (3/4)	0.635(0.025)	48	18.69 (0.736)	0.559 (0.022)	17.32 (0.682)
Turbo BII LP	19.05 (3/4)	0.635(0.025)	48	18.75 (0.738)	0.559 (0.022)	17.27 (0.680)

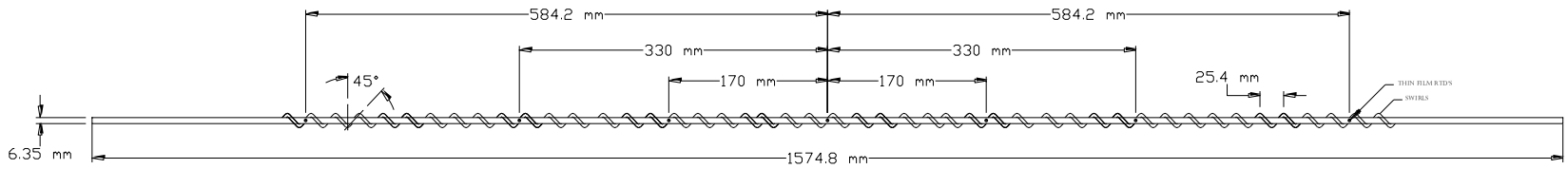

Figure 3-8 Instrumented tube

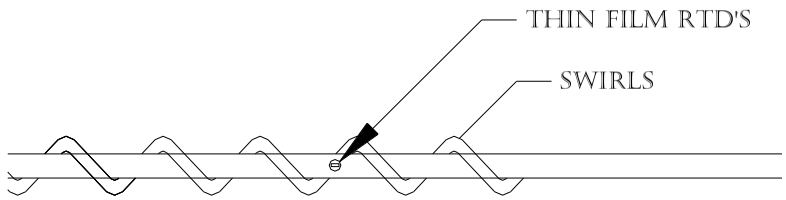

Figure 3-9 Close up on instrumented tube

The stainless steel tube is helically wrapped with a 3.81 mm (0.15 in.) outer diameter insulated tinned copper wire. The wire wrapping is approximately at 45 degrees angle and a pitch of 25.4 mm (1 in.). This configuration provides a helical channel path for the water to flow inside. The purpose of the wire wrap will be explained next in a separate subsection. Figure 3-9 shows a close up on the instrumented tube.

3.2.2 The function of the wire wraps (swirls).

Prior to deciding on using the wire warp in its current configuration, data were collected using the instrumented tube without any wrapping with just the RTD's. Those preliminary data showed inconsistent results that often varied with heat flux and flow rate. In other words, one down stream RTD among the 5 RTD's may read a higher temperature than some RTD up stream of it.

To clear any doubts concerning the functioning or calibration of the RTD's, the flow was reduced to the laminar regime and laminar flow heat transfer data were collected. In this case, the RTD's read a consistent temperature drop along length of the tube. This result confirms that both velocity and thermal boundary layers have a significant effect on the temperature measurement of the RTD's.

A theoretical prediction of the temperature profile was used as a guide to judge the best tube configuration. Through a number of experimental results, it was found that a helical channel for the water to flow within the most effective way to minimize the effect of the velocity and the thermal boundary layers. Specifically, the predicted and measured temperatures often correlate within ±0.03 °C, indicating that the channel is functioning as intended.

It is necessary to point out that, adding the helical wire wrap creates only a flow pattern and it does not directly participate in the heat transfer process. Only the calculations of the hydraulic diameter and the characteristic length are based on the water passage of the helical channel.

3.2.3 The hydraulic diameter and characteristic length definitions.

Figures 3-10 below shows a cross section of the instrumented tube. The flow pattern illustrated by the arrows assumes that the majority of the flow is flowing in the channel the swirls create and follows the swirl angle. Thus the characteristic length is defined as the straight length of the wire warp or $L_c = 1.905\ \text{m}$ and the hydraulic diameter is defined as,

$$D_h = \frac{4 \cdot \left(W \cdot D_w - \frac{\pi}{4} \cdot D_w{}^2 \right)}{2\left(W + D_w\right) - \pi \cdot D_w} \tag{3.1}$$

$$D_h = 7.3517 \times 10^{-3}\ \text{m}$$

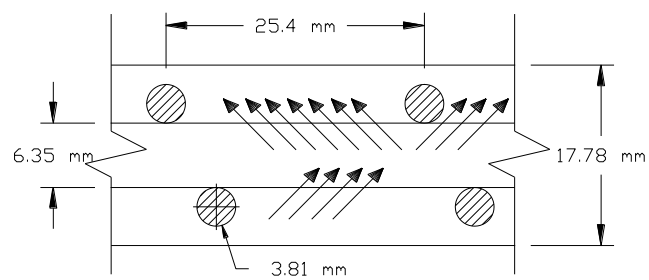

Figure 3-10 Instrumented tube cross section and flow pattern

3.2.4 The thin film RTD's.

The RTD element used on the instrumented tube is of the type, Omega 1000 ohms, (2 mm X 2 mm X 0.8 mm) thin film DIN class B element. This thin film RTD element with its three wires is casted inside an encapsulant cylinder as shown in Figures 3-11 and 3-12 below. The encapsulant cylinder is 3.17 mm (1/8 in.) in outer diameter and 3.17 mm (1/8 in.) in height. The RTD element protrudes about 1 mm (0.04 in.) from the encapsulant.

Figure 3-11 RTD element inside an encapsulant.

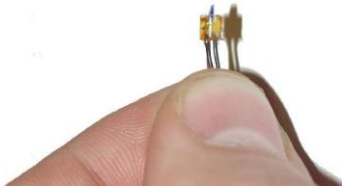

Figure 3-12 Picture of the RTD's size.

3.2.5 RTD's calibration.

Prior to starting the RTD's calibration process, the constant temperature bath used for the calibration was calibrated with a mercury thermometer of 0.01 °C divisions. After manufacturing the RTD like Figure 3-11, the RTD's are inserted inside the instrumented tube through the designated holes. Then all the RTD's are connected to the data acquisition switch unit, and immersed in the constant temperature bath.

The RTD's are calibrated over a wide range of temperature, from 4.0 °C to 30 °C with a step of 1 °C. The data acquisition system records the electrical resistance of each RTD at the corresponding set point of the constant temperature bath. After the constant temperature bath reaches steady state for a certain set temperature, an average of 20 minutes worth of data is recorded.

The 17 recorded resistances are curve fitted with the corresponding temperatures of the constant temperature bath. The best curve fit was found to be a third degree polynomial. The encapsulants are then placed and glued in the designated locations on the instrumented tube's surface.

3.2.6 The refrigerant saturated pressure and temperature measurements.

A tee is installed on the top of the test section, as shown in Figure 3-7, connects the pressure transducer and a safety pressure relief valve to the shell of the test facility. The safety pressure relief valve releases the refrigerant to a designated recovery bottle in case the R-134a refrigerant expands and the pressure reaches 861.84 kPa abs. (125 PSIA).

The pressure transducer is used for measuring the saturated vapor pressure. Two different pressure transducers, manufactured by Viatran, model 245, are used one at a time for each refrigerant. One pressure transducer with a range 0-517.1 kPa abs. (0-75 PSIA) is used for R-134a and the other with a range 0-103.42 kPa abs. (0-15 PSIA) is used for R-123. Using the refrigerant properties, the pressure transducer reading is converted to the equivalent saturated temperature.

A 6.35 mm (1/4 in.) ball valve is installed on the bottom of the pressure transducer. The purpose of the valve is to isolate the test section from the pressure transducer. The valve is kept closed anytime the system is not running, so when the refrigerant expands (due to any increase in the ambient temperature) inside the test section it doesn't over range the pressure transducer.

A RTD is installed on the same center line of the pressure transducer and on the bottom of the test section. It measures the saturated liquid temperature. This RTD is of the type Omega 100 ohms, quick disconnect probe with miniature mating connector. It is used to check the agreement of its temperature reading with the reading received from the pressure transducer.

Two identical sight glasses are installed before each other on each side of the test section. This arrangement helps observing the boiling process by projecting light beam on one of the sight glasses and looking though the opposite side. Also, the sight glasses are useful in determining the level of the refrigerant during system charging. A smaller sight glass is installed on the test section's outlet pipe.

3.3 The Water Circuit.

Due to the restricted water flow area inside the test tube, a large pressure drop (upto 355 kPa or 51.5 PSI at the highest flow rate) occurs along the test section. Two centrifugal pumps are used to overcome the pressure drop and to make a wide the range of test conditions available.

The up stream pump, which supplies the water to the test section, is a Goulds Pump model 3656, impeller diameter of 130.17 mm (5 1/8 in.), size 1 1/2 X 2-6 coupled to a 3-phase 208 VAC, 3 HP Baldor motor. The up stream pump's speed is controlled by a VFD (variable frequency drive). The VFD is manufactured by Magnetek model GPD 315. The purpose of the VFD is not only changing the mass flow rate of the water, but also to control the work (or energy) which the pump induces on the system.

The down stream pump, that sucks the water from the test section, is a STA-RITE pump model JBHC-61S coupled to a single phase 110 VAC, 1/2 HP motor. The down stream pump delivers the water to two electric water heaters with a capacity of 3 kW each. Each electric heater is a single phase 220 VAC and is controlled by an analogue VARIAC (variable autotransformers). The heaters are followed by two Aqua-Pure water filters mounted in parallel, the filter cartridge is nominal 5 micron. Following the water filters is a 19.05 mm (3/4 inch) ball valve is mounted between the filters and water flow meter.

The water flow meter is Micro Motion type Elite CMF050 sensor coupled to a Micro Motion transmitter model RFT9739. The flow meter is the last component in the water circuit, after which, the water discharges to a 9 liters (5 gallons) reservoir, which is the highest point of the system. This reservoir is 61 cm (2 ft.) higher than the test tube, and 1.52 m (5 feet) above the up stream pump's suction. The height of the reservoir provides enough NPSH (net positive suction head) for this pump.

3.4 Refrigerant Circuit.

The water flowing inside the test tube carries the input energy $\left(Q_{in}\right)$ to the system. The source of the input energy is the water heaters and the work of the pumps. The system reaches steady state when the amount of input energy is equals to the energy being rejected $\left(Q_{out}\right)$ in the condenser, or when $Q_{in} = Q_{out}$ at the 4.4 °C saturation temperature. The main component of the refrigerant circuit is a condenser, a brazed plate heat exchanger, that is manufactured by Alfa-Laval of the series CB 26-54H, it has a capacity of 15 kW (4.3 Tons-Refrigerant) and it works counter flow.

The liquid refrigerant exits the condenser at 0.91 m (3 ft) higher than the two entrance pipes of the test section. The line size carrying the liquid refrigerant is 12.7 mm (1/2 in.). A 12.7 mm (1/2 in.) Swagelok needle valve with Swagelok-type fittings is installed on the liquid line and half-way between the condenser and the test section. This valve allows precise control on the amount of liquid refrigerant entering the test section or the amount of energy absorbed by the refrigerant. This needle valve is the facility's maestro. It plays a major role in bringing the system to steady state, even with a very small adjustment. A RTD Omega 100 ohms, quick disconnect probe with miniature mating connector is installed before the test section entrance. It's used to measure the liquid refrigerant temperature.

The cooling source to the condenser is 50% water-glycol solution. The water-glycol solution is drawn from a large water-glycol tank (it provides the cooling source to the whole research institute) and the return is pumped back to it. The pump used for the glycol circuit is ITT A-C type 2000 centrifugal pump, size 2X1.5-9, 5 L/s (80 GPM), 56.38 meters of head (185 ft), 3600 RPM coupled to 3 phase 10HP, 208 VAC motor manufactured by US-Motors. The speed of the pump is controlled by a VFD. The VFD is manufactured by Magnetek model GPD 506. The water-glycol solution is cooled by the institute's chiller, which has a capacity of 23 Tons-Refrigerant.

3.5 Facility Operation.

The condenser glycol pump is started first, with the refrigerant valve fully opened. Then the water pumps start with the VFD adjusted to the desired water flow rate. Boiling starts and the saturation temperature starts to decrease quickly. As the saturation temperature approaches 6 °C, the water heaters are turned on with the desired amount of heat controlled via the VARIAC. The refrigerant valve is used to bring the facility to the steady state condition at 4.4 °C. Any point between 4.2 °C and 4.6 °C is considered a satisfactory steady state saturation temperature. The system is considered at steady state when the inlet water temperature change doesn't exceed 0.05 °C (less than ± the calibrated RTD uncertainty) over 20 minutes.

These procedures are the same for both high and low pressure refrigerants. For the low pressure refrigerant, after the system is charged with refrigerant and before starting the system, a recovery machine is connected to the highest point in the refrigerant loop to remove the non-condensable gases. When the saturated liquid temperature agrees with the saturated vapor temperature within 0.1 °C, the recovery machine is stopped and disconnected and the system is ready for testing.

3.6 Data Acquisition.

The data acquisition switch unit used is Agilent 34970A. This multimeter has an accuracy of 6½ digits. The unit is connected to a PC through a GPIB (general purpose interface bus). The unit is controlled by the National Instruments software Labview 8.2. When the system reaches steady state, the software starts recording data every 5 seconds over a 20 minute period. Recorded data is saved in a Microsoft Excel™ (.csv) sheet.

3.7 Conclusion.

This chapter presented new useful methodologies in designing a single tube water heated pool boiling facility. The equipments used in this facility helped determining the heat transfer coefficients with low uncertainty. Such as the use of the Micromotion Elite sensor, the thin film RTD's, and the Viatran pressure transducers. Due to their accurate calibration capability, the use of RTD's was found very useful. The thin film RTD's are excellent in their fast response to temperature change. The 1000 Ω RTD are better than the 100 Ω because of the better resolution on resistance measuring. The swirls were very functional in reducing the effect of velocity and thermal boundary layers. Positioning the inlet and outlet RTD's on the instrumented tube and close to the heat transfer region, helped determining the boundary conditions with the least effect of the ambient condition. Also, the location of the water pressure transducers was useful in determining the boundary conditions accurately.

CHAPTER 4 - Data Reduction

4.1 Introduction.

This chapter describes the methods and equations that lead to the determination of the refrigerant side heat transfer coefficient. It chapter presents the derivation of both the average and the local refrigerant heat transfer coefficients. First it presents the derivation of the general equation for the refrigerant side heat transfer coefficient, and then discusses the inputs needed for the determination of both the average and the local refrigerant side heat transfer coefficients. The chapter ends with the uncertainty analysis.

By solving the first law of thermodynamics and the heat transfer equations (Newton's law of cooling and Fourier's model) with the associated assumptions, the average refrigerant heat transfer coefficient is calculated by determining its dependant variables (the overall heat transfer coefficient and the water side heat transfer coefficient) as $h_{r,a} = h_{r,a}\left(U_o, h_w\right)$. The local refrigerant heat transfer coefficient is calculated by determining its dependant variables (local water temperature, local heat flux and the water side heat transfer coefficient) as $h_{r,l} = h_{r,l}\left(T_{local}, q''_{local}, h_w\right)$. The techniques and calculations needed to determine the dependant variables are present in later sections.

4.2 Finite Heat Transfer Analysis.

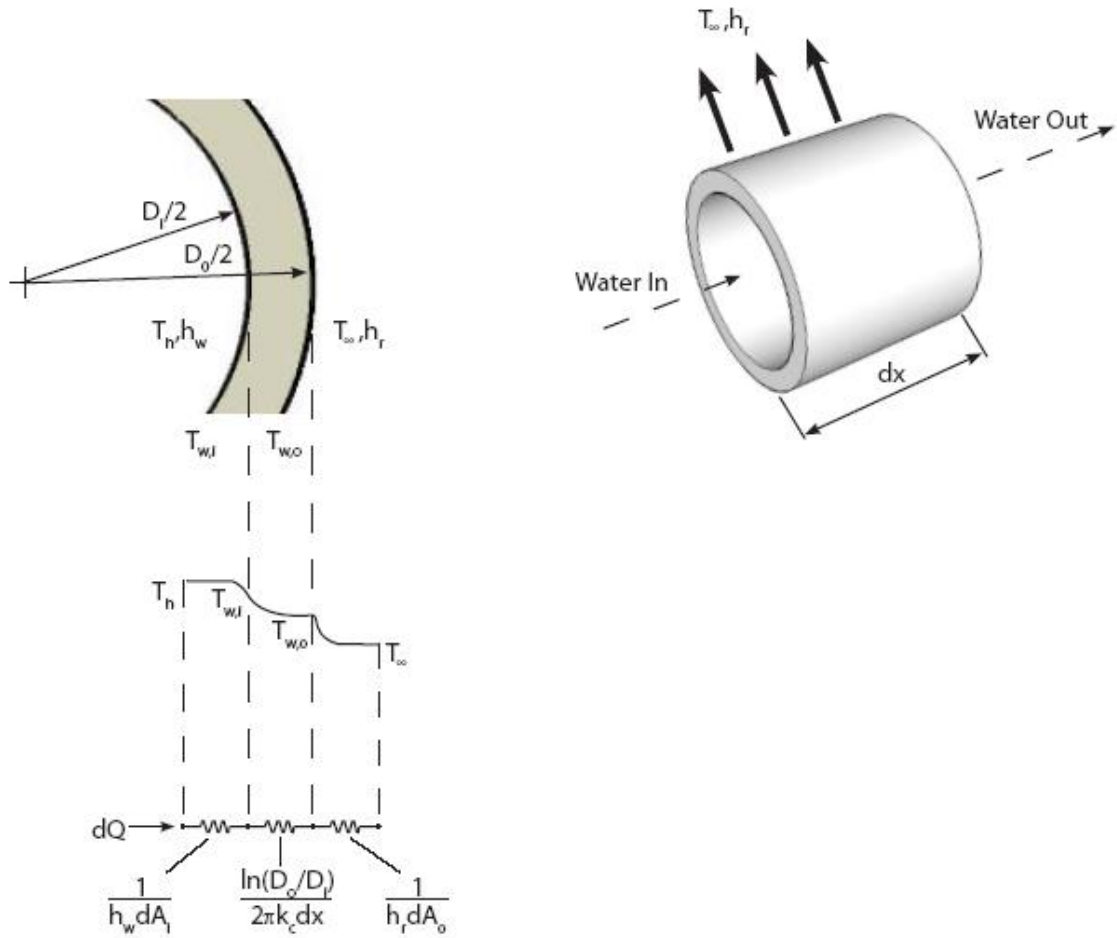

Figure 4-1 1-D finite control volume.

Applying the law of conservation of energy and the 1-D heat transfer equations on the finite control volume shown above in Figure 4-1. Heat is transferred by convection through the water, conduction through the cylindrical wall, and by convection through the refrigerant with the associated assumptions as,

1. Heat is being carried only in the radial direction.
2. Negligible fouling resistances.

Yields,

$$dQ = h_w dA_i \left(T_{hot} - T_{wall,in}\right) = \frac{2\pi k_c dx}{\ln\left(\frac{D_o}{D_i}\right)}\left(T_{wall,in} - T_{wall,out}\right) \tag{4.1}$$

And,

$$h_r dA_o \left(T_{wall,out} - T_{cold}\right) = \frac{2\pi k_c dx}{\ln\left(\frac{D_o}{D_i}\right)}\left(T_{wall,in} - T_{wall,out}\right) \tag{4.2}$$

Where,

$$dA_i = \pi D_i dx \tag{4.3}$$

$$dA_o = \pi D_o dx \tag{4.4}$$

An extended form of Newton's law of cooling is,

$$dQ = U \cdot dA_o \left(T_{hot} - T_{cold}\right) \tag{4.5}$$

Defining the thermal resistance of the tube's wall as,

$$R_{wall} = \frac{D_o}{2k_c} \ln\left(\frac{D_o}{D_i}\right) \tag{4.6}$$

Using Equations 4.1, 4.2, 4.5 and 4.6 the following general thermal resistances model is obtained,

$$\frac{1}{U} = \frac{1}{h_w} \cdot \frac{D_o}{D_i} + R_{wall} + \frac{1}{h_r} \tag{4.7}$$

Solving for h_r which is of interest in this study,

$$h_r = \left(\frac{1}{U} - R_{wall} - \frac{1}{h_w} \frac{D_o}{D_i} \right)^{-1} \tag{4.8}$$

It is necessary to notice that the above equation does not correlate to any particular distance. Thus, it can be applied for any distance of the heat exchanger, either dx or L. Based on this fact, all the elements of Equation (4.8) can be applied on a local sense or an average sense. To determine those elements on an average sense (the average heat transfer coefficients and the overall heat transfer coefficient), first the total heat transfer analysis is to be considered.

4.3 Total Heat Transfer Analysis.

Defining the whole test section as the control volume and applying the 1st law of thermodynamics,

$$\frac{dE_{st}}{dt} = \dot{E}_{in} + \dot{E}_{gen} - \dot{E}_{out} \tag{4.9}$$

Assumptions,

1. Steady state problem.
2. No energy generation.
3. Negligible ambient loss, i.e. perfect insulation.

$$\dot{E}_{in} = \dot{E}_{out} \tag{4.10}$$

The energies entering the test section are the inlet water enthalpy and the refrigerant saturated liquid enthalpy, and the energies leaving the test section are outlet water enthalpy and the refrigerant saturated vapor enthalpy.

Or,

$$\dot{m} \cdot i_{in} + \dot{m}_r \cdot i_f = \dot{m}_r \cdot i_g + \dot{m} \cdot i_{out} \tag{4.11}$$

$$Q = \dot{m}_r \cdot i_{fg} \tag{4.12}$$

$$Q = \dot{m}\left(i_{in} - i_{out}\right) \tag{4.13}$$

Assuming incompressible flow on the water side yields,

$$Q = \dot{m}\left(C_p\left(T_{in} - T_{out}\right) + v\underbrace{\left(P_{in} - P_{out}\right)}_{\Delta P} \right) \tag{4.14}$$

It should be point out that in most cases the contribution of pressure drop to the enthalpy change is ignored.

4.4 The Average Heat transfer Coefficient Analysis.

For calculating the average heat transfer coefficient (i.e. for the whole heat exchanger) according to Equation (4.8), the overall heat transfer coefficient U has to be evaluated between the inlet and the outlet conditions, or $U \rightarrow U_o$. The overall heat transfer coefficient U_o is to be calculated according to the enthalpy-based heat transfer analysis.

Substituting U_o for U in Equation (4.8) yields,

$$h_{r,a} = \left(\frac{1}{U_o} - R_{wall} - \frac{1}{h_w}\frac{D_o}{D_i} \right)^{-1} \tag{4.15}$$

4.4.1 The enthalpy-based heat transfer analysis (EBHT).

Classically, the overall heat transfer coefficient of the whole heat exchanger was determined from the following equation,

$$Q = U_o A_o \Delta T_{LMTD} \tag{4.16}$$

Where ΔT_{LMTD} in Equation (4.16) is $\left(\Delta T_1 - \Delta T_2\right) \Big/ \ln\left(\frac{\Delta T_1}{\Delta T_2}\right)$. Therefore, to determine the overall heat transfer coefficient, Equation (4.14) with the pressure term equals to zero and Equation (4.16) are to be solved simultaneously.

The derivation of the LMTD method starts by defining the change of the water enthalpy as the product of the temperature difference and the fluid's specific heat. Actually, this is a simplified definition of the enthalpy, where the effect of the change in pressure is neglected. This simplification is useful, since it leads in the end to solving the overall heat transfer coefficient with a simple algebraic equations. As a matter of fact, the vast majority of the shell and tube heat exchangers do not experience large change of the water enthalpy due to pressure drop. In other words, the temperature difference term is much bigger than the pressure drop term. For such applications, it is acceptable and easier to just set the pressure drop term equals to zero and to use the LMTD method to determine the overall heat transfer coefficient.

As was explained in the facility description chapter, the water flow inside the test tube experiences a large pressure drop. This makes a significant change in the water enthalpy. Therefore, it is necessary to consider the pressure drop in the calculation of the overall heat transfer coefficient as well as in the energy equation (Equation (4.14)).

For all intents and purposes, a new method, the enthalpy-based heat transfer analysis, was derived from the first principles for calculating the overall heat transfer coefficient in terms of the heat exchanger temperatures and pressures. The derivation of this method follows the derivation of the LMTD method.

The enthalpy-based heat transfer analysis works for parallel flow and counter flow heat exchangers, both with no phase change and with phase change. For solving the phase change problem, the specific heat of the cold side is set equal to infinity in the case of boiling and the specific heat of the hot side is set equal to infinity in the case of condensation.

4.4.1.1 The governing equations of the enthalpy-based heat transfer analysis.

Hot side energy balance assuming incompressible flow,

$$dQ = -\dot{m}_h \left(C_{p,h} \cdot dT_h + v_h \cdot dP_h \right) \tag{4.17}$$

Or,

$$dT_h = -\frac{1}{C_{p,h}} \left(\frac{dQ}{\dot{m}_h} + v_h \cdot dP_h \right) \tag{4.18}$$

Cold side energy balance assuming incompressible flow,

$$dQ = \dot{m}_c \left(C_{p,c} \cdot dT_c + v_c \cdot dP_c \right) \tag{4.19}$$

Or,

$$dT_c = \frac{1}{C_{p,c}} \left(\frac{dQ}{\dot{m}_c} - v_c \cdot dP_c \right) \tag{4.20}$$

An extended form of Newton's law of cooling is,

$$dQ = U \cdot dA \cdot \Delta T \tag{4.21}$$

Where,

$$\Delta T \equiv T_h - T_c \tag{4.22}$$

Combining these equations result in the following,

$$\frac{d\left(\Delta T\left(x\right)\right)}{dx}+\left(\frac{1}{\dot{m}_h\cdot C_{p,h}}+\frac{1}{\dot{m}_c\cdot C_{p,c}}\right)\cdot U\cdot\frac{d}{dx}A(x)\cdot\left(\Delta T\right)=\frac{v_c}{C_{p,c}}\cdot\frac{d}{dx}P_c(x)-\frac{v_h}{C_{p,h}}\cdot\frac{d}{dx}P_h(x) \tag{4.23}$$

Solving the above 1st order ODE gives,

$$\Delta T\left(x\right)=e^{-\left(\frac{1}{\dot{m}_h\cdot C_{p,h}}+\frac{1}{\dot{m}_c\cdot C_{p,c}}\right)\cdot U\cdot A(x)}\int_0^x\left(\frac{v_c}{C_{p,c}}\cdot\frac{d}{dx}P_c(x)-\frac{v_h}{C_{p,h}}\cdot\frac{d}{dx}P_h(x)\right)\cdot e^{\left(\frac{1}{\dot{m}_h\cdot C_{p,h}}+\frac{1}{\dot{m}_c\cdot C_{p,c}}\right)\cdot U\cdot A(x)}dx+$$

$$C\cdot e^{-\left(\frac{1}{\dot{m}_h\cdot C_{p,h}}+\frac{1}{\dot{m}_c\cdot C_{p,c}}\right)\cdot U\cdot A(x)} \tag{4.24}$$

Where C is to be determined by using the inlet boundary condition $\Delta T\left(x\right)=\Delta T_1\big|_{x=0}$. For the case of pool boiling, the specific heat of the cold side is set equal to infinity. The pressure drop of the water side is assumed linear along the test section and the area is defines as,

$$A(x)=\pi D_o x \tag{4.25}$$

Equation (4.24) reduces to the following equation which gives the difference between the water side and the refrigerant side at any distance x,

$$\Delta T\left(x\right)=\frac{-\left(\dot{m}_h\cdot v_h\cdot\Delta p_h\right)}{U\cdot A}+\left(\frac{\Delta T_1\cdot U\cdot A+\left(\dot{m}_h\cdot v_h\cdot\Delta p_h\right)}{U\cdot A}\right)\cdot e^{-\left(\frac{U\cdot\pi\cdot D_o}{\dot{m}_h\cdot C_{p,h}}\right)\cdot x} \tag{4.26}$$

Substituting the outlet boundary condition $\Delta T(x) = \Delta T_2\big|_{x=L}$ in Equation (4.26) and rearranging yields,

$$\ln\left(\frac{\Delta T_2 + \dfrac{\left(\dot{m}_h \cdot v_h \cdot \Delta p_h\right)}{U_o \cdot A}}{\Delta T_1 + \dfrac{\left(\dot{m}_h \cdot v_h \cdot \Delta p_h\right)}{U_o \cdot A}}\right) + \frac{U_o \cdot A}{\dot{m}_h \cdot C_{p,h}} = 0 \qquad (4.27)$$

Now, the only unknown in the above Equation is the overall heat transfer coefficient, which is to be determined by trial and error. Note that Equation (4.27) reduces to the LMTD as Δp_h goes to zero.

4.4.2 The water side heat transfer coefficient.

The water side heat transfer coefficient for no phase change can be found from the Nusselt number as follows,

$$h_i = \frac{Nu_D \cdot k_w}{D_h} \qquad (4.28)$$

It can be calculated using one of the Nusselt Number correlations for convective turbulent internal flow. The water properties are evaluated at the average of inlet and outlet temperatures.

The modified Petukhov's correlation (1970) or Gnielinski's correlation (1976) is the one widely used in this type of situations. The Gnielinski's correlation has the advantage of the validity over a wide range of both Reynolds number (3000 to 5E06) and Prandtle number (0.5 to 2000) with an accurate result.

$$Nu_D = \frac{(f/8)(\mathrm{Re}_D - 1000)\mathrm{Pr}}{1 + 12.7(f/8)^{1/2}(\mathrm{Pr}^{2/3} - 1)}, \tag{4.29}$$

$$f = \left(0.79\ln(\mathrm{Re}_D) - 1.64\right)^{-2} \tag{4.30}$$

The friction factor proposed by Gnielinski in the above equations is that of a smooth tube. Since the tubes used in this research are smooth and internally enhanced, the friction factor is calculated according to its basic definition (Equation (4.31) below) by measuring the pressure drop across the test tube. The friction factor is calculated according to,

$$f = \frac{\Delta P}{\rho} \cdot \frac{D_h}{L_c} \cdot \frac{2}{V^2} \tag{4.31}$$

In the case of the internally enhanced tubes, the micro-fins and swirls affect the accuracy of measuring both the characteristic length and the hydraulic diameter used in the above equation. The Gnielinski correlation needs a correction factor multiplier, this correction factor is determined using the modified Wilson plot technique. After determining the correction factor, the water-side heat transfer coefficient can then be calculated as,

$$h_w = C_i \cdot h_i \tag{4.32}$$

4.4.3 The modified Wilson plot technique.

The modified Wilson plot technique was introduced by Briggs and Young (1969) for shell and tube heat exchangers. This technique is used to obtain the heat transfer coefficients for both the shell and the tubes sides. Given the heat flux, the overall heat transfer coefficient and the Nusselt number correlations, the thermal resistances equation (Equation (4.33) below) can be transformed in to a straight line equation (Equation (4.35)).

$$\frac{1}{U_o} = \frac{1}{h_r} + R_{wall} + \frac{1}{h_w} \cdot \frac{A_o}{A_i} \tag{4.33}$$

Data points are then collected at different flow rates on either side. Using a linear regression for the data-points results in a straight line equation. The inverse of the intercept is the correction factor for the tube side heat transfer coefficient and inverse of the slope is the correction factor for the shell side heat transfer coefficient.

In the case of pool boiling, a simple model for the boiling heat transfer coefficient is chosen. Specially, the refrigerant heat transfer coefficient is assumed to be only a function of the heat flux and can be expressed as,

$$h_r = C_o \left(q''\right)^n \tag{4.34}$$

Substituting the expressions for the refrigerant side heat transfer coefficient (Equation (4.34)) and the water side heat transfer coefficient (Equation (4.32)), rearranging and multiplying both side by $\left(h_i \cdot A_i\right)$ in Equation (4.33) yields,

$$\underbrace{\left(\frac{h_i A_i}{U_o A_o} - R_{wall} h_i A_i\right)}_{Y} = \underbrace{\frac{1}{C_i} + \frac{1}{C_o}\underbrace{\left(\frac{h_i A_i}{(q'')^n A_o}\right)}_{X}}_{Y_{predicted}} \tag{4.35}$$

For each tube of this study, six data points were taken at different water flow rates which cover the full range of Reynolds number of the test facility. The number of points was selected to give the narrowest confident interval of the linear regression.

In order to perform the linear regression between Y and X in the above straight line equation (Equation (4.35)), the exponent n must be assumed at first. By trail and error, n was selected to give the minimum sum of the absolute percentage difference between Y and $Y_{predicted}$.

To lessen the effect of the chosen boiling model, the points were taken at one selected value of heat flux with a maximum change of 8% between the six taken points.

After selecting the optimum n, both C_i and C_o can be determined from linear regression. The correction factor for the water side heat transfer coefficient C_i is then ready to be used in Equation (4.32) for determining the final expression of the water side heat transfer coefficient. Thereafter, the average refrigerant side heat transfer coefficient can be backed out according to Equation (4.15) at all ranges of heat fluxes.

It is worth mentioning that Equation (4.34) is useful for the Wilson plot analysis only, or to be used over a narrow heat flux range, and is not to be applied on the full heat flux range of the pool boiling study. For a wide heat flux range, the refrigerant side heat transfer coefficient for some refrigerant-tube combination may experience increasing and decreasing trends with heat flux.

4.5 The Local Refrigerant Heat Transfer Coefficient Analysis.

The local analysis studies of the change of the refrigerant heat transfer coefficient along the heat exchanger. In the previous average analysis, the average heat transfer coefficient is calculated based on the overall heat transfer coefficient and the total heat transfer of the heat exchanger, which was calculated based on the inlet and outlet water conditions. Similarly, the local analysis is based on the local-overall heat transfer coefficient and local heat flux. The local-overall heat transfer coefficient can be evaluated from extending the Newton's law of cooling as,

$$q''_{local} = U_{local} \cdot \left(T_{hot} - T_{cold}\right) \tag{4.36}$$

Replacing T_{hot} with the local water temperature $\left(T_{local}\right)$ and replacing T_{cold} with the saturated refrigerant temperature $\left(T_{\infty}\right)$ gives,

$$q''_{local} = U_{local} \cdot \left(T_{local} - T_{\infty}\right) \tag{4.37}$$

Replacing $\frac{1}{U}$ with $\frac{1}{U_{local}}$ in Equation (4.8) gives,

$$h_{r,l} = \left(\frac{1}{U_{local}} - R_{wall} - \frac{1}{h_w} \frac{D_o}{D_i} \right)^{-1} \tag{4.38}$$

Substituting the expression of U_{local} from Equation (4.37) yields,

$$h_{r,l} = \left(\frac{\left(T_{local} - T_\infty\right)}{q''_{local}} - R_{wall} - \frac{1}{h_w} \frac{D_o}{D_i} \right)^{-1} \tag{4.39}$$

To apply this equations, three new items must be measured, local water temperature (T_{local}), local heat flux (q''_{local}), and the water heat transfer coefficient $\left(h_w\right)$.

4.5.1 Comments on the use of the water side heat transfer coefficient in the local analysis.

The water heat transfer coefficient is assumed to be constant along the test tube and it does not change locally when solving for the local refrigerant heat transfer coefficient. So, the water heat transfer coefficient which was determined from the modified Wilson plot technique is used in this local analysis.

As was mentioned above in Section 4.4.7, the water heat transfer coefficient is a function of the water flow rate and water properties evaluated at the average of inlet and outlet temperatures. What validates the assumption of the constant water heat transfer coefficient is that the water flow rate does not change along the tube and the water properties do not change by much within a reasonable temperature difference. To avoid any significant change of the water properties, the local analysis is best done at a maximum temperature difference of 3 °C between the inlet and the outlet.

4.5.2 The local heat flux.

As was mentioned in the facility description chapter, the water temperature distribution inside the test tube was measured using 7 RTD's. The seven RTD's are the inlet and the outlet plus five internal RTD's. The five internal RTD's are the five local water temperatures in the test tube.

Recalling Equation (4.17) of the hot side in Section (4.4.1.1),

$$dQ = -\dot{m}\left(C_p \cdot dT + v \cdot dP\right) \tag{4.40}$$

Dividing both sides by $\left(\pi \cdot D_o \cdot dx\right)$ gives,

$$\frac{dQ}{\pi \cdot D_o \cdot dx} = \frac{-\dot{m}}{\pi \cdot D_o}\left(C_p \cdot \frac{dT}{dx} + v \cdot \frac{dP}{dx}\right) \tag{4.41}$$

But,

$$\frac{dQ}{\pi \cdot D_o \cdot dx} = q''_{local} \tag{4.42}$$

Then,

$$q''_{local} = \frac{-\dot{m}}{\pi \cdot D_o}\left(C_p \cdot \frac{dT}{dx} + v \cdot \frac{dP}{dx}\right) \tag{4.43}$$

Equation 4.43 indicates that the local heat flux can be formed from the temperature gradient and pressure gradient through the test tube. As was assumed in calculating the overall heat transfer coefficient, the change of water pressure is linear.

Thus,

$$q''_{local} = \frac{\dot{m}}{\pi \cdot D_o}\left(-C_p \cdot \frac{dT}{dx} + v \cdot \frac{\Delta P}{L}\right) \tag{4.44}$$

4.5.4 The water temperature gradient.

The water temperature drops as it flows inside the test tube. This temperature drop can be expressed as a function of distance by curve fitting the seven RTD's temperature measurements with the corresponding RTD position. The most suitable curve fit was found to be a second order polynomial. Equation 4.45 can be easily differentiated and used in Equation 4.44 to determine the local heat flux.

$$T(x) = C_1 + C_2 \cdot x + C_3 \cdot x^2 \tag{4.45}$$

4.5.5 The Monte Carlo Simulation of the local temperature curve fit.

According to Equation (4.26), or the original LMTD, the temperature drop takes an exponential form. Therefore, the temperature drop between any two points over a distance x takes an exponential-shape function. Given the inlet temperature and the overall heat transfer coefficient and any distance x such that $0 < x < L$, the temperature at any x can be determined theoretically.

A Monte Calro simulation was conducted prior to starting the experimental phase of this project to determine the best functional form for the curve fit for the internal RTD's reading with distance. For different assumed heat fluxes, refrigerant and water heat transfer coefficients and inlet water temperatures, this simulation was performed by adding a random error representing the uncertainty of the RTD's, to the values of theoretical T_{local}'s .

Different curve fits were tried. The best curve fit is the one which returns the minimum percentage error between the average of the five local heat transfer coefficients and the assumed heat transfer coefficients.

4.6 Uncertainty Analysis.

The uncertainty analysis is performed on both the average and the local refrigerant heat transfer coefficients using the Kline-McClintock (1953) second order law. The analysis is applied on the following input variables.

4.6.1 Inputs.

The measured variables are the water flow rate, the temperature reading of the seven water film RTD's, the refrigerant saturation pressure (which is converted into saturation temperature), and the water inlet and outlet pressure. The flow meter uncertainty used is the uncertainty listed by the manufacturer, which is ±0.05% of reading. In the following subsections, the uncertainty of the measured variables and calculated inputs is discussed in details.

4.6.1.1 Temperature uncertainty.

Sources of uncertainty in the 1000 Ω RTD's temperature reading are, the constant temperature bath used for the RTD's calibration, the data acquisition system, and the calibration curve fit $T = f(R)$. The accuracy of the constant temperature bath (u_{CTB}) is 0.01 °C. The RTD resistance changes with the temperature with a slope of $\left(\frac{dT}{dR} \approx 0.257 \frac{^oC}{\Omega}\right)$. The accuracy of the data acquisition system, including measurement error, switching error and transducer conversion error (u_{RM}) is calculated according to, $(0.008\ \%\ \text{of reading} + 0.001\ \%\ \text{of range})$. Both the reading and the range are 1 kΩ. The accuracy of the curve fit is calculated as, (t-stat × the standard error). For all the seven RTD's, the highest uncertainty of the curve fit (u_{TCF}) is 0.016 °C. The total uncertainty of the RTD's can be calculated by propagation of error as,

$$u_T = \sqrt{\left(\left(u_{CTB}\right)^2 + \left(\frac{dT}{dR} \cdot u_{RM}\right)^2 + \left(u_{TCF}\right)^2 \right)} \tag{4.46}$$

$$\therefore u_T = \pm 0.03\ ^oC$$

4.6.1.2 Saturation temperature uncertainty for R-134a.

First, the uncertainty in the pressure transducer reading is determined by the propagation of error of the uncertainty in the data acquisition system and the calibration curve fit equation $P = f\left(V\right)$. The accuracy of the data acquisition system, including measurement error, switching error and transducer conversion error $\left(u_{VM}\right)$ is calculated according to, 0.002% reading + 0.0005% of range. The reading is 5 VDC and the range is 10 VDC. The slope of the calibration curve fit is $\left(\frac{dP}{dV} \square 103.455 \frac{VDC}{kPa}\right)$. The uncertainty of the curve fit $\left(u_{PVCF}\right)$ is 0.0806 kPa (t-stat × the standard error). Applying the propagation of error yields,

$$u_P = \sqrt{\left(\frac{dP}{dV} \cdot u_{VM}\right)^2 + \left(u_{PVCF}\right)^2} \tag{4.47}$$

$$\therefore u_P = \pm 0.08 \text{ kPa}$$

The uncertainty given by the manufacturer $\left(u_{PM134a}\right)$ is 0.05% of the range 0-75 PSIA or ±0.25 kPa. This uncertainty is much higher than the uncertainty calculated above. So, for more conservative calculations, the manufacturer's uncertainty shall be used for determining the uncertainty in the saturation temperature.

The saturation temperature used in the data reduction is calculated by converting the pressure transducer reading into temperature using the saturated refrigerant properties with the

curve fit equation $T_{sat} = f\left(P_{sat}\right)$. The slope of the curve fit is $\left(\frac{dT}{dP} \approx 0.0835 \frac{^oC}{kPa}\right)$. The sources of the uncertainty in the saturation temperature are the pressure transducer uncertainty $\left(u_{PM134a}\right)$ and the curve fit uncertainty. The uncertainty of the curve fit $\left(u_{PTCF}\right)$ is 0.000386 °C (t-stat × the standard error). The uncertainty of the saturation temperature is,

$$u_{T_{sat}} = \sqrt{\left(\frac{dT}{dP} \cdot u_{PM134a}\right)^2 + \left(u_{PTCF}\right)^2} \tag{4.48}$$

$$\therefore u_{T_{sat,134a}} = \pm 0.02\ ^oC$$

4.6.1.3 Saturation temperature uncertainty for R-123.

Like the case of R-134a, the uncertainty listed by the manufacturer will be used. The manufacturer's uncertainty $\left(u_{PM123}\right)$ is 0.05% of the range 0-15 PSIA or ±0.05 kPa. The saturation temperature used in the data reduction is calculated by converting the pressure transducer reading into temperature using the saturated refrigerant properties with the curve fit equation $T_{sat} = f\left(P_{sat}\right)$. The resulting slope is $\left(\frac{dT}{dP} \approx 0.557578 \frac{^oC}{kPa}\right)$. The sources of the uncertainty in the saturation temperature are the pressure transducer uncertainty $\left(u_{PM123}\right)$ and the curve fit uncertainty. The uncertainty of the curve fit $\left(u_{PTCF}\right)$ is 0.00333 °C (t-stat × the standard error). The uncertainty of the saturation temperature is,

$$u_{T_{sat}} = \sqrt{\left(\frac{dT}{dP} \cdot u_{PM123}\right)^2 + \left(u_{PTCF}\right)^2} \tag{4.49}$$

$$\therefore u_{T_{sat,123}} = \pm 0.028\ ^oC$$

4.6.1.4 Water pressure uncertainty.

The water pressure uncertainty used in the analysis is the uncertainty listed by the manufacturer.

$$u_{PW} = \pm 0.758 \text{ kPa}$$

4.6.1.5 Water specific heat uncertainty.

The specific heat is calculated at the average inlet and outlet water temperatures. The average temperature uncertainty $\left(u_{AT}\right)$ is $\pm \frac{0.03}{\sqrt{2}}\,{}^{o}C$. The sources of the uncertainty in the specific heat of the water are the average temperature uncertainty in the curve fit $C_p = f\left(T_{av}\right)$ and the uncertainty in the curve fit. The slope of the curve fit is $\left(\frac{dC_p}{dT} \approx -0.00118 \frac{kJ/kg \cdot {}^{o}C}{{}^{o}C}\right)$. The uncertainty of the curve fit $\left(u_{CPCF}\right)$ is $0.0006\, kJ/kg \cdot {}^{o}C$ (t-stat × the standard error). The uncertainty of the specific heat is,

$$u_{C_p} = \sqrt{\left(\left(\frac{dC_p}{dT} \cdot u_{AT}\right)^2 + \left(u_{CPCF}\right)^2\right)} \tag{4.50}$$

$$\therefore u_{C_p} = \pm 6 \cdot 10^{-04} \;\; kJ/kg \cdot {}^{o}C$$

4.6.1.6 Water density Uncertainty.

The water density is calculated at the average inlet and outlet water temperatures. The average temperature uncertainty $\left(u_{AT}\right)$ is $\pm \frac{0.03}{\sqrt{2}}\,{}^{o}C$. The sources of the uncertainty in the water density are the average temperature uncertainty in the curve fit $\rho = f\left(T_{av}\right)$ and the uncertainty

in the curve fit. The slope of the curve fit $\left(\frac{d\rho}{dT} \approx -0.1413 \frac{kg/m^3}{^oC}\right)$. The uncertainty of the curve fit $\left(u_{\rho CF}\right)$ is 0.006 kg/m³ (t-stat × the standard error). The uncertainty of the density is,

$$u_\rho = \sqrt{\left(\left(\frac{d\rho}{dT} \cdot u_{AT}\right)^2 + \left(u_{\rho CF}\right)^2\right)} \tag{4.51}$$

$$\therefore u_\rho = \pm 7 \cdot 10^{-03} \ kg/m^3$$

4.6.1.7 Water heat transfer coefficient uncertainty.

The water heat transfer coefficient is a function of the water flow rate, water properties and the correction factor obtained from the Wilson plot technique. The correction factor is the dominant uncertainty of the water heat transfer coefficient. The correction factor uncertainty was assumed to be the 95% confidence interval of the slope of the linear curve fit of the Wilson plot data. The 95 % correction factor confidence interval for R-134a on Turbo BII HP tube is 4 %, for R-134a on smooth tube is 2 %, for R-123 on Turbo BII LP is 4 %, and for R-123 on smooth tube is 17 %.

$$u_{h_{w,134aS}} = 0.02 \cdot h_{w,134aS} \tag{4.52}$$

$$u_{h_{w,134aT}} = 0.04 \cdot h_{w,134aT} \tag{4.53}$$

$$u_{h_{w,123S}} = 0.17 \cdot h_{w,123S} \tag{4.54}$$

$$u_{h_{w,123T}} = 0.04 \cdot h_{w,123T} \tag{4.55}$$

4.6.1.8 Length uncertainty.

The length or distance measurements uncertainty is 1.6 mm based on the uncertainty of the measuring tape.

$$u_d = \pm 1.6 \text{ mm}$$

4.6.2 Average refrigerant heat transfer coefficient uncertainty.

For the average heat transfer coefficient, the input variables are discussed above. The final uncertainty can be determined by applying the propagation of uncertainties on the equation,

$$h_{r,a} = \left(\frac{\dfrac{\left(\Delta T_1 - \Delta T_2\right)}{\ln\left(\dfrac{\Delta T_1}{\Delta T_2}\right)} \cdot A_o}{\dot{m}\left(C_P\left(T_{in} - T_{out}\right) + v\left(P_{in} - P_{out}\right)\right)} - R_w - \frac{1}{h_w} \cdot \frac{D_o}{D_i} \right)^{-1} \tag{4.56}$$

Due to the difficulty of solving for the overall heat transfer coefficient using the EBHT (solution by trail and error), the overall heat transfer coefficient term in the above equation is replaced with the total heat transfer (Equation (4.14)) divided by the LMTD. This does not significantly change the estimated uncertainty in the average heat transfer coefficient.

$$u_{h_{r.a}} = \sqrt{\left(\left(\left(\frac{\partial h_{r.a}}{\partial \Delta T_1}\right) \cdot u_{\Delta T_1}\right)^2 + \left(\left(\frac{\partial h_{r.a}}{\partial \Delta T_2}\right) \cdot u_{\Delta T_2}\right)^2 + \left(\left(\frac{\partial h_{r.a}}{\partial A_o}\right) \cdot u_{A_o}\right)^2 + \left(\left(\frac{\partial h_{r.a}}{\partial \dot{m}}\right) \cdot u_{\dot{m}}\right)^2 + \ldots\ldots \right)} \tag{4.57}$$

Uncertainties were calculated for each data point taken and can be seen as error bars on the results graph given in next chapter.

4.6.3 Local Refrigerant Heat Transfer Coefficient Uncertainty.

According to the Equation 4.58 below, two more input uncertainties are needed for determining the final uncertainty of the local refrigerant heat transfer coefficient using the propagation of uncertainty technique. These two inputs are the uncertainty in T_{local} and the uncertainty in $\frac{dT}{dx}$. The propagation of error can be applied to Equation 4.58 resulting in an equation similar to Equation 4.57. Uncertainties were calculated for each data point taken and can be seen as error bars on the results graph given in next chapter.

$$h_{r,l} = \left(\frac{\left(T_{local} - T_{sat}\right)}{\frac{\dot{m}}{\pi \cdot D_o}\left(-C_P \frac{dT}{dx} + v\frac{\Delta P}{L}\right)} - R_w - \frac{1}{h_w} \cdot \frac{D_o}{D_i} \right)^{-1} \tag{4.58}$$

4.6.3.1 Uncertainty of the local temperature slope.

The uncertainty in the temperature derivative (temperature slope) can not be determined using the propagation of error method as the other inputs. A Monte Carlo simulation was conducted to determine the temperature slope uncertainty. First, the inlet temperature and the overall heat transfer coefficient are assumed as certain values, then they were used in Equation 4.59 below to determine the theoretical values of 5 internal local temperatures. The theoretical temperatures are determined from,

$$T_{theor}(x) = \frac{-\dot{m}_h \cdot v_h \cdot \Delta p_h}{U \cdot A} + \left(\frac{\Delta T_1 \cdot U \cdot A + \left(\dot{m}_h \cdot v_h \cdot \Delta p_h\right)}{U \cdot A} \right) \cdot e^{-\left(\frac{U \cdot \pi \cdot D}{\dot{m}_h \cdot C_{p,h}}\right) \cdot x} + T_\infty \tag{4.59}$$

A normal distribution of 12,000 random number sets (each set is a 1 column and seven rows matrix) between -0.03 °C and +0.03 °C (representing the uncertainty in the temperature) on the theoretical values was added, each set at a time. Also, a normal distribution of 12,000 random

number sets (each set is a 1 column and seven rows matrix) between -1.6 mm and 1.6 mm on each RTD's position was assumed. A 2nd order polynomial curve fit was used to fit all the 12,000 sets of temperatures and distances to produce a 12,000 curve fits as,

$$T_{actual} = C_1 + C_2 \cdot x + C_3 \cdot x^2 \tag{4.60}$$

The slope of the 2nd order function was compared to the theoretical slope,

$$\left.\frac{dT}{dx}\right|_{theor.} = -\left(\frac{U \cdot \pi \cdot D_o}{\dot{m} \cdot C_p}\right)\left(\left(T(x) - T_\infty\right) + \frac{\left(\dot{m} \cdot v \cdot \Delta P\right)}{U \cdot A}\right) \tag{4.61}$$

$$\left.\frac{dT}{dx}\right|_{actual} = C_2 + 2 \cdot C_3 \cdot x \tag{4.62}$$

$$u_{dTdx} = \frac{\left.\frac{dT}{dx}\right|_{actual} - \left.\frac{dT}{dx}\right|_{theor.}}{\left.\frac{dT}{dx}\right|_{theor.}} \tag{4.63}$$

The 12,000 points of the 5 slopes (corresponding to the 5 local temperature) were sorted from min. to max.; the 11400th point (95% confidence interval of the 12,000 points) was taken as the uncertainty in the temperature slope.

4.6.3.2 Uncertainty of the local temperature.

In addition to the temperature uncertainty (section 4.6.1.1), an uncertainty $\left(u_d\right)$ of 1.6 mm was assumed in the positioning of the RTD's on the instrumented tube. It was found the distance uncertainty does not have a significant effect on the temperature uncertainty. The final uncertainty of the local temperature is determined as,

$$u_{T_{local}} = \sqrt{\left(\left(u_T\right)^2 + \left(\left.\frac{dT}{dx}\right|_{local} \cdot u_d\right)^2\right)} \tag{4.64}$$

4.7 Conclusion.

This chapter introduced two related methods for determining the refrigerant heat transfer coefficient, the average and local methods. This study is the first study to present the engagement of the water pressure in the calculation of the refrigerant heat transfer coefficient, or the enthalpy-based heat transfer analysis, which is useful for solving many heat exchanger problems that experience large pressure drop. Also of significance is that, a Monte Carlo simulation was used twice in this study. The first time is for determining the best polynomial degree for curve fitting the local temperatures with distance. The second time is for determining the uncertainty in the temperature slope $\frac{dT}{dx}$ of the local heat transfer coefficient. Uncertainty analysis is applied to each average heat transfer coefficient and for each of the of five local heat transfer coefficients.

CHAPTER 5 - Results

This chapter incorporates the results of the four tubes tested with R-134a and R-123. The results are that of, the average refrigerant heat transfer coefficients, the local refrigerant heat transfer coefficients, and the comparison between the average and local results. The results of the modified Wilson plot analysis are given in the average heat transfer coefficient section. All tests were conducted at a saturation temperature of 4.44 °C. Testing ranges of heat flux and Reynolds number for each tube is defined.

5.1 Average Heat Transfer Coefficient Results.

5.1.1 Modified Wilson Plot Results.

Four modified Wilson plots were conducted, one for each tube-fluid combination. The best linear regression was selected for each case. As was explained in the data reduction chapter, the correction factor for the water side heat transfer coefficient is determined from the linear regression. Also, the 95% confidence interval of the correction factor is used as the uncertainty in the water side heat transfer coefficient.

Both the insert tube with the wire wrap and the internal enhancement of the enhanced tubes cause a significant increase in the water side heat transfer coefficient. This makes the refrigerant side thermal resistance the dominant thermal resistance. This also increases the resolution on determining the refrigerant heat transfer coefficient. When performing Wilson plot analysis for R-134a on smooth tube, the refrigerant thermal resistance is as high as 4.8 times greater that the water thermal resistance and as low as 1.3 times the water thermal resistance. For R-123 on smooth tube, the ratio is between 19 and 5. For R-134a on Turbo BII HP, the ratio is between 4.2 and 1.6. For R-123 on Turbo BII LP, the ratio is between 3 and 1.4. Six points were taken for performing the modified Wilson plot. Data were taken over a narrow heat flux range

with a maximum change of 8% between points. Wilson plots for the four cases are shown in Figures 5-1 through 5-4 and the results summary is presented in Table 5-1.

Looking at the water side correction factors and the corresponding relative uncertainty (95% confidence interval) provided in Table 5-1, gives an important conclusion. The correction factors for smooth tube under both R-134a and R-123 are close to one, within the 95 % confidence interval, which indicates that the choice of the hydraulic diameter and the characteristic length was good and satisfactory to be applied in the definition of the friction factor equation (Equation 4.31). This also indicates that the effect of the pressure drop has been factored out correctly (through the EBHT) in performing the modified Wilson plot analysis. The two enhanced tubes correction factors are close to 2 because of the presence of the internal micro fins.

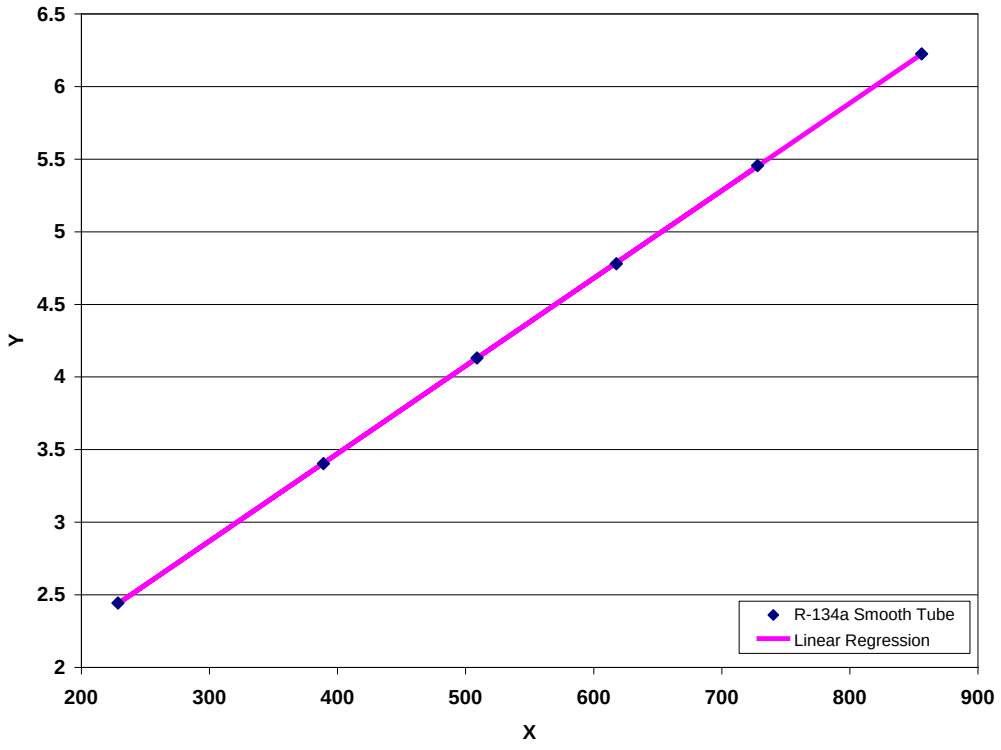

Figure 5-1 R-134a on smooth tube modified Wilson plot.

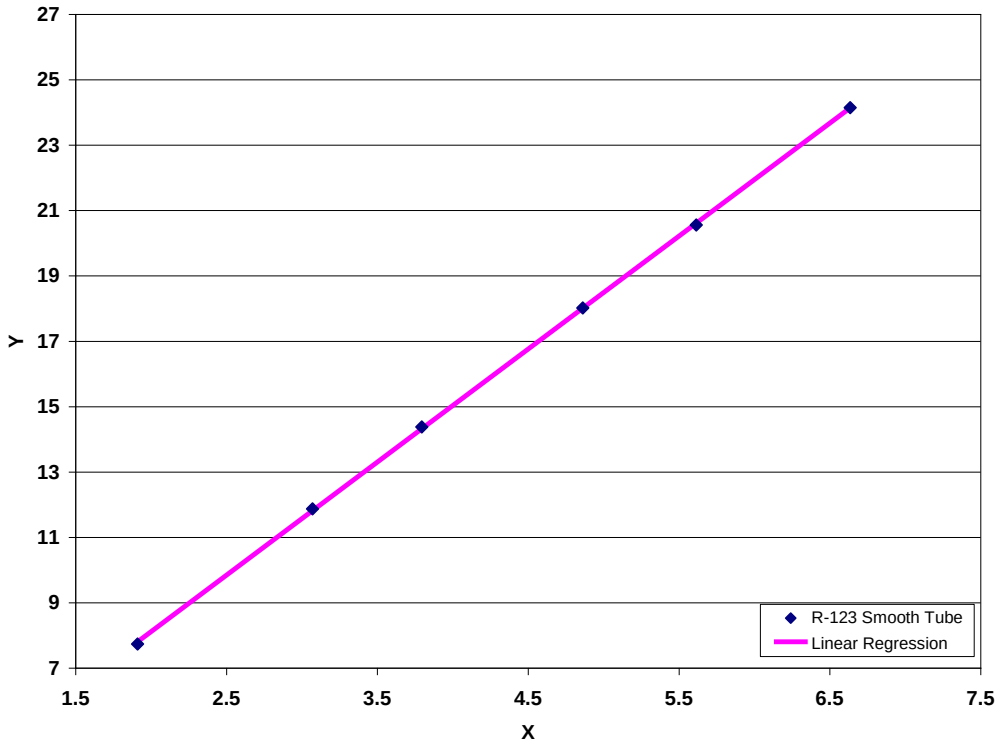

Figure 5-2 R-123 on smooth tube modified Wilson plot.

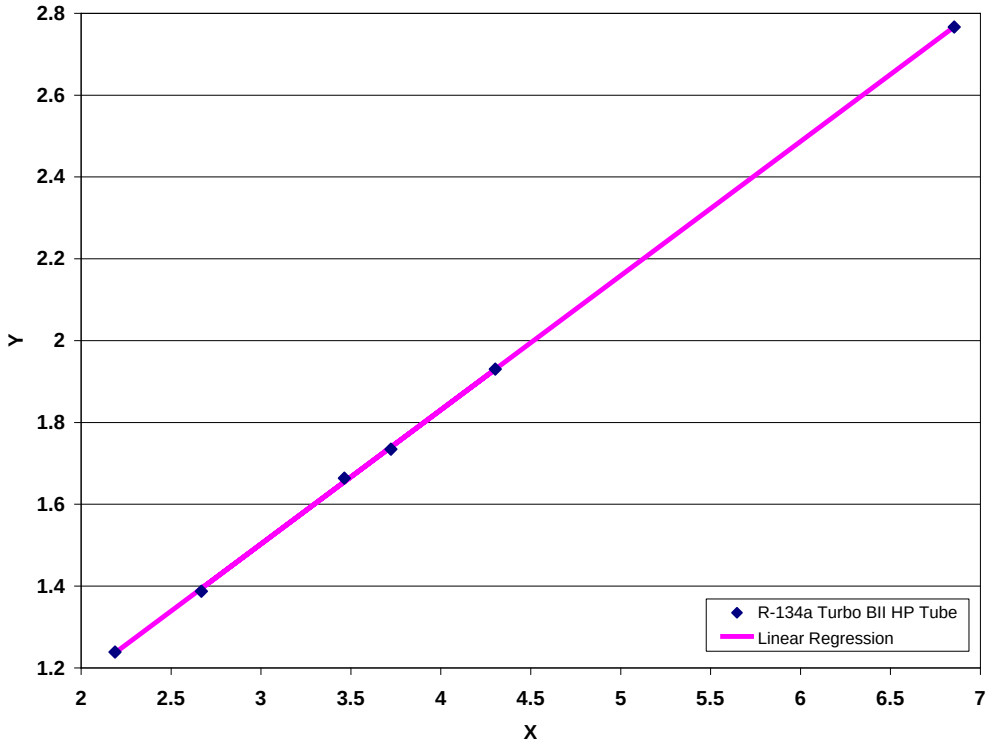

Figure 5-3 R-134a on Turbo BII HP tube modified Wilson plot.

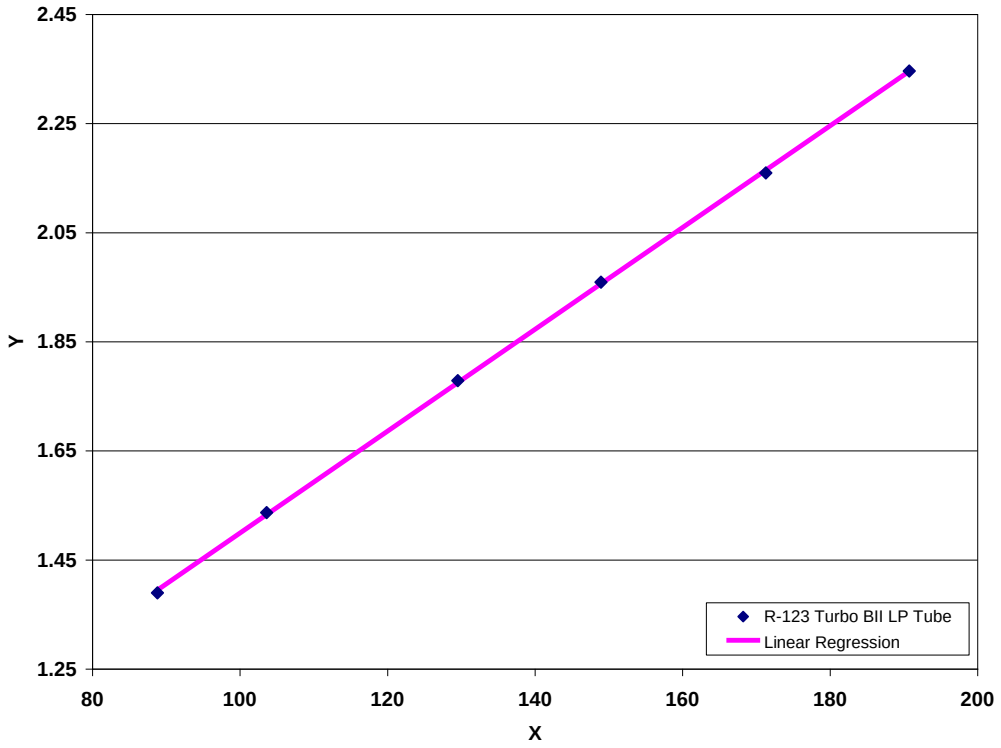

Figure 5-4 R-123 on Turbo BII LP tube modified Wilson plot.

Table 5-1 Modified Wilson plot summary table.

	R-134a Smooth Tube	**R-123 Smooth Tube**	**R-134a Turbo BII HP Tube**	**R-123 Turbo BII LP Tube**
Heat Flux Range (kW/m^2)	24.1-24.3	11.8-12.6	80-82	14-15
Reynolds Number Range (× 1000)	8-37	9-38	12-35	7-17
Resulting correction Factor (C_i)	0.9424	0.8356	1.928	1.765
Relative Uncertainty in (C_i)	2%	17%	4%	4%

5.1.2 R-134a and R-123 smooth tube results.

Figures 5-5 and 5-6 below show the results of the average smooth tube refrigerant heat transfer coefficient for R-134a and R-123 and some literature data for comparison. Literature data points were collected by scanning the graphs available in published papers of interest, and then picking the data points using a program called DigXY. So, the literature data points in the plots presented here are expected to have some uncertainty.

The heat flux range for testing with R-134a on smooth tube, to the nearest decimal number, is 9.2-126.6 kW/m² and the range of Reynolds number is 7,964.7-61,897.8. The heat flux range for testing with R-123 on smooth tube is 9.2-58 kW/m² and the range of Reynolds number is 9,344.7-51,644.4. The heat flux range for the R-123 is limited than that of the R-134a because R-134a's vapor density is more than 6 times the vapor density of R-123, and this requires a larger shell size to accommodate the vapor generation of R-123 at high heat fluxes.

The data of R-123 shows a better agreement with the literature than that of R-134a, but both agreements are considered good. Both curves show an increasing trend with heat flux. The heat transfer coefficients of R-134a show that they are about 2.5 times the corresponding values of the heat transfer coefficient of R-123 at the same heat flux.

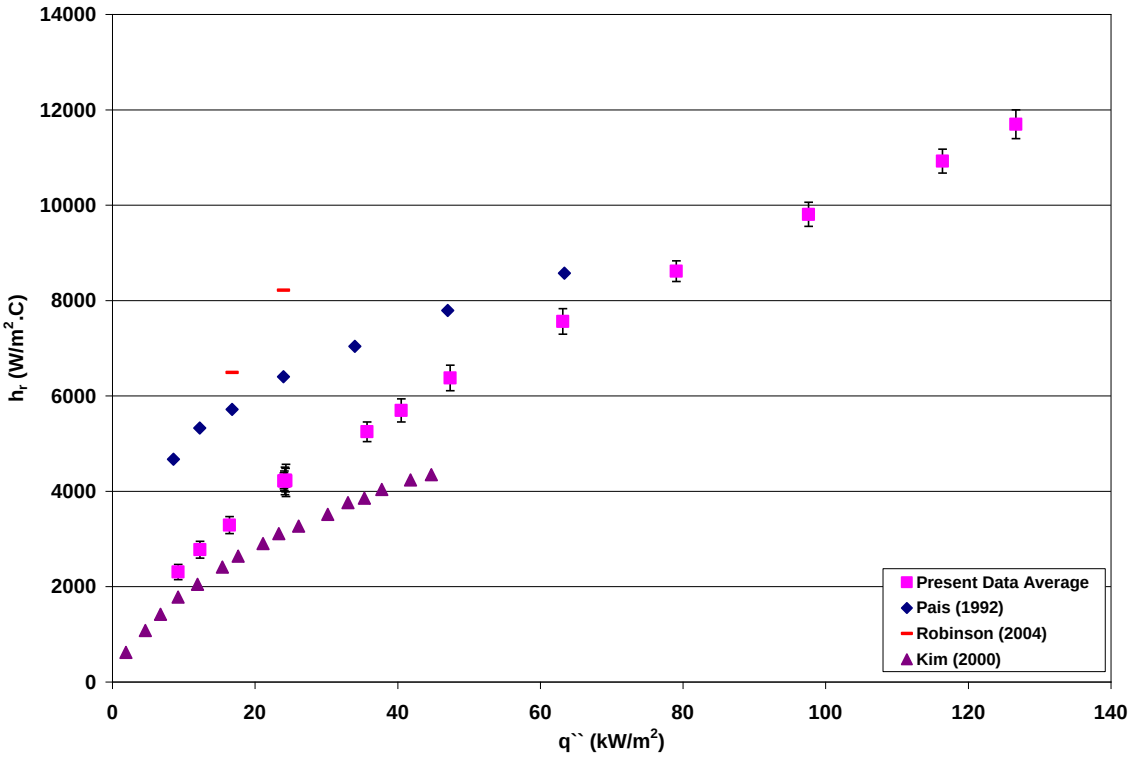

Figure 5-5 R-134a on smooth tube average heat transfer coefficient plot.

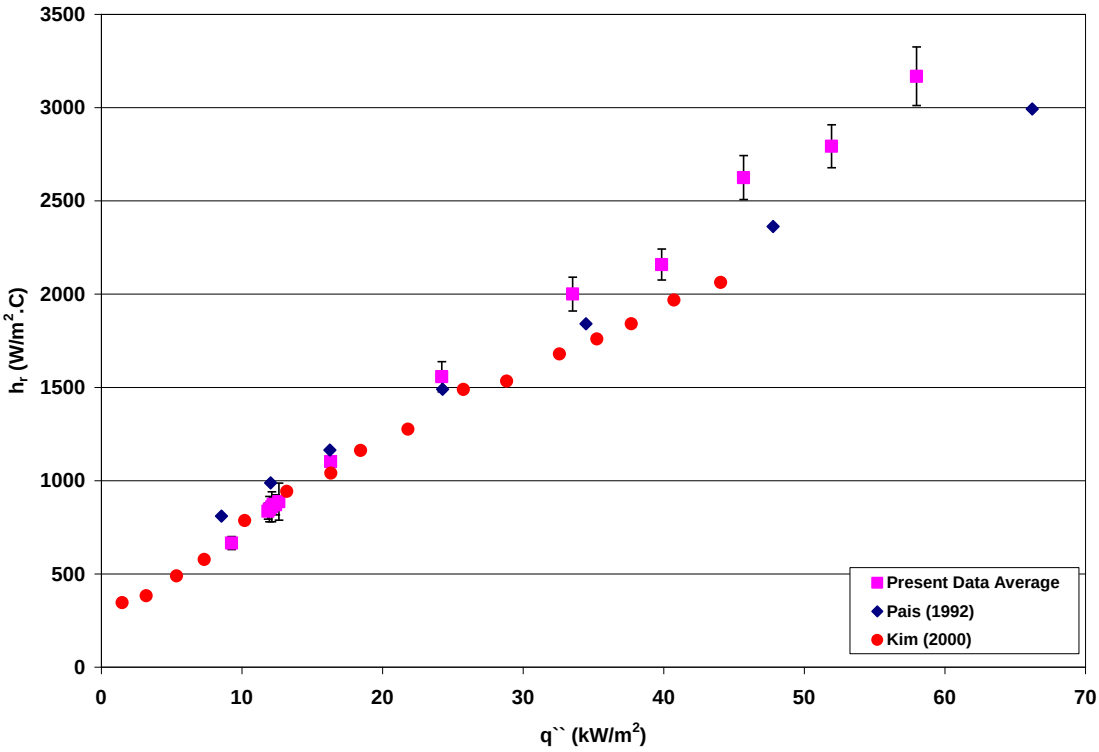

Figure 5-6 R-123 on smooth tube average heat transfer coefficient plot.

5.1.3 R-134a and R-123 enhanced tubes results.

For R-134a and R-123 on enhanced tubes, Figures 5-7 and 5-8 show the results of the refrigerant heat transfer coefficient and the available literature data for comparison. All available literature data for Turbo BII HP were used for comparison with the present data. No published literature data is available for Turbo BII LP tube, except for the data by Mark A. Kedzierski (1995). This data though would not give a fair comparison because it is a surface of Turbo BII LP boiling and not tube boiling.

The heat flux range for testing with R-134a on Turbo BII HP, to the nearest decimal number, is 4.1-135.1 kW/m² and the range of Reynolds number is 7,018.8-38,527.3. The heat flux range for testing with R-123 on Turbo BII LP is 4.7-59.8 kW/m² and the range of Reynolds number is 5,282.4-31,089.1.

The heat flux range of Turbo BII HP is the widest range ever among the available literature. Only Robinson and Thome (2004) and Ribatski and Thome (2006) had their testing with water heated tubes, Chen and Tuzla (1996) and Tatara and Payvar (2000) had electric heated tubes. This wide range of data gives a clear picture of the heat transfer coefficient trend change with heat flux. The heat transfer coefficient trend show a steep increase with heat flux then the curve changes to a decreasing trend, and then it recovers to an increasing trend again. This trend is also seen in Chen and Tuzla's data (1996) and Robinson and Thome's data (2004), and is discussed in the literature. Chien and Webb (1996) parts I and II explain the effect of tunnel dimensions and pore diameter and pore pitch on enhanced tubes performance. They concluded, from their study of the effect of pore diameter and pore pitch, that at a certain reduced heat flux, part of the tunnel will become flooded and this results in decreasing the performance.

For the tested heat flux range, Turbo BII LP shows a continuous increasing trend of the heat transfer coefficient with heat flux. Just as the case of the smooth tube, the heat flux range for the R-123 is limited than that of the R-134a because R-134a's vapor density is more than 6 times the vapor density of R-123, and this requires a larger shell size to accommodate the vapor generation of R-123 at high heat fluxes.

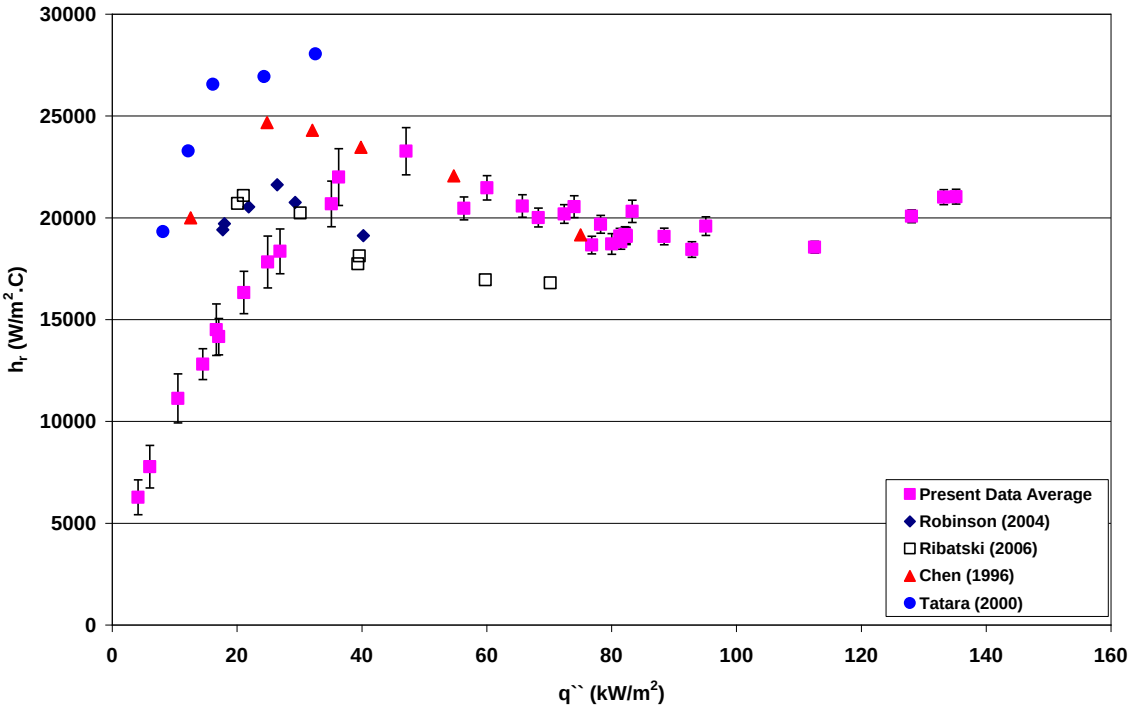

Figure 5-7 R-134a on Turbo BII HP tube average heat transfer coefficient plot.

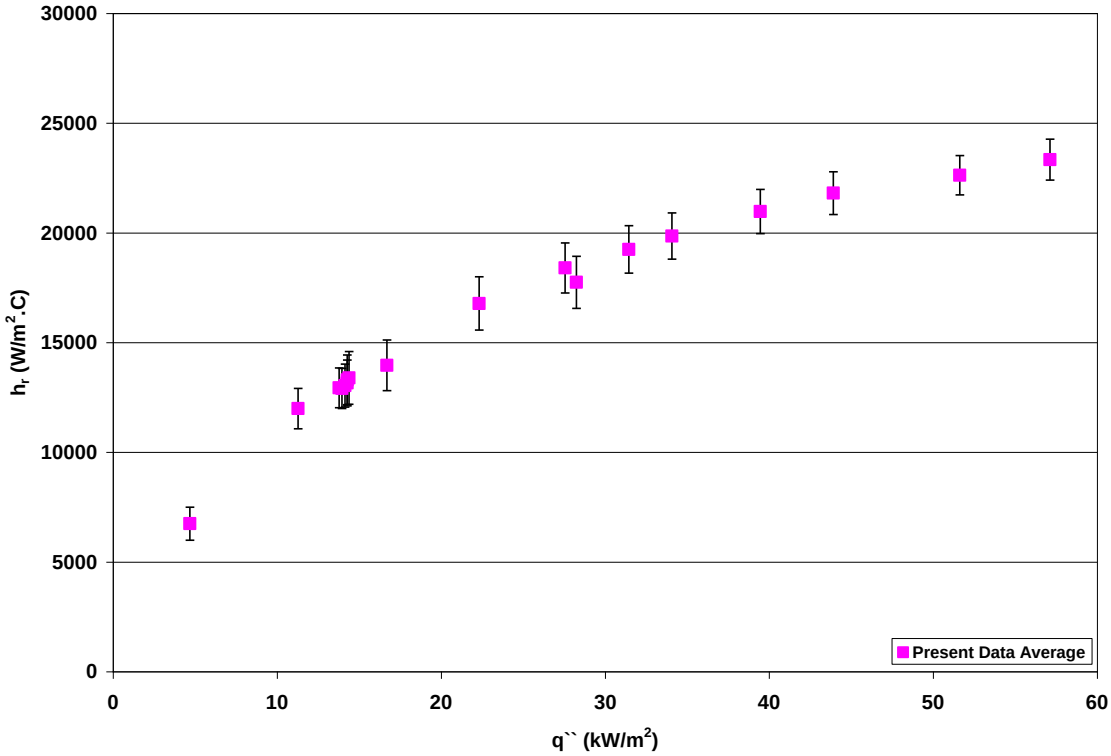

Figure 5-8 R-123 on Turbo BII LP tube average heat transfer coefficient plot.

5.1.4 Smooth to enhanced comparison plots.

Figures 5-9 and 5-10 show two comparison plots (one for each refrigerant), for comparing the performance of the smooth tube to the enhanced tube. Just for the comparison purpose, the data points were curve fitted and the heat transfer coefficients were compared at the same heat flux. R-123 Turbo BII LP tube to smooth tube heat transfer coefficient ratio changes from 24 at low heat flux to 7 at high heat flux. R-134a Turbo BII HP tube to smooth tube heat transfer coefficient ratio changes from 4 at low heat flux to 1.7 at high heat flux.

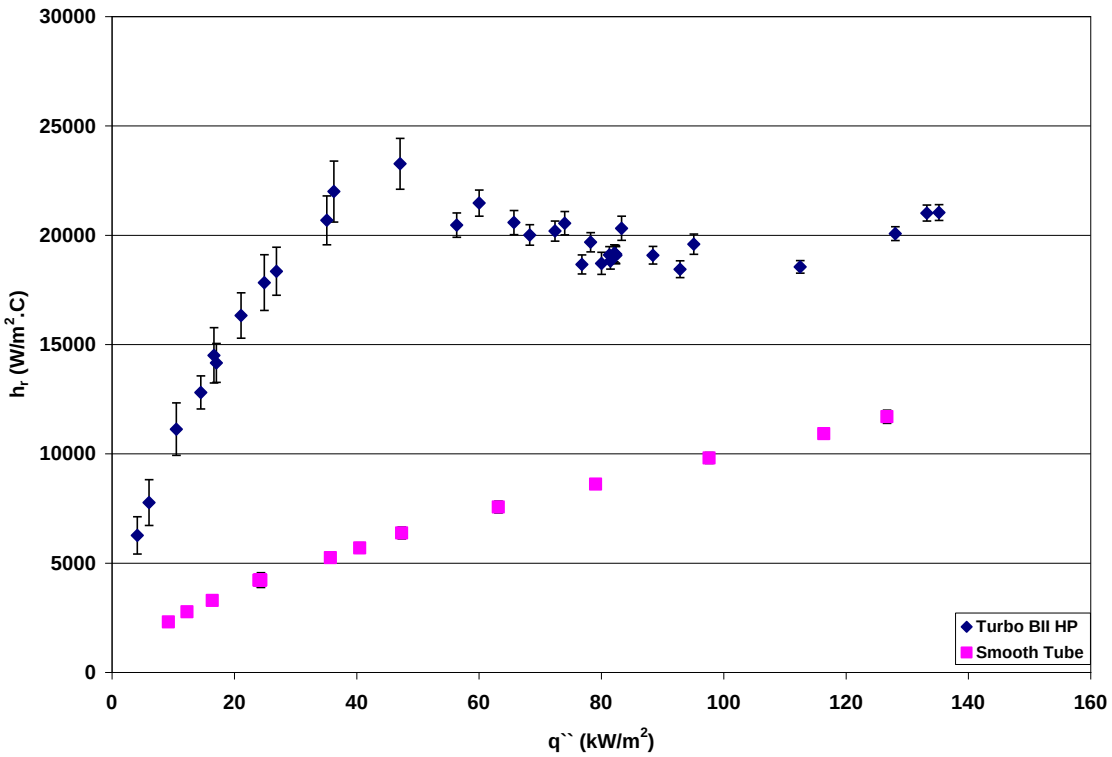

Figure 5-9 R-134a Turbo BII HP tube and smooth tube comparison.

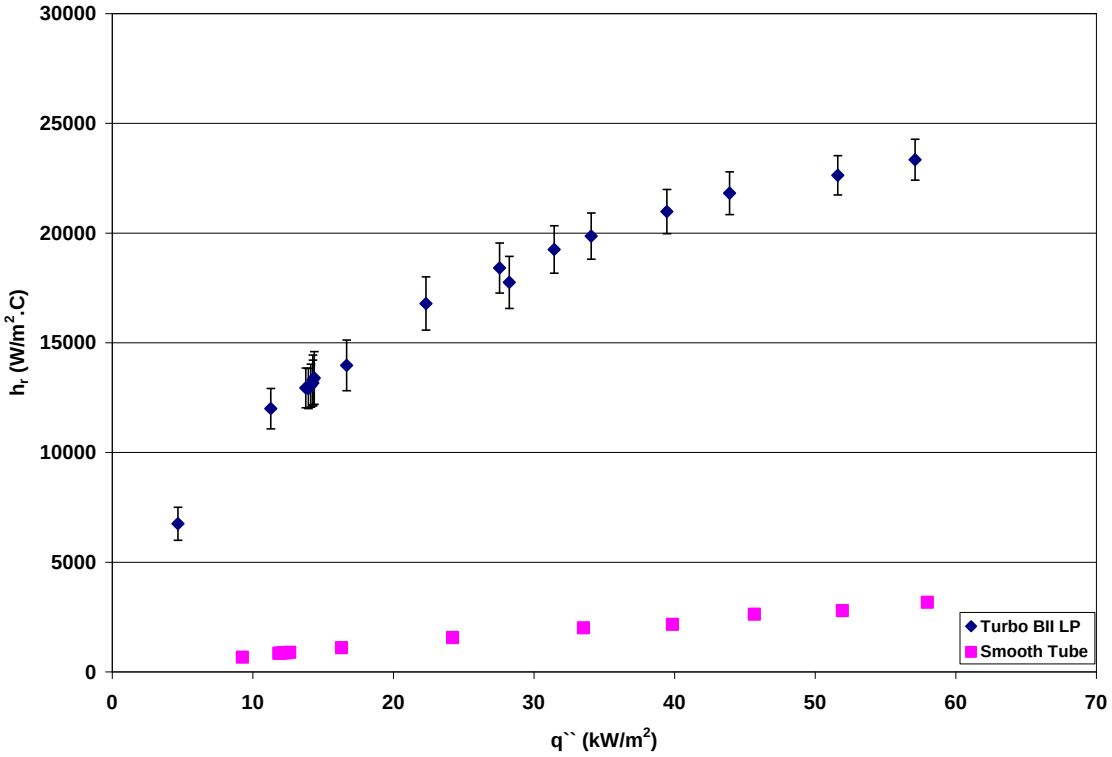

Figure 5-10 R-123 Turbo BII LP tube and smooth tube comparison plot.

5.1.5 Turbo BII HP and Turbo BII LP comparison.

Figure 5-11 below show the comparison between the performance of R-134a on Turbo BII HP tube and R-123 on Turbo BII LP tube. Although the performance of the smooth tube in a pool of R-123 is much lower than the performance of the smooth tube in a pool of R-134a (Section 5.1.2), the Turbo BII LP tube in R-123 shows a performance that is almost the same as Turbo BII HP in R-134a over the tested heat flux of the Turbo BII LP. Within the uncertainty limits, both tubes have the same performance.

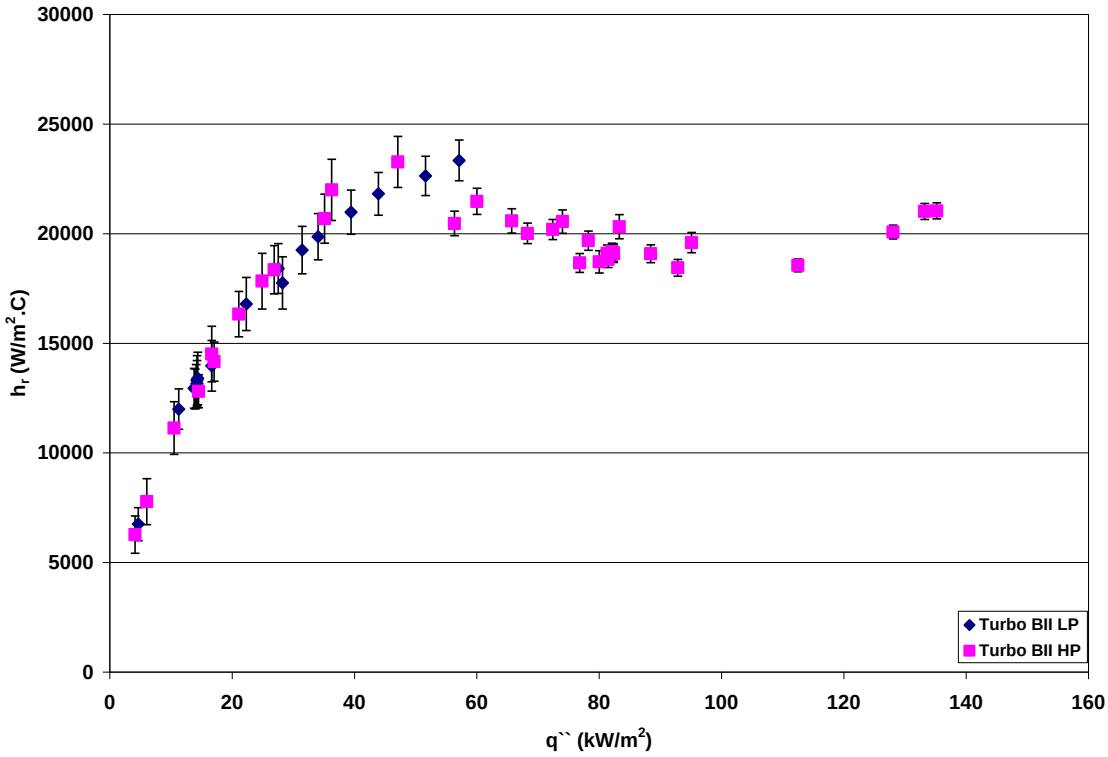

Figure 5-11 Turbo BII HP and Turbo BII LP comparison plot.

5.2 Local Heat Transfer Coefficient Results.

The local heat transfer coefficient results below are the product of the analysis made on the same data taken for the average heat transfer coefficient. The same literature data used for the comparison of the average data is applied in the local data as well. A comparison between the average data and local data is presented in a later section.

5.2.1 Test tube water temperature profile.

Figures 5-12 through Figure 5-15 are four selected data points' temperature profiles, one for each of the four test cases. Each plot shows the water temperature profile at a certain heat flux and Reynolds number (or water flow rate). Each plot contains the reading of the seven RTD's (the inlet, the outlet and the five internal RTD's) and the predicted theoretical profile according the EBHT.

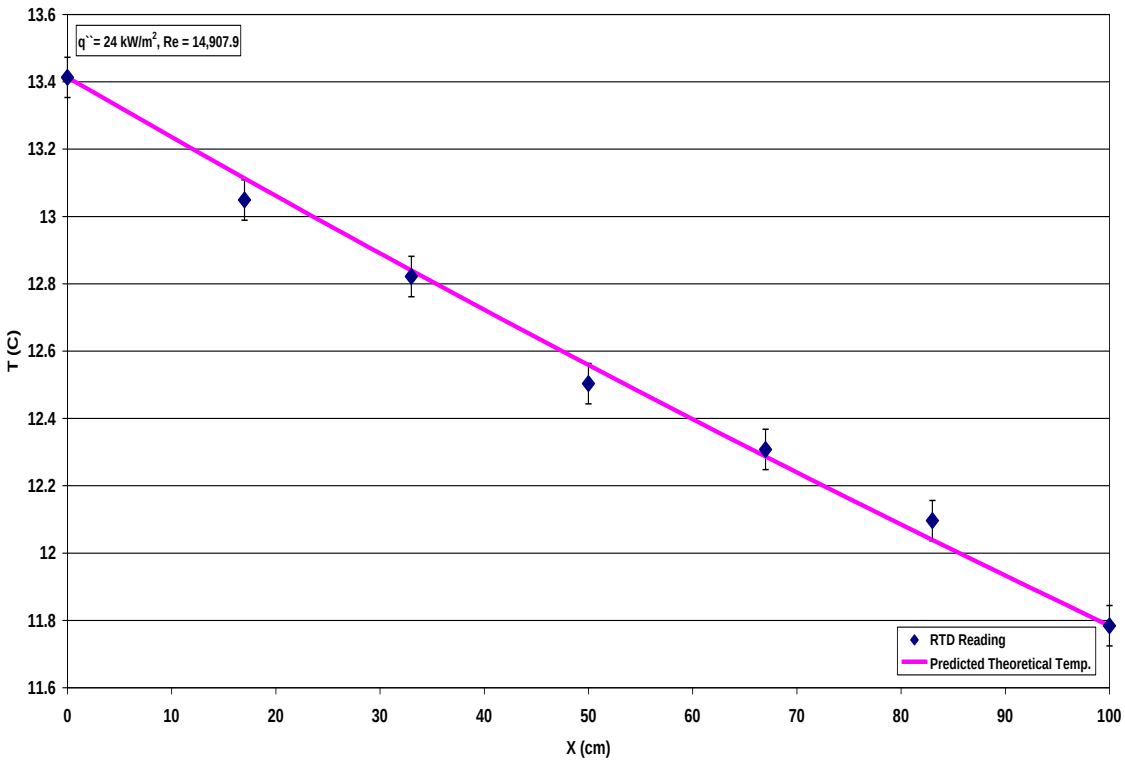

Figure 5-12 R-134a smooth tube temperature profile plot.

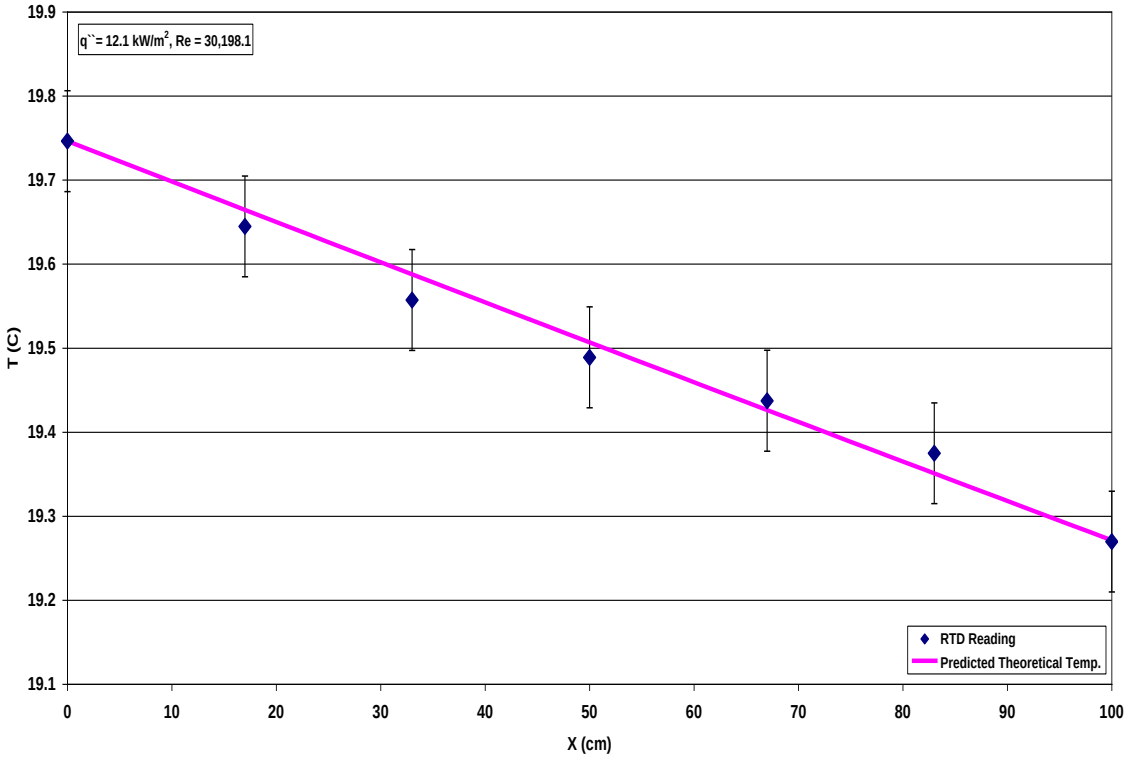

Figure 5-13 R-123 smooth tube temperature profile plot.

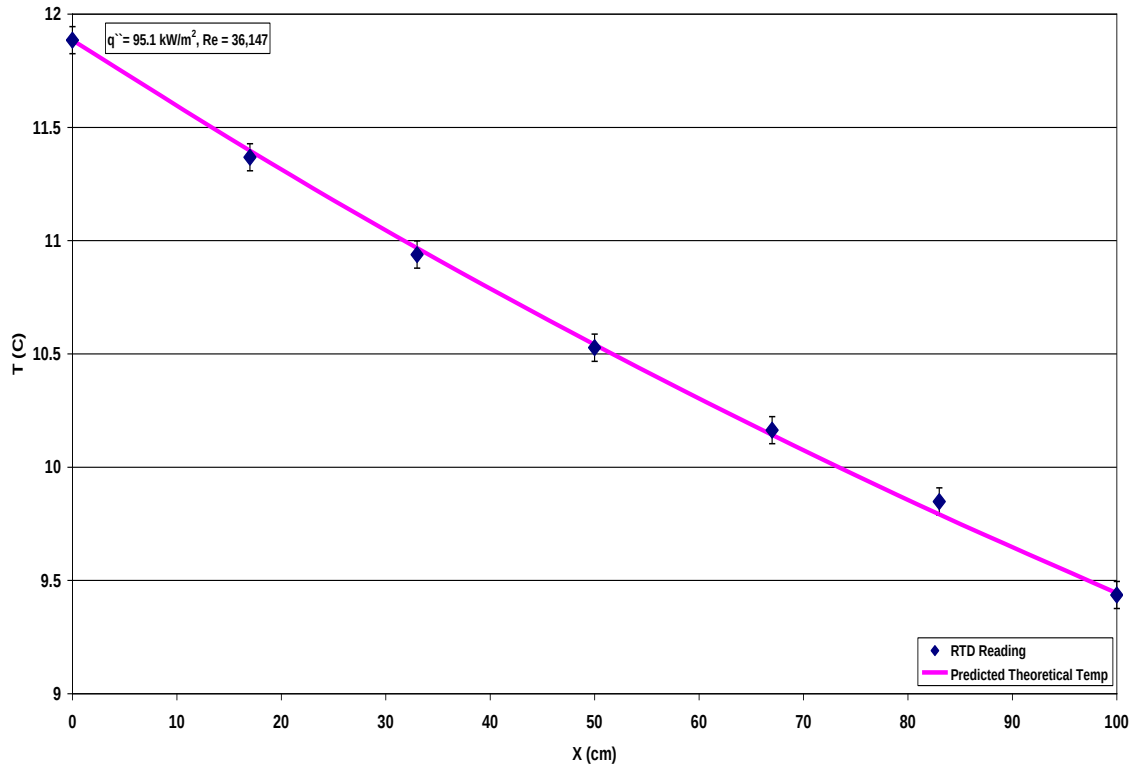

Figure 5-14 R-134a Turbo BII HP tube temperature profile plot.

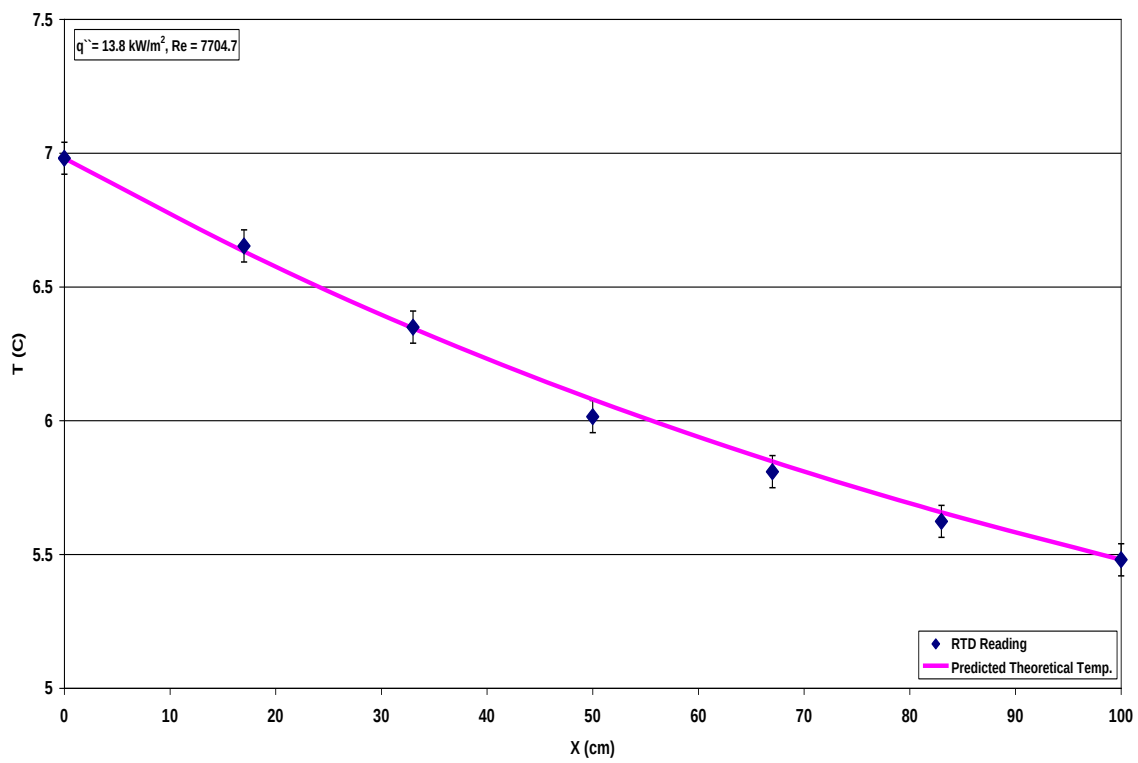

Figure 5-15 R-123 Turbo BII LP tube temperature profile plot.

5.2.2 R-134a and R-123 smooth tube results.

Figures 5-16 and 5-17 show the local heat transfer coefficient results of R-134a and R-123 on smooth tube. The change of the heat transfer coefficient for each run is represented by five local heat transfer coefficients corresponding to the five internal RTD's. The middle point always has the least uncertainty among the five points, unlike the two end points, which have the highest uncertainty among the five points. Almost all the local heat transfer coefficient points in Figure 30 show increasing trend with heat flux except for two runs, the first one shows a slight decrease with heat flux and the other one shows no change of the heat transfer coefficient with heat flux. The local data for both plots agree well with the literature.

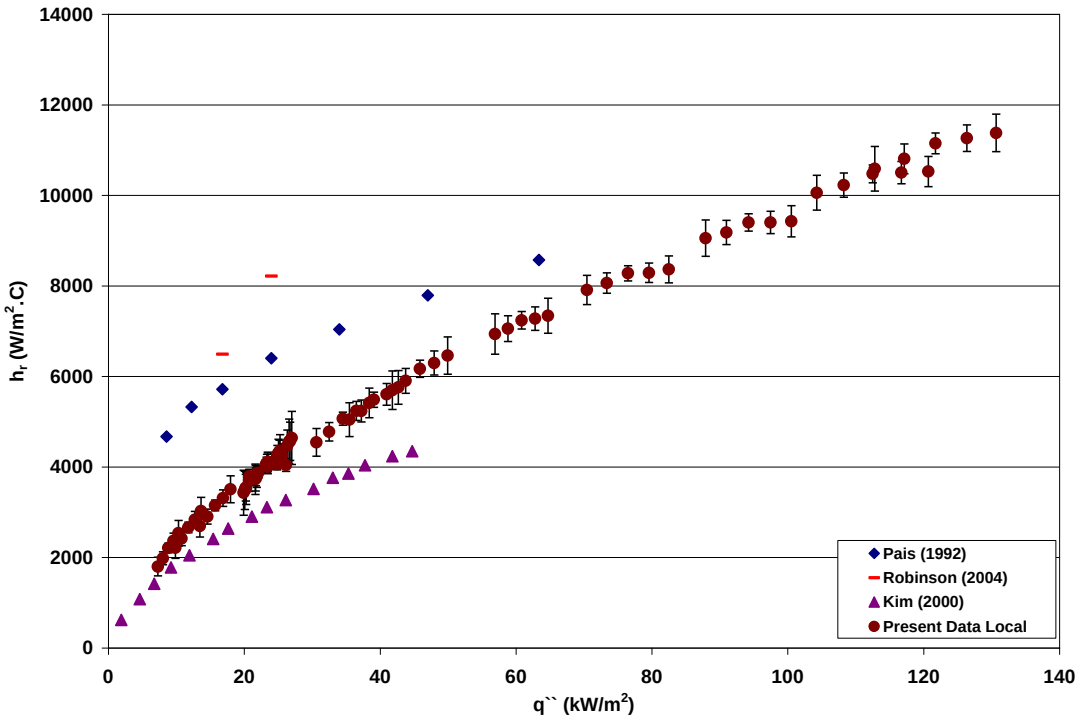

Figure 5-16 R-134a on smooth tube local heat transfer coefficient plot.

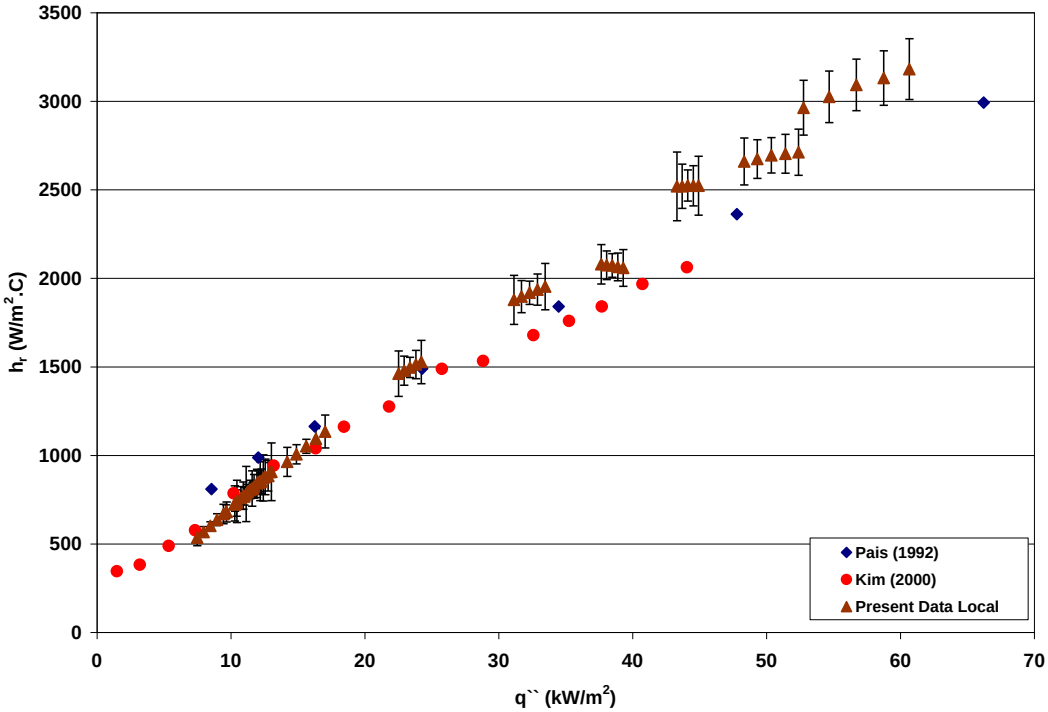

Figure 5-17 R-123 on smooth tube local heat transfer coefficient plot.

5.2.3 R-134a and R-123 enhanced tube results.

The local heat transfer coefficients of the Turbo BII HP tube in Figure 5-18 follow the same trend as the average heat transfer coefficient in Figure 5-7, except for some outliers. The local analysis shows the same trend change after the point of 40 kW/m². The local Turbo BII HP tube agrees well with the literature. Figure 5-19 shows the local heat transfer coefficients of the Turbo BII LP tube. The local data show an increasing trend with the heat flux. Comparing the uncertainty bars of the two enhanced tubes illustrate that the Turbo BII LP tube has higher uncertainty. This is because the saturation temperature uncertainty of R-123 (0.028 °C) is higher than the saturation temperature of R-134a (0.02 °C).

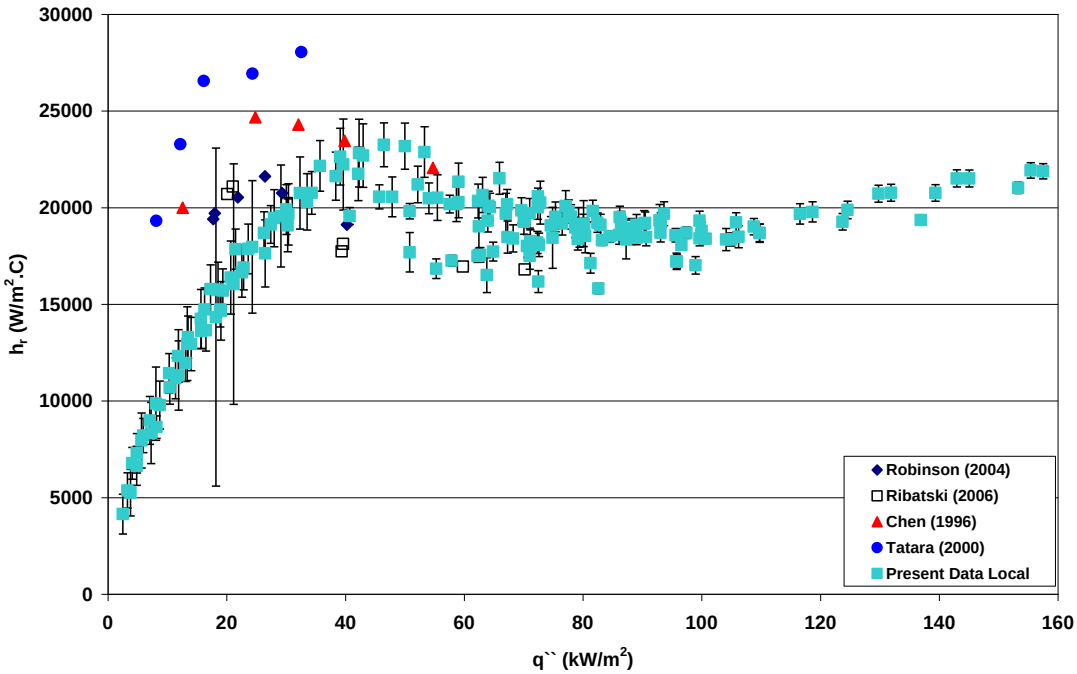

Figure 5-18 R-134a on Turbo BII HP tube local heat transfer coefficient plot.

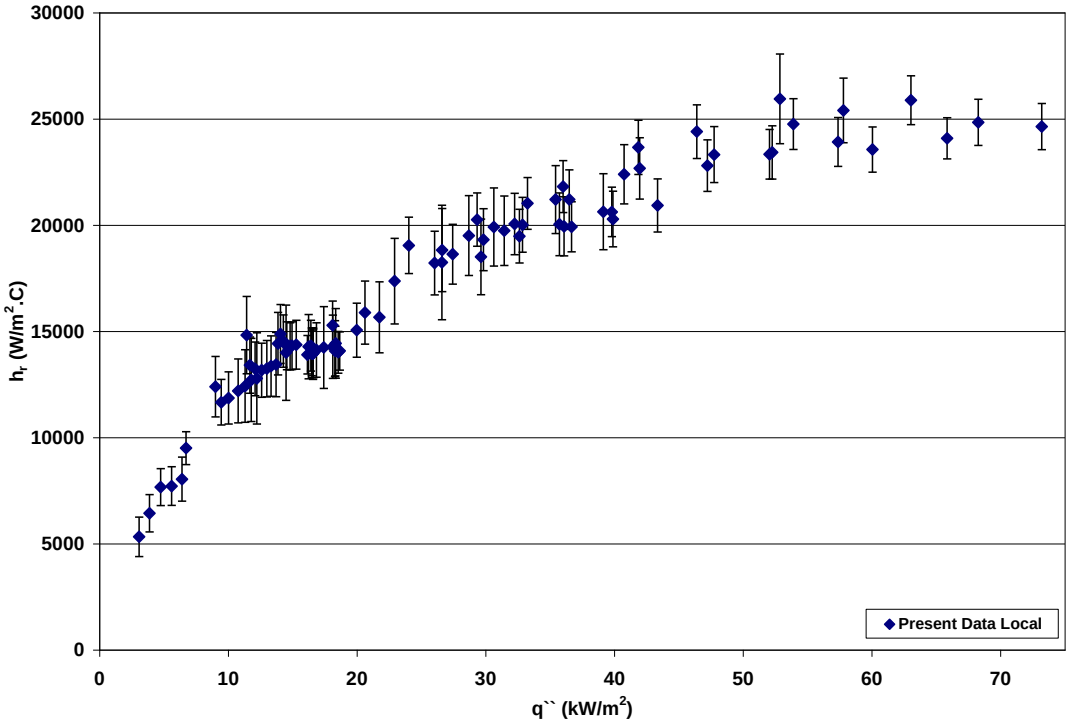

Figure 5-19 R-123 on Turbo BII LP tube local heat transfer coefficient plot.

5.3 Average and Local Results Comparison.

The four following plots, Figures 5-20 through 5-23, are for comparing the average and local data for each case. Comparing the average and local results is important for judging the performance of the local analysis. Eliminating the two ends' heat transfer coefficients (corresponding to the two RTD's next to the inlet and the outlet on temperature profile curve) and considering only the three internal RTD's of a taken data point gives a better agreement between the local and the average. This is because usually the two ends' heat transfer coefficients have high uncertainty.

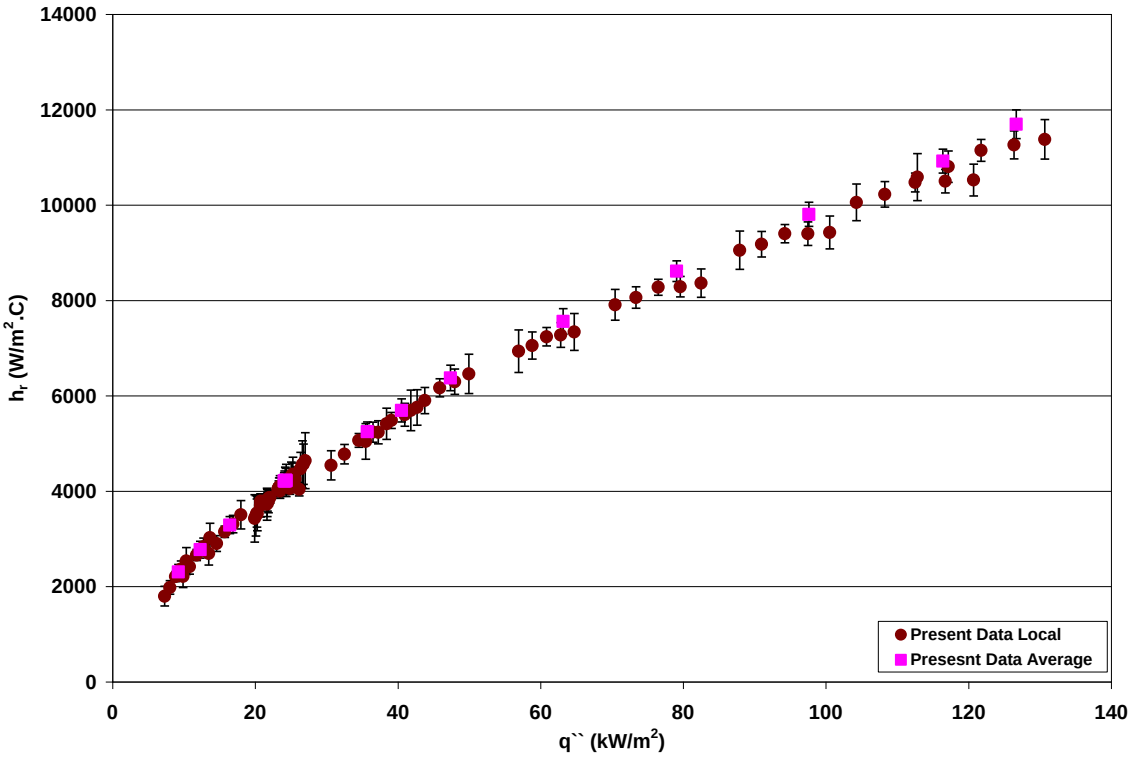

Figure 5-20 R-134a smooth tube average and local comparison plot.

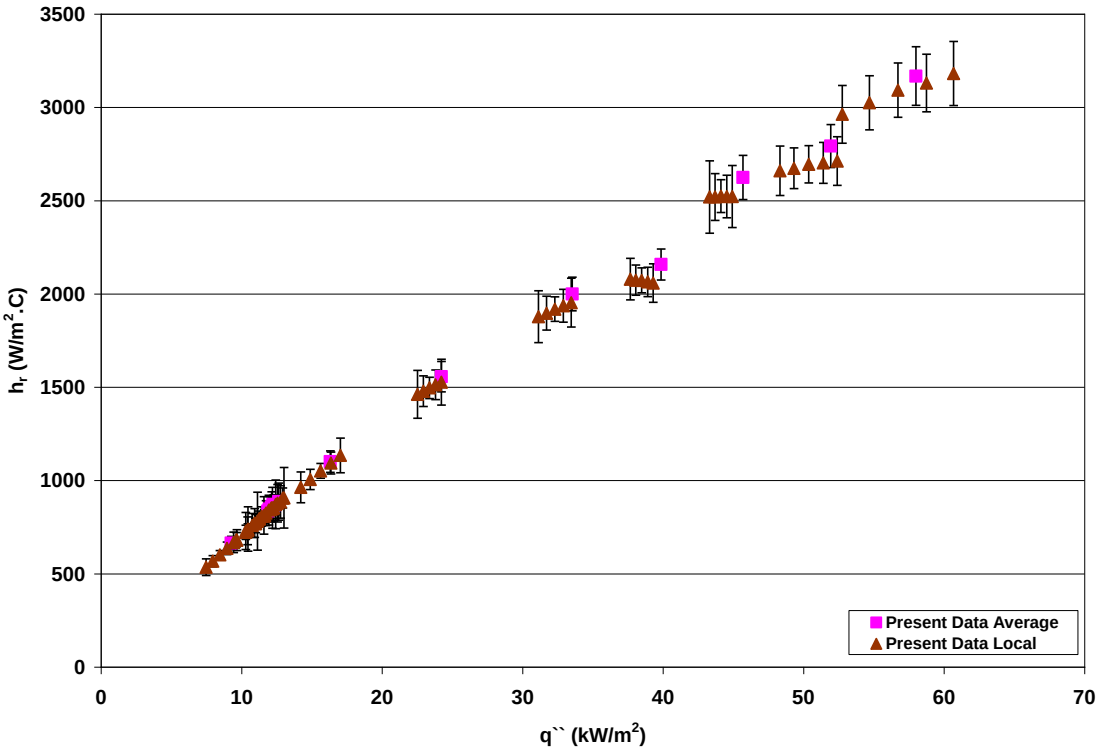

Figure 5-21 R-123 smooth tube average and local comparison plot.

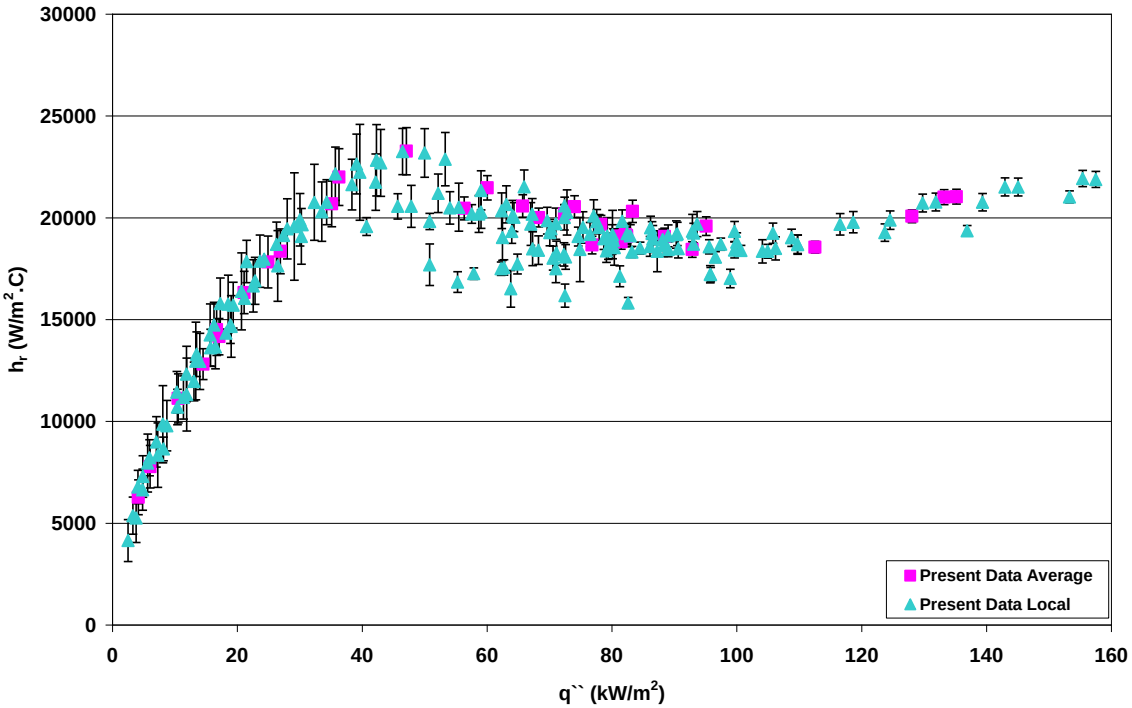

Figure 5-22 R-134a Turbo BII HP tube average and local comparison plot.

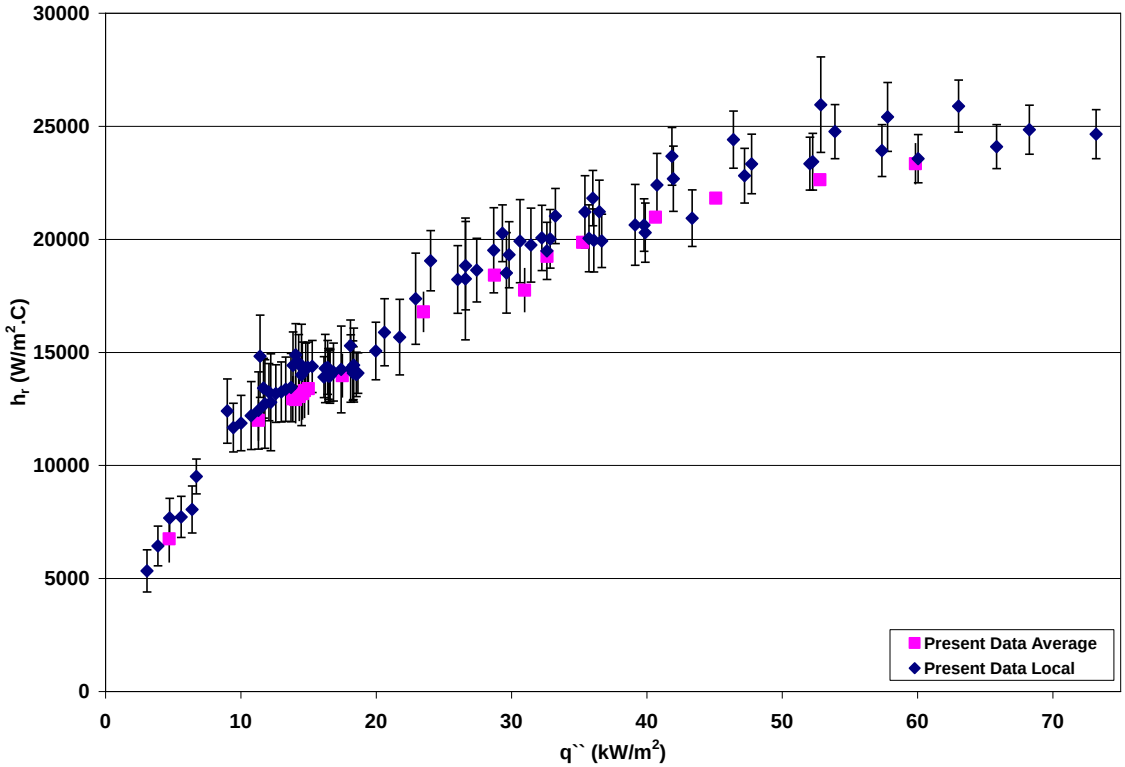

Figure 5-213 R-123 Turbo BII LP average and local comparison plot.

5.4 Conclusion.

The modified Wilson plot data were taken where the dominant thermal resistance on the refrigerant side. Also, modified Wilson plot data were taken over a narrow heat flux range with a maximum change of 8% between points. Both R-134a and R-123 on smooth tube and the Turbo BII LP tube show a continuously increasing trend of the heat transfer coefficient. Turbo BII HP is the only tube among the four tubes that shows a trend change with heat flux, this is also seen in the data reported by Chen and Tuzla (1996), and Robinson and Thome(2004). The smooth tube shows a much better performance (250%) in R-134a than in R-123. The performance of Turbo BII HP and Turbo BII LP are similar. The average results showed a good agreement with the literature for all cases.

The water temperature profiles show a consistent drop in temperature even at the low temperature difference between the inlet and the outlet. Figure 5-13 shows a clear consistent temperature drop even at a temperature difference of only 0.47 °C between the inlet and the outlet. The local data show a good agreement with the average data as well as the literature. For a better agreement between the average data and the local data, the two ends' heat transfer coefficients can be eliminated and only the three internal RTD's are considered.

CHAPTER 6 - Overall Conclusion

6.1 Research Conclusion

This chapter presents the overall conclusion for this entire thesis. This project presented a complete pool boiling study of R-134a on smooth tube and Turbo BII HP tube and R-123 on smooth tube and Turbo BII LP tube. This was accomplished by first determining the water side heat transfer coefficient using the modified Wilson plot analysis, then the refrigerant side heat transfer coefficient. The refrigerant side heat transfer coefficient was determined using two related methods, average and local. The data determined will be used in the 2nd phase of this study, which studies the tube pitch impact on the shell side boiling heat transfer. Both the modified Wilson plot data and the pool boiling coefficient will be used in modeling the tube bundle.

The facility design of this project presented new useful methodologies in building a single tube water heated pool boiling facility. The equipments used in this facility helped determining the heat transfer coefficients with low uncertainty. Such as the use of the Micromotion Elite sensor (±0.05 % of reading uncertainty), the thin film RTD's (±0.03 °C uncertainty), and the Viatran pressure transducers (±0.25 kPa for R-134a and ±0.05 kPa for R-123 uncertainties). Due to their accurate calibration capability, the use of RTD's was found very useful in temperature measurement. The thin film RTD's are excellent in their fast response to temperature change. The 1000 Ω RTD are better than the 100 Ω because of the better resolution on resistance measuring. The swirls were very functiuonal in reducing the effect of velocity and thermal boundary layers. Positioning the inlet and outlet RTD's on the instrumented tube and close to the heat transfer region, helped determining the boundary conditions with the least effect of the ambient condition. Also, the positioning of the water pressure transducers was useful in determining the boundary conditions accurately.

The data reduction introduced two related methods for determining the refrigerant heat transfer coefficient, the average and local methods. This study is the first study to present the engagement of the water pressure in the calculation of the refrigerant heat transfer coefficient, or

the enthalpy-based heat transfer analysis (EBHT), which is useful for solving many heat exchanger problems that experience large pressure drop. A Monte Carlo simulation was used twice in this study. The first time is for determining the best polynomial degree for curve fitting the local temperatures with distances. The second time is for determining the uncertainty in the temperature slope $\frac{dT}{dx}$ of the local heat transfer coefficient. Uncertainty analysis was applied to each average heat transfer coefficient and for each of the of five local heat transfer coefficients.

The modified Wilson plot analysis was conducted prior to performing the complete pool boiling data for each of the four boiling cases. Data were taken over a narrow heat flux range with a maximum change of 8% between points. Also, the modified Wilson plot data were taken where the dominant thermal resistance on the refrigerant side. The resulting water heat transfer coefficient correction factor for both case of the smooth tube is close to 1 and for the two enhanced tubes is about two.

Both R-134a and R-123 on smooth tube and the Turbo BII LP tube show a continuously increasing trend of the heat transfer coefficient. Turbo BII HP is the only tube among the four tubes that shows a trend change with heat flux, this is also seen in the data reported by Chen and Tuzla (1996), and Robinson and Thome(2004). The smooth tube shows a much better performance (250%) in R-134a than in R-123. The performance of Turbo BII HP and Turbo BII LP are similar. The average results show a good agreement with the literature for all cases.

The water temperature profiles show a consistent drop in temperature even at the low temperature difference between the inlet and the outlet, even at a temperature difference of only 0.47 °C between the inlet and the outlet. The local data show a good agreement with the average data as well as the literature. For a better agreement between the average data and the local data, the two ends' heat transfer coefficients can be eliminated and only the three internal RTD's are considered.

6.2 Recommendations

Although this research presented a good understanding of the nucleate boiling of R-134a and R-123 on smooth and enhanced tubes, there still some work for future researches to be recommended. The following are some recommendations.

Expanding the heat flux range for testing with R-123 on the Turbo BII LP tube is important. Although Chien and Webb (1996) presented an explanation of the performance decreasing of some enhanced tubes with increasing heat flux, studying the case of the Turbo BII HP tube is important for comparison with their explanation. Specially that the Turbo BII LP tube has a very similar performance as the Turbo BII HP and yet it doest not experience the same phenomenon.

Further studying for the effect of the velocity and thermal boundary layers and the wire wrap function will be beneficial for more accurate local heat transfer coefficient analysis. If possible, increasing the number of the internal local RTD's for comparison with the present local data, and studying whether it is helpful or redundant.

Bibliography

Briggs, D.E., and E.H.Young. 1969. Modified Wilson plot techniques for obtaining heat transfer correlations for shell and tube heat exchangers. *Chemical Engineering Progress Symposium Series* 92(65):35-45.

Chang, J.Y., and S.M. You. 1997. Enhanced boiling heat transfer from micro-porous cylindrical surfaces in saturated FC-87 and R-123. *Transactions of the ASME. Journal of Heat Transfer* 119(2):319-25

Chien, L.H., and R.L. Webb. 1998. A parametric study of nucleate boiling on structured surfaces. I. Effect of tunnel dimensions. *Transactions of the ASME. Journal of Heat Transfer* 120(4):1042-8

Chien, L.H., and R.L. Webb. 1998. A parametric study of nucleate boiling on structured surfaces. II. Effect of pore diameter and pore pitch. *Transactions of the ASME. Journal of Heat Transfer* 120(4):1049-54

Chien, L.-H., and R.L. Webb. 2001. Effect of geometry and fluid property parameters on performance of tunnel and pore enhanced boiling surfaces. *Journal of Enhanced Heat Transfer* 8(5):329-339

Chiou, C.B., D.C. Lu, and C.C. Wang. 1997. Pool boiling of R-22, R-124 and R-134a on a plain tube. *International Journal of Heat and Mass Transfer* 40(7):1657-66

Collier, J.G., and J.R. Thome. 1994. *Convictive Boiling and Condensation*. 3rd edition, A.L. Cullen, L.C. Woods, J.M. Brady , C.E. Brennen, E.R. Eatock Taylor, M.Y. Hussaini, T.V. Jones, J. Van Bladel, Oxford University Press, Inc.

Hahne, E., Q. R. Chen, and R. Windisch. 1991. Pool boiling heat transfer on finned tubes-an experimental and theoretical study. *International Journal of Heat and Mass Transfer* 34(8):2071-9.

Hsieh, S.S., and C.J. Weng. 1997. Nucleate pool boiling from coated surfaces in saturated R-134a and R-407c. *International Journal of Heat and Mass Transfer* 40(3):519-532

Hsieh, S.S., and T.Y. Yang. 2001. Nucleate pool boiling from coated and spirally wrapped tubes in saturated R-134a and R-600a at low and moderate heat flux. *Transactions of the ASME. Journal of Heat Transfer* 123(2):257-70

Incropera, F.P., and D.P. Dewitt. 2002. *Fundamentals of Heat and Mass Transfer*. 5th edition, John Wiley and Sons, Inc.

Jung, D., K. An, and J. Park. 2004. Nucleate boiling heat transfer coefficients of HCFC22, HFC134a, HFC125, and HFC32 on various enhanced tubes. *International Journal of Refrigeration* 27(2):202-6

Kedzierski, M.A. 1995. Calorimetric and visual measurements of R-123 pool boiling on four enhanced surfaces. Report NISTIR 5732, U.S. Department of Commerce, Washington, D.C.

Khartabil H.F., and R.N. Christensen. 1992. An improved scheme for determining heat transfer correlations from heat exchanger regression models with three unknowns. *Experimental Thermal and Fluid Science* 5(6):808-819.

Kim, N. H., and K.K. Choi. 2001. Nucleate pool boiling on structured enhanced tubes having pores with connecting gaps. *International Journal of Heat and Mass Transfer* 44(1):17-28

Memory, S.B., D.C. Sugiyama, and P.J. Marto. 1995. Nucleate pool boiling of R-114 and R-114-oil mixtures from smooth and enhanced surfaces. I. Single tubes. *International Journal of Heat and Mass Transfer* 38(8):1347-61.

Ribatski G., and J.R. Thome. 2006. Nucleate boiling heat transfer of R134a on enhanced tubes. *Applied Thermal Engineering* 26(10):1018-31

Richard, S.F., and D.E. Beasley. 1991. *Theory and Design for Mechanical Measurements*. Wiley & Sons, Inc.

Robinson, D.M., and J.R. Thome. 2004. Local bundle boiling heat transfer coefficients on a turbo-BII HP tube bundle (RP-1089). *HVAC and R Research* 10(4):441-457

Saidi, M.H., M. Ohadi, and M. Souhar. 1999. Enhanced pool boiling of R-123 refrigerant on two selected tubes . *Applied Thermal Engineering* 19(8):885-895

Shah, R.K. 1990. Assessment of modified Wilson plot techniques for obtaining heat exchanger design data. *Heat Transfer, Proceedings of the International Heat Transfer Conference* 5:51-56.

Tatara, R.A., and P. Payvar. 2000. Pool boiling of pure R134a from a single Turbo-BII-HP tube. *International Journal of Heat and Mass Transfer* 43(12):2233-6

Thome, J.R. 1990. *Enhanced Heat Transfer*, S.E. Zinninger, L. McCullough, Hemisphere Publishing Corporation.

Thome, J.R. 2007 (the date in which website was browsed). Design Book III, http://www.wlv.com/products/databook/db3/data/db3ch9.pdf

Webb, R.L., and C. Pais.1991. Pool boiling data for five refrigerants on three tube geometries. *ASHRAE Transactions* n(1):72-78.

Webb, R.L., and C. Pais. 1992. Nucleate pool boiling data for five refrigerants on plain, integral-fin and enhanced tube geometries. *International Journal of Heat and Mass Transfer* 35(8):1893-904.

Webb, R.L., L.H. Chien, and W.F. McQuade, and H.E. Imadojemu. 1995. Pool boiling of oil-refrigerant mixtures on enhanced tubes. *Proceedings of the ASME-JSME Thermal Engineering Joint Conference, Maui, HI,* 2:247-255

Webb, R.L., and N.H. Kim. 2005. *Principles of Enhanced Heat Transfer*. 2nd edition, Taylor & Francis Group, LLC.

Yang, C.Y., and C.F. Fan. 2006. Pool boiling of refrigerants R-134a and R-404A on porous and structured tubes part II. Heat transfer performance. *Journal of Enhanced Heat Transfer* 13(1):85-97

Appendix A - Data Tables

Table 6-1 R-134a on smooth tube average data

Run #	$T_{w,in}$ (°C)	$T_{w,out}$ (°C)	ΔP_w (kPa)	Re	T_{sat} (°C)	q"(kW/m²)	h_r (W/m².°C)
R134aS1	11.85	11.09	87.82	30527.40	4.28	24.20	4216.24
R134aS2	16.35	13.07	8.19	7964.75	4.36	24.31	4215.15
R134aS3	13.41	11.78	24.22	14907.91	4.23	24.05	4218.02
R134aS4	12.67	11.49	41.86	20213.60	4.31	24.11	4215.25
R134aS5	12.19	11.26	62.73	25343.33	4.29	24.29	4233.31
R134aS6	11.78	11.16	122.30	36966.02	4.48	24.32	4226.58
R134aS7	16.62	14.98	121.41	41816.40	4.44	63.16	7560.83
R134aS8	14.89	13.53	102.82	36280.82	4.28	47.36	6375.92
R134aS9	14.49	13.13	78.57	30761.26	4.25	40.51	5694.95
R134aS10	11.81	10.73	25.60	14803.13	4.47	16.41	3289.33
R134aS11	14.45	12.93	52.91	24386.47	4.26	35.70	5246.90
R134aS12	10.94	10.03	20.70	12775.11	4.53	12.27	2774.30
R134aS13	10.15	9.33	15.02	10364.56	4.35	9.22	2306.16
R134aS14	21.11	18.64	193.30	61897.89	4.47	126.69	11696.15
R134aS15	21.67	18.64	119.80	47003.62	4.28	116.37	10922.70
R134aS16	19.96	17.42	119.90	45218.51	4.26	97.62	9806.90
R134aS17	19.66	16.89	72.69	33424.07	4.47	79.07	8616.08

Table 6-2 R-134a on smooth tube local data

Run #	RTD #	T_w (°C)	$\lvert dT/dx \rvert$ (°C/m)	$\Delta P_w/\Delta x$ (kPa/m)	Re	T_{sat} (°C)	q''_{local} (kW/m²)	$h_{r,local}$ (W/m².°C)
R134aS1	Inlet	11.85			30527.40	4.28		
	1	11.69	0.84	76.83			26.61	4561.69
	2	11.57	0.79	76.83			25.03	4310.86
	3	11.39	0.73	76.83			23.35	4080.96
	4	11.35	0.68	76.83			21.67	3751.56
	5	11.24	0.63	76.83			20.09	3483.42
	Outlet	11.09						
R134aS2	Inlet	16.35			7964.75	4.36		
	1	15.65	3.52	7.17			26.13	4042.59
	2	15.07	3.34	7.17			24.83	4059.33
	3	14.55	3.16	7.17			23.45	4002.91
	4	14.14	2.97	7.17			22.06	3867.99
	5	13.67	2.80	7.17			20.76	3793.21
	Outlet	13.07						
R134aS3	Inlet	13.41			14907.91	4.23		
	1	13.05	1.73	21.19			25.59	4255.23
	2	12.82	1.65	21.19			24.41	4125.80
	3	12.50	1.57	21.19			23.16	4037.00
	4	12.31	1.48	21.19			21.90	3857.20
	5	12.10	1.40	21.19			20.72	3702.60
	Outlet	11.78						
R134aS4	Inlet	12.67			20213.60	4.31		
	1	12.42	1.29	36.62			26.35	4470.16
	2	12.24	1.22	36.62			24.86	4263.36
	3	11.98	1.14	36.62			23.28	4074.92
	4	11.88	1.06	36.62			21.70	3781.54

	5	11.72	0.99	36.62			20.21	3541.91
	Outlet	11.49						
R134aS5	Inlet	12.19			25343.33	4.29		
	1	12.01	1.03	54.88			26.75	4565.99
	2	11.85	0.97	54.88			25.18	4331.78
	3	11.64	0.90	54.88			23.51	4112.32
	4	11.57	0.84	54.88			21.84	3789.79
	5	11.44	0.78	54.88			20.27	3526.41
	Outlet	11.26						
R134aS6	Inlet	11.78			36966.02	4.48		
	1	11.66	0.69	107.00			26.99	4640.08
	2	11.55	0.65	107.00			25.27	4357.55
	3	11.40	0.60	107.00			23.45	4089.35
	4	11.37	0.55	107.00			21.63	3727.29
	5	11.29	0.50	107.00			19.91	3430.39
	Outlet	11.16						
R134aS7	Inlet	16.62			41816.40	4.44		
	1	16.31	1.68	106.22			64.71	7340.80
	2	16.04	1.63	106.22			62.82	7276.16
	3	15.71	1.58	106.22			60.82	7239.88
	4	15.55	1.53	106.22			58.81	7054.01
	5	15.33	1.48	106.22			56.93	6937.36
	Outlet	14.98						
R134aS8	Inlet	14.89			36280.82	4.28		
	1	14.62	1.44	89.95			49.93	6460.54
	2	14.41	1.38	89.95			47.96	6295.40
	3	14.12	1.32	89.95			45.86	6168.00
	4	13.99	1.26	89.95			43.77	5901.43
	5	13.81	1.20	89.95			41.79	5694.76
	Outlet	13.53						

R134aS9	Inlet	14.49			30761.26	4.25		
	1	14.22	1.44	68.74			42.69	5758.60
	2	14.01	1.38	68.74			40.94	5604.02
	3	13.72	1.31	68.74			39.09	5485.79
	4	13.59	1.25	68.74			37.23	5235.97
	5	13.41	1.19	68.74			35.49	5044.25
	Outlet	13.13						
R134aS10	Inlet	11.81			14803.13	4.47		
	1	11.56	1.18	22.39			17.97	3505.79
	2	11.41	1.11	22.39			16.88	3310.93
	3	11.18	1.03	22.39			15.72	3149.88
	4	11.08	0.95	22.39			14.56	2902.42
	5	10.94	0.88	22.39			13.47	2696.39
	Outlet	10.73						
R134aS11	Inlet	14.45			24386.47	4.26		
	1	14.15	1.63	46.29			38.39	5414.59
	2	13.89	1.55	46.29			36.51	5239.72
	3	13.58	1.47	46.29			34.51	5066.50
	4	13.43	1.38	46.29			32.51	4777.00
	5	13.23	1.30	46.29			30.63	4542.57
	Outlet	12.93						
R134aS12	Inlet	10.94			12775.11	4.53		
	1	10.74	1.02	18.11			13.65	3024.81
	2	10.60	0.95	18.11			12.73	2835.01
	3	10.40	0.87	18.11			11.76	2662.18
	4	10.32	0.80	18.11			10.78	2417.38
	5	10.21	0.73	18.11			9.86	2212.39
	Outlet	10.03						
R134aS13	Inlet	10.15			10364.56	4.35		
	1	9.97	0.93	13.14			10.33	2535.57

	2	9.84	0.86	13.14			9.59	2367.54
	3	9.65	0.79	13.14			8.81	2211.41
	4	9.60	0.72	13.14			8.02	1982.45
	5	9.49	0.65	13.14			7.29	1798.94
	Outlet	9.33						
R134aS14	Inlet	21.11			61897.89	4.47		
	1	20.63	2.55	169.11			130.68	11379.06
	2	20.21	2.46	169.11			126.35	11264.02
	3	19.74	2.37	169.11			121.75	11148.93
	4	19.50	2.28	169.11			117.14	10806.44
	5	19.16	2.19	169.11			112.81	10586.50
	Outlet	18.64						
R134aS15	Inlet	21.67			47003.62	4.28		
	1	21.10	3.14	104.81			120.69	10525.71
	2	20.57	3.04	104.81			116.71	10502.62
	3	20.01	2.93	104.81			112.48	10476.07
	4	19.67	2.82	104.81			108.25	10224.92
	5	19.28	2.71	104.81			104.27	10057.81
	Outlet	18.64						
R134aS16	Inlet	19.96			45218.51	4.26		
	1	19.49	2.62	104.90			100.53	9428.38
	2	19.05	2.54	104.90			97.47	9401.48
	3	18.56	2.45	104.90			94.22	9399.59
	4	18.30	2.37	104.90			90.97	9181.53
	5	17.96	2.29	104.90			87.91	9054.05
	Outlet	17.42						
R134aS17	Inlet	19.66			33424.07	4.47		
	1	19.11	2.89	63.59			82.50	8364.64
	2	18.67	2.79	63.59			79.58	8289.09
	3	18.13	2.68	63.59			76.47	8278.94

	4	17.81	2.57	63.59			73.37	8063.34
	5	17.45	2.47	63.59			70.44	7909.41
	Outlet	16.89						

Table 6-3 R-123 on smooth tube average data

Run #	$T_{w,in}$ (°C)	$T_{w,out}$ (°C)	ΔP_w (kPa)	Re	T_{sat} (°C)	q"(kW/m²)	h_r (W/m².°C)
R123S1	19.43	19.05	83.14	38008.71	4.22	12.64	887.16
R123S2	19.75	19.27	54.77	30198.16	4.49	12.13	859.70
R123S3	19.86	19.30	39.95	25279.77	4.42	11.96	846.80
R123S4	20.29	19.52	25.56	19601.57	4.31	12.41	869.89
R123S5	20.57	19.59	15.59	14859.95	4.27	11.86	836.13
R123S6	21.84	20.19	6.52	9344.72	4.38	12.24	872.65
R123S7	20.33	19.37	10.38	11813.32	4.35	9.26	665.15
R123S8	21.24	20.28	28.30	21322.22	4.31	16.32	1101.53
R123S9	22.14	21.18	55.95	32159.77	4.38	24.22	1556.60
R123S10	23.84	22.66	67.76	37359.97	4.37	33.53	1999.93
R123S11	24.43	23.26	118.04	51644.47	4.25	45.69	2624.66
R123S12	29.30	26.12	29.91	26743.75	4.27	57.99	3167.99
R123S13	28.16	25.76	41.18	31180.51	4.40	51.94	2792.90
R123S14	26.76	24.92	41.30	30392.83	4.29	39.86	2158.25

Table 6-4 R-123 on smooth tube local data

Run #	RTD #	T_w (°C)	$\lvert dT/dx \rvert$ (°C/m)	$\Delta P_w/\Delta x$ (kPa/m)	Re	T_{sat} (°C)	q''_{local} (kW/m²)	$h_{r,local}$ (W/m².°C)
R123S1	Inlet	19.43			38008.71	4.22		
	1	19.36	0.40	72.74			13.02	907.55
	2	19.28	0.38	72.74			12.56	878.54

	3	19.22	0.37	72.74			12.07	846.15
	4	19.18	0.35	72.74			11.59	812.90
	5	19.13	0.34	72.74			11.13	782.10
	Outlet	19.05						
R123S2	Inlet	19.75			30198.16	4.49		
	1	19.64	0.49	47.92			12.42	872.21
	2	19.56	0.47	47.92			11.94	841.75
	3	19.49	0.45	47.92			11.43	807.72
	4	19.44	0.43	47.92			10.92	772.64
	5	19.37	0.41	47.92			10.45	740.27
	Outlet	19.27						
R123S3	Inlet	19.86			25279.77	4.42		
	1	19.74	0.58	34.95			12.19	854.13
	2	19.64	0.56	34.95			11.73	825.18
	3	19.56	0.53	34.95			11.24	793.03
	4	19.50	0.51	34.95			10.75	759.78
	5	19.42	0.49	34.95			10.29	729.07
	Outlet	19.30						
R123S4	Inlet	20.29			19601.57	4.31		
	1	20.10	0.79	22.36			12.78	885.13
	2	19.98	0.76	22.36			12.21	849.13
	3	19.87	0.72	22.36			11.60	809.47
	4	19.78	0.68	22.36			10.99	768.74
	5	19.68	0.65	22.36			10.42	730.59
	Outlet	19.52						
R123S5	Inlet	20.57			14859.95	4.27		
	1	20.31	1.01	13.64			12.28	854.24
	2	20.17	0.96	13.64			11.65	813.39
	3	20.03	0.91	13.64			10.97	768.82
	4	19.92	0.85	13.64			10.30	722.61

	5	19.80	0.80	13.64			9.67	680.25
	Outlet	19.59						
R123S6	Inlet	21.84			9344.72	4.38		
	1	21.38	1.74	5.70			12.93	906.37
	2	21.16	1.63	5.70			12.13	853.34
	3	20.93	1.52	5.70			11.28	796.67
	4	20.72	1.41	5.70			10.43	738.02
	5	20.53	1.30	5.70			9.63	682.78
	Outlet	20.19						
R123S7	Inlet	20.33			11813.32	4.35		
	1	20.06	0.98	9.08			9.43	668.36
	2	19.94	0.93	9.08			8.96	636.52
	3	19.81	0.87	9.08			8.45	602.29
	4	19.70	0.82	9.08			7.95	567.69
	5	19.58	0.77	9.08			7.48	535.40
	Outlet	19.37						
R123S8	Inlet	21.24			21322.22	4.31		
	1	21.02	0.99	24.76			17.04	1134.73
	2	20.88	0.95	24.76			16.35	1093.98
	3	20.72	0.91	24.76			15.62	1051.54
	4	20.59	0.87	24.76			14.89	1006.23
	5	20.47	0.83	24.76			14.21	963.39
	Outlet	20.28						
R123S9	Inlet	22.14			32159.77	4.38		
	1	21.94	0.95	48.95			24.22	1527.36
	2	21.79	0.94	48.95			23.81	1513.19
	3	21.65	0.92	48.95			23.37	1496.42
	4	21.51	0.90	48.95			22.93	1478.56
	5	21.37	0.88	48.95			22.52	1461.87
	Outlet	21.18						

R123S10	Inlet	23.84			37359.97	4.37		
	1	23.60	1.18	59.29			33.46	1953.58
	2	23.42	1.16	59.29			32.90	1936.65
	3	23.23	1.14	59.29			32.30	1918.69
	4	23.07	1.11	59.29			31.70	1897.01
	5	22.90	1.09	59.29			31.13	1878.23
	Outlet	22.66						
R123S11	Inlet	24.43			51644.47	4.25		
	1	24.20	1.15	103.27			44.93	2522.78
	2	24.02	1.14	103.27			44.53	2522.60
	3	23.83	1.13	103.27			44.11	2524.41
	4	23.67	1.12	103.27			43.70	2519.63
	5	23.50	1.11	103.27			43.30	2519.64
	Outlet	23.26						
R123S12	Inlet	29.30			26743.75	4.27		
	1	28.66	3.33	26.17			60.67	3181.89
	2	28.19	3.23	26.17			58.75	3131.12
	3	27.59	3.11	26.17			56.71	3092.45
	4	27.14	3.00	26.17			54.68	3024.96
	5	26.71	2.90	26.17			52.76	2963.34
	Outlet	26.12						
R123S13	Inlet	28.16			31180.51	4.40		
	1	27.68	2.42	36.03			52.39	2712.30
	2	27.31	2.38	36.03			51.40	2703.13
	3	26.90	2.33	36.03			50.36	2694.84
	4	26.58	2.28	36.03			49.31	2673.71
	5	26.23	2.23	36.03			48.32	2659.94
	Outlet	25.76						
R123S14	Inlet	26.76			30392.83	4.29		
	1	26.40	1.82	36.13			39.29	2058.64

	2	26.12	1.80	36.13			38.90	2064.53
	3	25.81	1.78	36.13			38.48	2072.77
	4	25.56	1.76	36.13			38.06	2073.83
	5	25.29	1.74	36.13			37.66	2079.46
	Outlet	24.92						

Table 6-5 R-123 on Turbo BII LP tube average data

Run #	$T_{w,in}$ (°C)	$T_{w,out}$ (°C)	ΔP_w (kPa)	Re	T_{sat} (°C)	q"(kW/m²)	h_r (W/m².°C)
R123T1	5.71	4.99	18.37	5282.35	4.24	4.70	6748.22
R123T2	7.09	6.28	373.84	29819.08	4.42	30.97	17750.18
R123T3	8.88	7.25	373.33	31089.07	4.50	59.84	23338.17
R123T4	7.04	5.30	18.41	5437.45	4.22	11.30	11995.05
R123T5	6.16	5.48	141.95	17347.34	4.28	15.00	13392.66
R123T6	6.24	5.47	113.48	15380.61	4.29	14.70	13303.49
R123T7	6.32	5.43	86.45	13267.32	4.25	14.56	13163.31
R123T8	6.56	5.53	65.21	11419.73	4.35	14.32	13040.34
R123T9	6.81	5.51	42.56	9034.63	4.32	14.05	12910.68
R123T10	6.98	5.48	31.87	7704.77	4.29	13.84	12942.10
R123T11	6.63	5.91	171.43	19411.48	4.58	17.51	13967.60
R123T12	6.81	5.97	217.09	22222.17	4.47	23.50	16786.40
R123T13	7.24	6.19	217.11	22451.40	4.51	28.75	18406.70
R123T14	7.41	6.22	216.97	22527.67	4.40	32.63	19244.65
R123T15	7.83	6.54	217.06	22796.52	4.63	35.26	19860.81
R123T16	7.95	6.46	215.82	22806.35	4.37	40.64	20975.00
R123T17	8.30	6.64	215.80	23004.45	4.40	45.10	21813.98
R123T18	8.81	6.83	216.96	23034.51	4.32	52.80	22633.34

Table 6-6 R-123 on Turbo BII LP tube local data

Run #	RTD #	T_w (°C)	$\lvert dT/dx \rvert$ (°C/m)	$\Delta P_w/\Delta x$ (kPa/m)	Re	T_{sat} (°C)	q''_{local} (kW/m²)	$h_{r,local}$ (W/m².°C)
R123T1	Inlet	5.71			5282.35	4.24		
	1	5.54	0.99	16.08			6.40	8047.03
	2	5.41	0.86	16.08			5.59	7721.20
	3	5.23	0.73	16.08			4.74	7671.97
	4	5.15	0.60	16.08			3.88	6437.69
	5	5.06	0.47	16.08			3.07	5330.88
	Outlet	4.99						
R123T2	Inlet	7.09			29819.08	4.42		
	1	6.94	1.04	327.07			39.12	20636.78
	2	6.81	0.95	327.07			36.09	19947.89
	3	6.59	0.86	327.07			32.86	20019.41
	4	6.49	0.77	327.07			29.63	18513.12
	5	6.30	0.68	327.07			26.59	18247.53
	Outlet	6.28						
R123T3	Inlet	8.88			31089.07	4.50		
	1	8.61	2.01	326.63			73.19	24645.85
	2	8.31	1.87	326.63			68.26	24846.51
	3	7.92	1.72	326.63			63.02	25888.24
	4	7.67	1.57	326.63			57.79	25408.64
	5	7.36	1.43	326.63			52.86	25949.57
	Outlet	7.25						
R123T4	Inlet	7.04			5437.45	4.22		
	1	6.62	2.48	16.11			16.14	13902.95
	2	6.24	2.13	16.11			13.86	14425.25
	3	5.87	1.76	16.11			11.43	14827.45
	4	5.64	1.38	16.11			9.00	12400.97

	5	5.44	1.03	16.11			6.71	9508.89
	Outlet	5.30						
R123T5	Inlet	6.16			17347.34	4.28		
	1	6.03	0.85	124.19			18.33	14434.99
	2	5.91	0.78	124.19			16.85	14126.88
	3	5.74	0.70	124.19			15.28	14376.11
	4	5.66	0.62	124.19			13.70	13442.12
	5	5.56	0.55	124.19			12.22	12790.77
	Outlet	5.48						
R123T6	Inlet	6.24			15380.61	4.29		
	1	6.09	0.95	99.28			18.11	14282.33
	2	5.96	0.87	99.28			16.57	13957.47
	3	5.77	0.78	99.28			14.94	14328.99
	4	5.67	0.69	99.28			13.31	13368.50
	5	5.56	0.61	99.28			11.77	12714.95
	Outlet	5.47						
R123T7	Inlet	6.32			13267.32	4.25		
	1	6.14	1.13	75.64			18.28	14187.60
	2	5.98	1.02	75.64			16.59	13967.13
	3	5.77	0.91	75.64			14.79	14299.35
	4	5.66	0.79	75.64			12.99	13248.37
	5	5.53	0.69	75.64			11.30	12430.87
	Outlet	5.43						
R123T8	Inlet	6.56			11419.73	4.35		
	1	6.35	1.32	57.05			18.31	14077.09
	2	6.16	1.19	57.05			16.48	13947.42
	3	5.92	1.05	57.05			14.54	14326.73
	4	5.78	0.91	57.05			12.59	13176.27
	5	5.64	0.77	57.05			10.76	12200.54
	Outlet	5.53						

R123T9	Inlet	6.81			9034.63	4.32		
	1	6.53	1.71	37.23			18.54	14019.71
	2	6.28	1.52	37.23			16.47	14042.71
	3	5.98	1.31	37.23			14.27	14549.75
	4	5.81	1.11	37.23			12.08	13241.43
	5	5.64	0.92	37.23			10.01	11870.37
	Outlet	5.51						
R123T10	Inlet	6.98			7704.77	4.29		
	1	6.65	2.02	27.88			18.65	14080.85
	2	6.35	1.78	27.88			16.42	14330.70
	3	6.02	1.52	27.88			14.05	14884.03
	4	5.81	1.27	27.88			11.68	13415.26
	5	5.62	1.02	27.88			9.45	11670.26
	Outlet	5.48						
R123T11	Inlet	6.63			19411.48	4.58		
	1	6.47	0.90	149.98			21.73	15669.66
	2	6.37	0.83	149.98			19.97	15060.41
	3	6.19	0.75	149.98			18.10	15289.51
	4	6.10	0.67	149.98			16.24	14283.26
	5	5.95	0.59	149.98			14.48	14000.16
	Outlet	5.91						
R123T12	Inlet	6.81			22222.17	4.47		
	1	6.64	1.12	189.93			30.63	19917.03
	2	6.51	1.00	189.93			27.43	18638.33
	3	6.23	0.87	189.93			24.02	19051.29
	4	6.19	0.74	189.93			20.61	15886.08
	5	6.05	0.62	189.93			17.41	14243.77
	Outlet	5.97						
R123T13	Inlet	7.24			22451.40	4.51		
	1	7.03	1.31	189.94			35.72	20043.84

	2	6.86	1.19	189.94			32.62	19485.52
	3	6.56	1.07	189.94			29.32	20265.75
	4	6.48	0.94	189.94			26.02	18223.33
	5	6.31	0.82	189.94			22.92	17372.27
	Outlet	6.19						
R123T14	Inlet	7.41			22527.67	4.40		
	1	7.18	1.47	189.82			39.87	20294.25
	2	6.99	1.35	189.82			36.66	19926.65
	3	6.66	1.22	189.82			33.24	21028.52
	4	6.55	1.09	189.82			29.82	19318.17
	5	6.36	0.96	189.82			26.60	18833.81
	Outlet	6.22						
R123T15	Inlet	7.83			22796.52	4.63		
	1	7.59	1.60	189.91			43.34	20930.17
	2	7.37	1.46	189.91			39.79	20628.91
	3	7.02	1.32	189.91			36.01	21819.31
	4	6.90	1.18	189.91			32.23	20061.65
	5	6.69	1.04	189.91			28.68	19512.57
	Outlet	6.54						
R123T16	Inlet	7.95			22806.35	4.37		
	1	7.67	1.94	188.82			52.26	23431.68
	2	7.40	1.75	188.82			47.21	22810.35
	3	6.99	1.54	188.82			41.85	23667.47
	4	6.83	1.34	188.82			36.48	21211.81
	5	6.60	1.15	188.82			31.44	19743.87
	Outlet	6.46						
R123T17	Inlet	7.83			23004.45	4.40		
	1	7.59	1.60	189.91			43.34	20930.17
	2	7.37	1.46	189.91			39.79	20628.91
	3	7.02	1.32	189.91			36.01	21819.31

	4	6.90	1.18	189.91			32.23	20061.65
	5	6.69	1.04	189.91			28.68	19512.57
	Outlet	6.54						
R123T18	Inlet	8.81			23034.51	4.32		
	1	8.38	2.47	189.81			65.83	24097.62
	2	8.08	2.25	189.81			60.04	23565.15
	3	7.59	2.02	189.81			53.89	24761.19
	4	7.33	1.78	189.81			47.74	23328.56
	5	7.02	1.56	189.81			41.95	22677.89
	Outlet	6.83						

Table 6-7 R-134a on Turbo BII HP Tube average data

Run #	$T_{w,in}$ (°C)	$T_{w,out}$ (°C)	ΔP_w (kPa)	Re	T_{sat} (°C)	q"(kW/m²)	h_r (W/m².°C)
R134aT1	5.56	5.09	23.68	7018.84	4.39	4.14	6270.37
R134aT2	5.68	5.25	52.39	11141.75	4.43	6.04	7772.38
R134aT3	6.05	5.50	92.59	15386.96	4.50	10.52	11128.06
R134aT4	7.38	5.71	23.75	7330.09	4.43	14.51	12806.46
R134aT5	6.35	5.67	143.73	19632.21	4.44	16.67	14503.06
R134aT6	7.04	5.80	52.65	11529.35	4.48	17.08	14158.95
R134aT7	7.02	5.91	92.64	15744.20	4.50	21.09	16326.77
R134aT8	6.74	5.91	205.19	23943.55	4.40	24.90	17829.27
R134aT9	7.07	5.96	143.96	19958.22	4.36	26.89	18350.20
R134aT10	7.36	6.17	205.23	24292.55	4.32	35.12	20679.55
R134aT11	6.93	6.04	353.01	31811.44	4.24	36.29	21996.25
R134aT12	7.85	6.67	352.85	32593.60	4.47	47.08	23268.29
R134aT13	11.64	7.56	52.65	12794.50	4.52	56.34	20460.72
R134aT14	10.72	7.53	93.01	17159.43	4.48	60.04	21469.07
R134aT15	10.53	7.78	144.18	21694.02	4.36	65.72	20577.40

R134aT16	13.10	8.15	52.77	13169.14	4.45	68.28	20010.52
R134aT17	12.16	8.30	92.50	17669.56	4.46	72.43	20188.21
R134aT18	10.81	8.26	205.68	26472.12	4.44	74.02	20547.25
R134aT19	17.67	8.90	23.57	9042.84	4.48	76.83	18661.28
R134aT20	11.81	8.53	143.67	22314.70	4.33	78.25	19678.57
R134aT21	10.86	8.78	355.64	34748.02	4.33	80.02	18710.53
R134aT22	14.58	8.82	55.05	13912.77	4.30	81.32	19096.64
R134aT23	13.36	9.03	92.53	18216.39	4.47	81.50	18823.44
R134aT24	12.79	8.78	109.25	19597.18	4.27	82.12	19173.17
R134aT25	12.48	9.03	145.09	22748.66	4.52	82.36	19132.02
R134aT26	16.24	9.00	37.24	11514.16	4.40	82.38	19079.61
R134aT27	10.77	8.63	353.23	35119.20	4.32	83.31	20315.67
R134aT28	12.31	9.25	206.28	27464.07	4.42	88.43	19083.28
R134aT29	12.64	9.69	246.18	30097.73	4.48	92.87	18441.64
R134aT30	11.88	9.44	353.23	36147.06	4.37	95.11	19587.57
R134aT31	15.47	10.73	146.60	24197.85	4.52	112.52	18552.09
R134aT32	15.32	10.89	206.35	29382.92	4.31	128.04	20072.04
R134aT33	14.47	11.02	355.37	38459.13	4.47	133.20	21009.97
R134aT34	14.58	11.07	354.77	38527.33	4.43	135.19	21034.61

Table 6-8 R-134a on Turbo BII HP tube local data

Run #	**RTD #**	**T_w (°C)**	**$\lvert dT/dx \rvert$ (°C/m)**	**$\Delta P_w/\Delta x$ (kPa/m)**	**Re**	**T_{sat} (°C)**	**q''_{local} (kW/m²)**	**$h_{r,local}$ (W/m².°C)**
R134aT1	Inlet	5.56			7018.84	4.39		
	1	5.44	0.65	20.72			5.62	7949.83
	2	5.36	0.56	20.72			4.87	7293.45
	3	5.24	0.47	20.72			4.07	6774.11
	4	5.20	0.37	20.72			3.27	5367.36
	5	5.15	0.29	20.72			2.51	4146.27

	Outlet	5.09						
R134aT2	Inlet	5.68			11141.75	4.43		
	1	5.57	0.58	45.83			8.07	9860.74
	2	5.49	0.51	45.83			7.03	8992.65
	3	5.39	0.43	45.83			5.93	8210.92
	4	5.35	0.34	45.83			4.83	6642.32
	5	5.30	0.27	45.83			3.79	5258.14
	Outlet	5.25						
R134aT3	Inlet	6.05			15386.96	4.50		
	1	5.92	0.70	81.00			13.33	12961.08
	2	5.81	0.62	81.00			11.86	12325.31
	3	5.70	0.53	81.00			10.29	11435.66
	4	5.65	0.45	81.00			8.72	9788.87
	5	5.58	0.37	81.00			7.24	8338.69
	Outlet	5.50						
R134aT4	Inlet	7.38			7330.09	4.43		
	1	6.92	2.48	20.78			21.49	17849.25
	2	6.56	1.99	20.78			17.28	15784.91
	3	6.25	1.56	20.78			13.49	13301.88
	4	6.02	1.20	20.78			10.41	10703.14
	5	5.86	0.94	20.78			8.16	8646.41
	Outlet	5.71						
R134aT5	Inlet	6.35			19632.21	4.44		
	1	6.19	0.85	125.74			20.67	16379.26
	2	6.05	0.76	125.74			18.54	15759.94
	3	5.93	0.66	125.74			16.27	14731.66
	4	5.85	0.56	125.74			14.01	12945.53
	5	5.77	0.47	125.74			11.88	11318.94
	Outlet	5.67						
R134aT6	Inlet	7.04			11529.35	4.48		

	1	6.73	1.72	46.07			23.63	17868.84
	2	6.47	1.41	46.07			19.36	15709.65
	3	6.25	1.14	46.07			15.73	13614.86
	4	6.08	0.94	46.07			13.04	11959.52
	5	5.94	0.82	46.07			11.38	11173.96
	Outlet	5.80						
R134aT7	Inlet	7.02			15744.20	4.50		
	1	6.76	1.48	81.05			28.00	19458.63
	2	6.52	1.21	81.05			22.85	16898.06
	3	6.33	1.00	81.05			18.89	14727.84
	4	6.19	0.87	81.05			16.49	13653.58
	5	6.06	0.82	81.05			15.65	14240.59
	Outlet	5.91						
R134aT8	Inlet	6.74			23943.55	4.40		
	1	6.55	1.03	179.52			30.38	19655.52
	2	6.38	0.92	179.52			27.42	19127.18
	3	6.23	0.81	179.52			24.29	17970.15
	4	6.14	0.70	179.52			21.15	16047.45
	5	6.03	0.60	179.52			18.19	14337.80
	Outlet	5.91						
R134aT9	Inlet	7.07			19958.22	4.36		
	1	6.81	1.39	125.95			33.55	20299.12
	2	6.58	1.24	125.95			30.03	19903.37
	3	6.39	1.09	125.95			26.29	18688.38
	4	6.25	0.93	125.95			22.55	16652.09
	5	6.11	0.78	125.95			19.03	14664.58
	Outlet	5.96						
R134aT10	Inlet	7.36			24292.55	4.32		
	1	7.10	1.44	179.55			42.16	21749.11
	2	6.86	1.30	179.55			38.36	21627.15

	3	6.66	1.16	179.55			34.31	20759.27
	4	6.51	1.02	179.55			30.26	19084.99
	5	6.35	0.89	179.55			26.46	17635.98
	Outlet	6.17						
R134aT11	Inlet	6.93			31811.44	4.24		
	1	6.75	1.05	308.84			42.29	22823.30
	2	6.57	0.97	308.84			39.10	22637.49
	3	6.40	0.88	308.84			35.72	22159.67
	4	6.30	0.79	308.84			32.33	20756.71
	5	6.18	0.70	308.84			29.14	19572.05
	Outlet	6.04						
R134aT12	Inlet	7.85			32593.60	4.47		
	1	7.61	1.34	308.71			53.31	22877.34
	2	7.39	1.26	308.71			49.99	23179.68
	3	7.18	1.16	308.71			46.47	23254.92
	4	7.02	1.07	308.71			42.95	22693.31
	5	6.86	0.98	308.71			39.64	22231.62
	Outlet	6.67						
R134aT13	Inlet	11.64			12794.50	4.52		
	1	10.67	5.09	46.06			70.23	19464.13
	2	9.86	4.57	46.06			63.07	20655.50
	3	9.23	4.02	46.06			55.46	20518.78
	4	8.58	3.47	46.06			47.85	20559.21
	5	8.07	2.95	46.06			40.69	19566.16
	Outlet	7.56						
R134aT14	Inlet	10.72			17159.43	4.48		
	1	9.99	3.85	81.37			72.40	20581.96
	2	9.36	3.50	81.37			65.93	21521.36
	3	8.87	3.13	81.37			59.05	21343.91
	4	8.38	2.77	81.37			52.16	21202.70

	5	7.96	2.42	81.37			45.69	20563.05
	Outlet	7.53						
R134aT15	Inlet	10.53			21694.02	4.36		
	1	9.93	3.12	126.14			74.60	19078.34
	2	9.41	2.91	126.14			69.62	19857.31
	3	9.00	2.69	126.14			64.32	20029.94
	4	8.58	2.47	126.14			59.03	20289.15
	5	8.20	2.26	126.14			54.04	20484.20
	Outlet	7.78						
R134aT16	Inlet	13.10			13169.14	4.45		
	1	11.93	6.04	46.17			83.22	18315.86
	2	10.97	5.47	46.17			75.37	19525.57
	3	10.22	4.86	46.17			67.02	19692.69
	4	9.43	4.26	46.17			58.67	20188.04
	5	8.81	3.68	46.17			50.82	19820.56
	Outlet	8.15						
R134aT17	Inlet	12.16			17669.56	4.46		
	1	11.31	4.51	80.93			84.50	18508.71
	2	10.56	4.16	80.93			77.97	19526.52
	3	9.98	3.79	80.93			71.02	19705.58
	4	9.38	3.41	80.93			64.08	20095.42
	5	8.87	3.06	80.93			57.54	20185.12
	Outlet	8.30						
R134aT18	Inlet	10.81			26472.12	4.44		
	1	10.26	2.85	179.95			82.42	19223.98
	2	9.80	2.68	179.95			77.56	19808.21
	3	9.41	2.49	179.95			72.39	20017.34
	4	9.03	2.31	179.95			67.22	20172.15
	5	8.67	2.14	179.95			62.35	20347.91
	Outlet	8.26						

R134aT19	Inlet	17.67			9042.84	4.48		
	1	15.32	11.29	20.62			98.94	17017.23
	2	13.67	9.96	20.62			87.27	18355.55
	3	12.34	8.54	20.62			74.87	18442.93
	4	10.94	7.13	20.62			62.47	19034.39
	5	9.93	5.79	20.62			50.79	17688.77
	Outlet	8.90						
R134aT20	Inlet	11.81			22314.70	4.33		
	1	11.09	3.74	125.70			89.02	18448.87
	2	10.48	3.48	125.70			82.95	19112.87
	3	9.99	3.21	125.70			76.50	19175.78
	4	9.49	2.94	125.70			70.05	19270.31
	5	9.03	2.68	125.70			63.97	19329.68
	Outlet	8.53						
R134aT21	Inlet	10.86			34748.02	4.33		
	1	10.42	2.45	311.15			93.64	19689.66
	2	10.06	2.25	311.15			86.40	19242.60
	3	9.60	2.05	311.15			78.72	18970.49
	4	9.40	1.84	311.15			71.03	17499.20
	5	9.10	1.64	311.15			63.80	16512.03
	Outlet	8.78						
R134aT22	Inlet	14.58			13912.77	4.30		
	1	13.18	7.14	48.16			100.68	18393.47
	2	12.06	6.40	48.16			90.30	19173.57
	3	11.13	5.62	48.16			79.27	19100.75
	4	10.32	4.83	48.16			68.24	18406.74
	5	9.61	4.10	48.16			57.85	17254.59
	Outlet	8.82						
R134aT23	Inlet	13.36			18216.39	4.47		
	1	12.37	5.14	80.95			96.60	18070.08

	2	11.54	4.70	80.95			88.27	18635.29
	3	10.84	4.22	80.95			79.41	18596.05
	4	10.25	3.75	80.95			70.56	18016.38
	5	9.67	3.31	80.95			62.23	17498.29
	Outlet	9.03						
R134aT24	Inlet	12.79			19597.18	4.27		
	1	11.87	4.76	95.58			97.43	18703.90
	2	11.11	4.35	95.58			89.01	19108.83
	3	10.44	3.91	95.58			80.06	19030.40
	4	9.91	3.47	95.58			71.11	18265.59
	5	9.38	3.06	95.58			62.69	17557.81
	Outlet	8.78						
R134aT25	Inlet	12.48			22748.66	4.52		
	1	11.71	4.01	126.93			95.59	18570.26
	2	11.06	3.69	126.93			88.14	18928.24
	3	10.48	3.36	126.93			80.23	18897.28
	4	10.04	3.03	126.93			72.32	18197.45
	5	9.57	2.71	126.93			64.88	17724.20
	Outlet	9.03						
R134aT26	Inlet	16.24			11514.16	4.40		
	1	14.37	9.23	32.58			104.95	18357.27
	2	12.97	8.17	32.58			92.91	19340.14
	3	11.82	7.04	32.58			80.11	19172.67
	4	10.77	5.92	32.58			67.31	18478.17
	5	9.92	4.86	32.58			55.27	16842.09
	Outlet	9.00						
R134aT27	Inlet	10.77			35119.20	4.32		
	1	10.33	2.33	309.04			90.48	19207.27
	2	9.96	2.21	309.04			86.20	19506.68
	3	9.60	2.09	309.04			81.64	19824.76

	4	9.29	1.97	309.04			77.09	20084.85
	5	9.00	1.86	309.04			72.81	20260.53
	Outlet	8.63						
R134aT28	Inlet	12.31			27464.07	4.42		
	1	11.63	3.45	180.48			99.62	18417.64
	2	11.08	3.22	180.48			93.07	18702.30
	3	10.61	2.97	180.48			86.10	18593.33
	4	10.16	2.73	180.48			79.13	18373.77
	5	9.74	2.50	180.48			72.58	18078.54
	Outlet	9.25						
R134aT29	Inlet	12.64			30097.73	4.48		
	1	12.00	3.46	215.38			108.79	19018.35
	2	11.45	3.18	215.38			99.98	18805.23
	3	10.89	2.88	215.38			90.63	18478.87
	4	10.57	2.58	215.38			81.27	17125.47
	5	10.16	2.29	215.38			72.47	16175.54
	Outlet	9.69						
R134aT30	Inlet	11.88			36147.06	4.37		
	1	11.37	2.73	309.04			105.78	19241.67
	2	10.94	2.57	309.04			99.63	19325.75
	3	10.53	2.40	309.04			93.09	19246.32
	4	10.16	2.22	309.04			86.55	18957.63
	5	9.85	2.06	309.04			80.39	18533.11
	Outlet	9.44						
R134aT31	Inlet	15.47			24197.85	4.52		
	1	14.37	5.78	128.26			136.88	19360.79
	2	13.45	5.22	128.26			123.72	19271.02
	3	12.62	4.63	128.26			109.74	18681.72
	4	12.02	4.03	128.26			95.75	17223.44
	5	11.42	3.47	128.26			82.59	15816.72

	Outlet	10.73						
R134aT32	Inlet	15.32			29382.92	4.31		
	1	14.26	5.32	180.54			153.29	21024.85
	2	13.44	4.83	180.54			139.35	20761.84
	3	12.73	4.31	180.54			124.55	19882.32
	4	12.08	3.79	180.54			109.74	18696.44
	5	11.54	3.31	180.54			95.81	17207.59
	Outlet	10.89						
R134aT33	Inlet	14.47			38459.13	4.47		
	1	13.66	4.03	310.91			155.39	21929.25
	2	13.05	3.71	310.91			142.96	21514.27
	3	12.49	3.36	310.91			129.75	20724.93
	4	11.97	3.01	310.91			116.55	19680.80
	5	11.55	2.68	310.91			104.12	18350.73
	Outlet	11.02						
R134aT34	Inlet	14.58			38527.33	4.43		
	1	13.77	4.09	310.38			157.51	21882.05
	2	13.15	3.76	310.38			145.08	21514.13
	3	12.57	3.41	310.38			131.87	20772.03
	4	12.04	3.06	310.38			118.66	19780.65
	5	11.62	2.74	310.38			106.23	18494.91
	Outlet	11.07						

Appendix B - Mathcad Example Calculation Sheet

The Mathcad sheet presented next is a selected sheet among the calculation sheets created for every data point (run). This sheet is used for calculating the overall heat transfer coefficient according the EBHT, the average heat transfer coefficient uncertainty, and the local heat transfer coefficients uncertainties.

An Excel sheet contains the recorded data from the data acquisition system as well as the necessary equations for calculating the average and local heat transfer coefficients was created for each run. So for each run two sheets were created, an Excel and a Mathcad sheets.

The Mathcad sheet starts by recalling the parameters from the corresponding Excel sheet. The first part of the Math Cad sheet is for calculating the overall heat transfer coefficient according to the EBHT. After determining the solution of the overall heat transfer coefficient, it delivers the solution back to the corresponding Excel sheet. A Mathcad function called “Find” is used for solving for the overall heat transfer coefficient by trail and error. The “Find” function requires a guess value for initiating the iterations.

Following to the determination of the overall heat transfer coefficient is the calculations of uncertainties in the average and local heat transfer coefficients as explained in Section 4.6 of this thesis. It is noticed that the propagation of error equations below are cut to fit the page. These equations are similar to Equation 4.52 presented in the Data Reduction chapter.

Data :=

C:\..\13.68.xls

$Ar := \pi \cdot 0.75 \cdot 0.0254$

$mdot := Data_{0,0}$

$U := Data_{0,24}$

$U = 11682.19781$

$Tsat := Data_{0,19}$

$Cp := Data_{0,13} 1000$

$\Delta T2 := \left(Data_{0,9} - Data_{0,19}\right)$

$\Delta P := \left(Data_{0,10} - Data_{0,2}\right) \cdot \frac{1m}{45in} \cdot 1000$

$v := \frac{1}{Data_{0,15}} \qquad \rho := \frac{1}{v}$

$\Delta T1 := \left(Data_{0,3} - Data_{0,19}\right)$

Given

$$\ln\left[\frac{\left(\Delta T2 + \frac{mdot \cdot v \cdot \Delta P}{U \cdot Ar}\right)}{\left(\Delta T1 + \frac{mdot \cdot v \cdot \Delta P}{U \cdot Ar}\right)}\right] + \frac{U \cdot Ar}{mdot \cdot Cp} = 0$$

$Uo := Find(U)$

$Uo = 11714.4842816937$

$$\ln\left[\frac{\left(\Delta T2 + \frac{mdot \cdot v \cdot \Delta P}{Uo \cdot Ar}\right)}{\left(\Delta T1 + \frac{mdot \cdot v \cdot \Delta P}{Uo \cdot Ar}\right)}\right] = -0.851612$$

$$\frac{Uo \cdot Ar}{mdot \cdot Cp} = 0.851612$$

C:\..\13.68U

Uo

Average Heat Transfer Coefficient Uncertainty Calculation

$umdot := \frac{0.05}{100} \cdot mdot$

$u\rho := 7 \cdot 10^{-3} \cdot \rho$

$u\Delta P := \sqrt{2} \cdot 758.423302$

$Tinlet := Data_{0,3}$

$Toutlet := Data_{0,9}$

$uT := 0.03$

$uCp := 6 \cdot 10^{-4} \cdot Cp$

$hw := Data_{0,29}$

$uhw := 0.02 \cdot hw$

$Rw := Data_{0,30}$

$uTsat := 0.02$

$L := 1$

$uL := 0.0015875 \qquad \frac{1}{16} in = 0.0015875\, m$

$$href(mdot, Cp, Tinlet, Toutlet, Tsat, \rho, \Delta P, hw, L) := \left[\frac{1}{\frac{mdot \cdot Cp \cdot (Tinlet - Toutlet) + mdot \cdot \frac{1}{\rho} \cdot (-\Delta P)}{\frac{Tinlet - Toutlet}{\ln\left(\frac{Tinlet - Tsat}{Toutlet - Tsat}\right)} \cdot \pi \cdot 0.75 \cdot 0.0254 \cdot L}} - Rw - \frac{1}{hw} \cdot \frac{0.75}{0.7} \right]^{-1}$$

$$uhref := \left[\left[\left(\frac{d}{dmdot} href(mdot, Cp, Tinlet, Toutlet, Tsat, \rho, \Delta P, hw, L) \right) \cdot umdot \right]^2 + \left[\left(\frac{d}{dCp} href(mdot, Cp, Tinlet, Toutlet, \right. \right. \right.$$

$uhref = 466.263$

$$\frac{uhref}{Data_{0,31}} \cdot 100 = 2.33$$

Local Heat Transfer Coefficient Uncertainty Calculations

Monte Carlo Simulation For Determining The Uncertainty in dT/dx

$Ti := Data_{0,3}$

$T1 := Data_{0,32}$ $\qquad$ $T1a := Data_{0,4}$

$T2 := Data_{0,33}$ $\qquad$ $T2a := Data_{0,5}$

$T3 := Data_{0,34}$ $\qquad$ $T3a := Data_{0,6}$

$T4 := Data_{0,35}$ $\qquad$ $T4a := Data_{0,7}$

$T5 := Data_{0,36}$ $\qquad$ $T5a := Data_{0,8}$

$To := Data_{0,9}$

$i := 0..12000$

$Z_i := rnorm(7,0,0.015)$

$Y_i := rnorm\left(7,0,7.9375 \times 10^{-4}\right)$

$$TT_i := \begin{pmatrix} Ti \\ T1 \\ T2 \\ T3 \\ T4 \\ T5 \\ To \end{pmatrix} + Z_i \qquad Dist_i := \begin{pmatrix} 0 \\ 0.17 \\ 0.33 \\ 0.5 \\ 0.67 \\ 0.83 \\ 1 \end{pmatrix} + Y_i$$

$REG_i := regress\left(Dist_i, TT_i, 2\right)$

$$Un17_i := \frac{\left[2\cdot(REG_i)_5\cdot(0.17) + (REG_i)_4 - Data_{0,37}\right]}{Data_{0,37}}$$

$$Un33_i := \frac{\left[2\cdot(REG_i)_5\cdot(0.33) + (REG_i)_4 - Data_{0,38}\right]}{Data_{0,38}}$$

$$Un50_i := \frac{\left[2\cdot(REG_i)_5\cdot(0.5) + (REG_i)_4 - Data_{0,39}\right]}{Data_{0,39}}$$

$$Un67_i := \frac{\left[2\cdot(REG_i)_5\cdot(0.67) + (REG_i)_4 - Data_{0,40}\right]}{Data_{0,40}}$$

$$Un83_i := \frac{\left[2\cdot(REG_i)_5\cdot(0.83) + (REG_i)_4 - Data_{0,41}\right]}{Data_{0,41}}$$

$$udTdx := \begin{pmatrix} sort(Un17)_{11400} \\ sort(Un33)_{11400} \\ sort(Un50)_{11400} \\ sort(Un67)_{11400} \\ sort(Un83)_{11400} \end{pmatrix}$$

$$dTdx1 := Data_{0,42}$$

$$dTdx2 := Data_{0,43}$$

$$dTdx3 := Data_{0,44}$$

$$dTdx4 := Data_{0,45}$$

$$dTdx5 := Data_{0,46}$$

$$\Delta P\Delta x := \frac{-(Data_{0,10} - Data_{0,2})\cdot 1000}{45\cdot 0.0254}$$

$$uT1a := \left[uT^2 + \left[dTdx1\cdot(1.5875\times 10^{-3})\right]^2\right]^{0.5}$$

$$uT2a := \left[uT^2 + \left[dTdx2\cdot(1.5875\times 10^{-3})\right]^2\right]^{0.5}$$

$$uT3a := \left[uT^2 + \left[dTdx3\cdot(1.5875\times 10^{-3})\right]^2\right]^{0.5}$$

$$uT4a := \left[uT^2 + \left[dTdx4\cdot(1.5875\times 10^{-3})\right]^2\right]^{0.5}$$

$$uT5a := \left[uT^2 + \left[dTdx5\cdot(1.5875\times 10^{-3})\right]^2\right]^{0.5}$$

1st Local HTC Uncertainty Calculation

$$q1''(mdot, Cp, dTdx1, \rho, \Delta P\Delta x) := \frac{mdot \cdot Cp \cdot dTdx1 + mdot \cdot \frac{1}{\rho} \cdot \Delta P\Delta x}{\pi \cdot 0.75 \cdot 0.0254}$$

$$uq1'' := \left[\left[\left(\frac{d}{dmdot} q1''(mdot, Cp, dTdx1, \rho, \Delta P\Delta x)\right) \cdot umdot\right]^2 + \left[\left(\frac{d}{dC}\right.\right.\right.$$

$$q1'' := q1''(mdot, Cp, dTdx1, \rho, \Delta P\Delta x)$$

$$hrl1(T1a, Tsat, q1'', Rw, hw) := \left[\frac{(T1a - Tsat)}{q1''} - Rw - \frac{1}{hw} \cdot \frac{0.75}{0.7}\right]^{-1}$$

$$uhrl1 := \left[\left[\left(\frac{d}{dT1a} hrl1(T1a, Tsat, q1'', Rw, hw)\right) \cdot uT1a\right]^2 + \left[\left(\frac{d}{dTsat} hr\right.\right.\right.$$

$$\frac{uhrl1}{Data_{0,47}} \cdot 100 = 1.492$$

2nd Local HTC Uncertainty Calculation

$$q2''(mdot, Cp, dTdx2, \rho, \Delta P\Delta x) := \frac{mdot \cdot Cp \cdot dTdx2 + mdot \cdot \frac{1}{\rho} \cdot \Delta P\Delta x}{\pi \cdot 0.75 \cdot 0.0254}$$

$$uq2'' := \left[\left[\left(\frac{d}{dmdot} q2''(mdot, Cp, dTdx2, \rho, \Delta P\Delta x)\right) \cdot umdot\right]^2 + \left[\left(\frac{d}{dC}\right.\right.\right.$$

$$q2'' := q2''(mdot, Cp, dTdx2, \rho, \Delta P\Delta x)$$

$$hrl2(T2a, Tsat, q2'', Rw, hw) := \left[\frac{(T2a - Tsat)}{q2''} - Rw - \frac{1}{hw} \cdot \frac{0.75}{0.7}\right]^{-1}$$

$$uhrl2 := \left[\left[\left(\frac{d}{dT2a} hrl2(T2a, Tsat, q2'', Rw, hw)\right) \cdot uT2a\right]^2 + \left[\left(\frac{d}{dTsat} hr\right.\right.\right.$$

$$\frac{uhrl2}{Data_{0,48}} \cdot 100 = 3.945$$

3rd Local HTC Uncertainty Calculation

$$q3''(mdot, Cp, dTdx3, \rho, \Delta P\Delta x) := \frac{mdot \cdot Cp \cdot dTdx3 + mdot \cdot \frac{1}{\rho} \cdot \Delta P\Delta x}{\pi \cdot 0.75 \cdot 0.0254}$$

$$uq3'' := \left[\left[\left(\frac{d}{dmdot} q3''(mdot, Cp, dTdx3, \rho, \Delta P\Delta x)\right) \cdot umdot\right]^2 + \left[\left(\frac{d}{dC}\right.\right.\right.$$

$$q3'' := q3''(mdot, Cp, dTdx3, \rho, \Delta P\Delta x)$$

$$hrl3(T3a, Tsat, q3'', Rw, hw) := \left[\frac{(T3a - Tsat)}{q3''} - Rw - \frac{1}{hw} \cdot \frac{0.75}{0.7}\right]^{-1}$$

$$uhrl3 := \left[\left[\left(\frac{d}{dT3a} hrl3(T3a, Tsat, q3'', Rw, hw)\right) \cdot uT3a\right]^2 + \left[\left(\frac{d}{dTsat} hr\right.\right.\right.$$

$$\frac{uhrl3}{Data_{0,49}} \cdot 100 = 5.327$$

4th Local HTC Uncertainty Calculation

$$q4''(mdot, Cp, dTdx4, \rho, \Delta P\Delta x) := \frac{mdot \cdot Cp \cdot dTdx4 + mdot \cdot \frac{1}{\rho} \cdot \Delta P\Delta x}{\pi \cdot 0.75 \cdot 0.0254}$$

$$uq4'' := \left[\left[\left(\frac{d}{dmdot} q4''(mdot, Cp, dTdx4, \rho, \Delta P\Delta x)\right) \cdot umdot\right]^2 + \left[\left(\frac{d}{dC}\right.\right.\right.$$

$$q4'' := q4''(mdot, Cp, dTdx4, \rho, \Delta P\Delta x)$$

$$hrl4(T4a, Tsat, q4'', Rw, hw) := \left[\frac{(T4a - Tsat)}{q4''} - Rw - \frac{1}{hw} \cdot \frac{0.75}{0.7}\right]^{-1}$$

$$uhrl4 := \left[\left[\left(\frac{d}{dT4a} hrl4(T4a, Tsat, q4'', Rw, hw)\right) \cdot uT4a\right]^2 + \left[\left(\frac{d}{dTsat} hr\right.\right.\right.$$

$$\frac{uhrl4}{Data_{0,50}} \cdot 100 = 4.481$$

5th Local HTC Uncertainty Calculation

$$q5''(mdot, Cp, dTdx5, \rho, \Delta P\Delta x) := \frac{mdot \cdot Cp \cdot dTdx5 + mdot \cdot \frac{1}{\rho} \cdot \Delta P\Delta x}{\pi \cdot 0.75 \cdot 0.0254}$$

$$uq5'' := \left[\left[\left(\frac{d}{dmdot} q5''(mdot, Cp, dTdx5, \rho, \Delta P\Delta x)\right) \cdot umdot\right]^2 + \left[\left(\frac{d}{dC}\right.\right.\right.$$

$$q5'' := q5''(mdot, Cp, dTdx5, \rho, \Delta P\Delta x)$$

$$hrl5(T5a, Tsat, q5'', Rw, hw) := \left[\frac{(T5a - Tsat)}{q5''} - Rw - \frac{1}{hw} \cdot \frac{0.75}{0.7}\right]^{-1}$$

$$uhrl5 := \left[\left[\left(\frac{d}{dT5a} hrl5(T5a, Tsat, q5'', Rw, hw)\right) \cdot uT5a\right]^2 + \left[\left(\frac{d}{dTsat} hr\right.\right.\right.$$

$$\frac{uhrl5}{Data_{0,51}} \cdot 100 = 2.004$$

$$uhref = 466.2627709$$

$$\begin{pmatrix} uhrl1 \\ uhrl2 \\ uhrl3 \\ uhrl4 \\ uhrl5 \end{pmatrix} = \begin{pmatrix} 273.2566794 \\ 770.2297129 \\ 1048.9653972 \\ 904.5311173 \\ 397.2098903 \end{pmatrix}$$